

Morphing UAVs: Integrating Extended Endurance, Agile Flight, and Enhanced
Functionalities through Hardware Innovations

By

Jerry Tang

A dissertation submitted in partial satisfaction of the

requirements for the degree of

Doctor of Philosophy

in

Engineering - Mechanical Engineering

in the

Graduate Division

of the

University of California, Berkeley

Committee in charge:

Professor Mark W. Mueller, Chair

Professor Hannah Stuart

Professor Koushil Sreenath

Spring 2025

Morphing UAVs: Integrating Extended Endurance, Agile Flight, and Enhanced
Functionalities through Hardware Innovations

Copyright 2025
by
Jerry Tang

Abstract

Morphing UAVs: Integrating Extended Endurance, Agile Flight, and Enhanced Functionalities through Hardware Innovations

by

Jerry Tang

Doctor of Philosophy in Engineering - Mechanical Engineering

University of California, Berkeley

Professor Mark W. Mueller, Chair

This dissertation presents a series of novel UAV designs that address notable limitations of conventional quadcopters through practical, hardware-centric modifications and corresponding control strategies. We first introduce an unactuated rotor tilting vehicle design (QUaRTM) that enables the quadcopter to passively adjust rotor orientation mid-flight, reducing frontal drag at higher speeds. By transitioning between untilted and tilted configurations using sprung hinges—without adding any actuators—QUaRTM achieves improved top speed, agility, and energy efficiency. Experiments show a 12.5% increase in max speed, better high-speed agility, and over 20% reduction in power consumption at 15–20 m/s. Building on this foundation, the active tilt-rotor concept PairTilt introduces pairwise rotor coupling to decouple forward translation from pitch rotation, enabling a balanced trade-off between mechanical simplicity and enhanced flight performance. This design reduces servo torque demands and gyroscopic effects by avoiding independent rotor tilting, while maintaining strong control authority. As a result, PairTilt supports faster and more energy-efficient cruising, improved agility during fast maneuvers, and enables novel capabilities such as sensor pointing and compact hovering in confined environments. Furthermore, the dissertation presents a dual-modal UAV design (Duawlfm) that, to the best of our knowledge, is the first to achieve ground locomotion without relying on aerodynamic propulsion and without adding any additional actuators. The same set of motors used for flight is mechanically repurposed to drive ground motion through a passive belt-and-differential drivetrain combined with one-way bearings, which automatically decouple the propellers during reverse motor operation. This unified actuation strategy enables seamless and efficient transitions between flying and driving, all within a compact and mechanically simple architecture. In addition, two co-authored studies—one on staging battery mass for extended flight time and another on midair reconfiguration using unactuated hinges—are briefly introduced here to underscore complementary design strategies that further enhance UAV capability. Collectively, these contributions not only extend the operational envelope of multirotor UAVs but

also provide practical solutions for applications requiring high-performance, long-range, and versatile aerial robotics.

Contents

Contents **i**

- 1 Introduction** **1**
 - 1.1 Motivation 1
 - 1.2 Overview of the Dissertation 2
 - 1.3 Dissertation Outline 5
 - 1.4 Conclusion 5

- 2 Literature Survey** **7**
 - 2.1 Quadcopters and the Need for Enhanced Efficiency 7
 - 2.2 Tilt-Rotor Designs for High-Speed Flight 7
 - 2.3 Innovations in Underactuated Tilt-Rotor UAVs 8
 - 2.4 Fully Actuated UAV Platforms 8
 - 2.5 Hybrid Aerial-Ground Mobility 8
 - 2.6 Summary 9

- 3 QUaRTM: A Quadcopter with Unactuated Rotor Tilting Mechanism** **10**
 - 3.1 Introduction 10
 - 3.2 System Overview 14
 - 3.3 Design 19
 - 3.4 Experimental Validation 29
 - 3.5 Conclusion 36

- 4 PairTilt: Design and Control of an Active Tilt-Rotor Quadcopter for Improved Efficiency and Agility** **38**
 - 4.1 Introduction 39
 - 4.2 Overview 42
 - 4.3 Design Analysis 45
 - 4.4 Control 57
 - 4.5 Experimental Validation 59
 - 4.6 Conclusion 66

5	Duawlfyn: A Drone with Unified Actuation for Wheeled Locomotion and Flight Operation	68
5.1	Introduction	69
5.2	Design	72
5.3	Control	75
5.4	Experimental Validation	78
5.5	Conclusion	84
6	Conclusion and Future Directions	85
6.1	Conclusion	85
6.2	Future Directions	86
	Bibliography	88

Acknowledgments

First and foremost, I would like to express my deepest gratitude to my parents, Jun Tang and Dongyan Xu, for their unwavering support throughout my education and life's development. Thank you for giving me the freedom to choose my own path and for always standing by me.

To my fiancée, Pei-Chi Tsao, thank you for your steadfast support and for helping me see many aspects of life that I often overlooked.

I am profoundly grateful to my advisor, Professor Mark Mueller, for taking me on as an undergraduate researcher and later admitting me to the Ph.D. program at UC Berkeley. None of this would have been possible without your guidance. Your support, deep knowledge, and critical yet constructive feedback have been instrumental throughout my journey.

I would like to thank my dissertation committee, Professor Mark Mueller, Professor Hannah Stuart, and Professor Koushil Sreenath, for your constructive feedback and support throughout the process. I also want to express that I truly enjoyed taking classes with you all during my time at Berkeley. A special thank you to Professor Hannah Stuart for hosting MECENG 270, through which I met my fiancée, Pei-Chi Tsao. I further thank my qualifying exam committee, which included Professor Hannah Stuart, Professor Koushil Sreenath, Professor Kosa Goucher-Lambert, and Professor Kameshwar Poolla, for their thoughtful and valuable comments.

I am grateful to all my fellow members at HiPeRLab, past and present, whose contributions built the experimental testbed I relied on — a full list is available at hiperlab.berkeley.edu/members. Special thanks to my Ph.D. colleagues Nathan Bucki, Karan Jain, Clark Zha, Xiangyu Wu, Daisy Zhang, Ting-Hao Wang, Carlo Bosio, Teaya Yang, and Ruiqi Zhang. I also appreciate the contributions of my undergraduate research assistants, Yiheng Ji and Mauricio Vergara, as well as my Master of Engineering Capstone Project team — Kaan Beyduz, Yiwei Jiang, Cody Wiebe, Haoyu Zhang, and Osaruese Asoro — whom I had the honor of advising. It was a pleasure working with you all.

I thank the Hong Kong Centre for Logistics Robotics (HKCLR) for supporting my Ph.D. studies and funding my two summer research exchanges to Hong Kong. I am also grateful to Professor Ben M. Chen at the Chinese University of Hong Kong (CUHK) for hosting me during those exchanges, which were truly inspiring experiences. I thank my peers and co-authors at CUHK — Guidong Yang, Benyun Zhao, Yizhou Chen, and Junda Huang — for the stimulating collaborations.

Additional thanks go to other funding sources: the Berkeley International Office Graduate Tuition & Fee Grant, the Mechanical Engineering Block Grant Award, the Mechanical Engineering Departmental Award, and the Graduate Division Conference Travel Grant. I would also like to thank Professor Van Carey for providing me with a GSI position that helped me cover one semester's expenses at a difficult time, and for offering me a research opportunity during my undergraduate years.

Chapter 1

Introduction

1.1 Motivation

Unmanned Aerial Vehicles (UAVs)—commonly referred to as drones—have become key agents in a wide variety of modern applications, including aerial photography, search and rescue, environmental monitoring, package delivery, and surveillance. Their versatility, compactness, and ability to operate without direct human presence in challenging or hazardous environments have driven substantial growth in both academic research and industrial development. At the core of UAV systems are design and control philosophies that seek to address constraints on energy consumption, flight time, maneuverability, and operational safety.

In particular, multirotor UAVs such as quadcopters have garnered widespread popularity. Their mechanical simplicity, near-hover agility, and ability to vertically take off and land (VTOL) have made them a default choice in many scenarios. However, conventional quadcopter platforms exhibit inherent limitations in areas such as:

- **Aerodynamic Efficiency and Speed:** In conventional quadcopters, forward flight requires pitching the entire body, which increases frontal drag and reduces overall flight efficiency. This constraint limits cruising speed, top-end performance, and energy efficiency—particularly in longer missions or high-speed applications.
- **Underactuation:** Fixed rotors couple translational and rotational degrees of freedom, preventing independent control of motion and attitude. This underactuation limits fast maneuvers in confined or dynamic environments, reduces responsiveness during high-acceleration commands, and forces separate actuators (e.g., servos or gimbals) for tasks like precise sensor or camera pointing.
- **Multi-Modal Functionality and Adaptability:** Conventional UAVs typically operate in a fixed configuration optimized solely for aerial flight, limiting their ability to adapt to diverse mission profiles. Extending their capabilities—such as transitioning between aerial and ground locomotion for regulatory compliance, safety considerations,

or energy efficiency; adapting geometry mid-flight to navigate confined environments; or strategically managing energy sources to prolong endurance—often demands the addition of complex actuators and propulsion systems, increasing mechanical complexity and weight. There is thus a clear need for UAV architectures that leverage clever, passive, or minimally actuated mechanical designs to seamlessly achieve multi-modal operation and dynamic adaptability without significant added hardware complexity.

To address these challenges, my doctoral research explores *innovative vehicle designs*: combining novel mechanical architectures and tailored control strategies to achieve better flight endurance, improved agility, and expanded operational capabilities. Specifically, I have investigated a range of morphological and actuation concepts that enhance performance across endurance, maneuverability, and efficiency dimensions.

1.2 Overview of the Dissertation

This thesis compiles my previously published works to form a cohesive narrative on innovative UAV design. Each chapter presents a distinct approach to enhancing multirotor performance by rethinking traditional mechanical architectures. The unifying theme throughout is that straightforward, hardware-centric design changes—when combined with targeted control strategies—can powerfully address the inherent limitations of standard quadcopters.

The main contributions are as follows:

1. **QUaRTM: A Quadcopter with Unactuated Rotor Tilting Mechanism Capable of Faster, More Agile, and More Efficient Flight.**

In this work, we present QUaRTM – a novel quadcopter design capable of tilting the propellers into the forward flight direction, which reduces the drag area and therefore allows for faster, more agile, and more efficient flight. The vehicle can morph between two configurations in mid-air, including the untilted configuration and the tilted configuration. The vehicle in the untilted configuration has a higher pitch torque capacity and a smaller vertical dimension. The vehicle in the tilted configuration has a lower drag area, leading to a higher top speed, higher agility at high speed, and better flight efficiency.

The morphing is accomplished without any additional actuators beyond the four motors of a quadcopter. The rigid connections between the quadcopter frame and the quadcopter arms are replaced with sprung hinges. This allows the propellers to be tilted when high thrusts are produced, and recover to the untilted configuration when the thrusts are brought low.

The effectiveness of such a vehicle is demonstrated by running experiments on a prototype vehicle with a shape similar to a regular quadcopter. Through the use of tilting, the vehicle is shown to have a 12.5% higher maximum speed, better high-speed agility

as the maximum crash-free cruise speed increased by 7.5%, and a better flight efficiency as the power consumption has dropped by more than 20% in the speed range of 15-20m s⁻¹.

2. **PairTilt: Design and Control of an Active Tilt-Rotor Quadcopter for Improved Efficiency and Agility.**

Building on the tilt-rotor concept, this work presents PairTilt, a novel quadcopter design featuring two pairs of tiltable rotors, balancing the mechanical simplicity of conventional quadcopters with the enhanced agility of more complex tilt-rotor systems. While the system remains underactuated—specifically, the lateral translational degree of freedom is not directly controlled—this design choice is justified because it reduces complexity and minimizes energy use. The coupling of rotors reduces angular momentum issues, enhancing stability and efficiency without the challenges associated with tilting each motor individually, which would require higher servo torque due to significant gyroscopic torques.

PairTilt’s tiltable mechanism minimizes drag in high-speed flight, extending the operational range and making it well-suited for various aerial applications. Additionally, the design partially decouples translational and rotational dynamics, enabling agile maneuvers in confined spaces. The system’s dynamics are analyzed, and a cascaded controller is implemented to ensure stable flight across various scenarios. Through simulations and real-world experiments, we demonstrate the vehicle’s superior agility, compact hovering, sensor pointing ability, and energy efficiency at higher speeds compared to conventional quadcopters.

The primary contribution of this work lies in PairTilt’s distinctive design, which achieves a unique balance of simplicity, efficiency, and agility. This balance is made possible by the pairwise rotor coupling, which reduces complexity and gyroscopic torque effects, and the strategic prioritization of key degrees of freedom. This design approach opens new possibilities for aerial robotics applications requiring both maneuverability and efficient high-speed flight.

3. **Duawlfyn: A Drone with Unified Actuation for Wheeled Locomotion and Flight Operation:**

This work presents Duawlfyn, a drone with unified actuation for wheeled locomotion and flight operation that achieves efficient, bidirectional ground mobility. Hybrid aerial-ground vehicles offer significant advantages in terms of operational flexibility, yet existing designs either rely on propeller thrust for ground locomotion that consumes considerable power or require additional actuators that add weight and complexity. This paper presents a new approach: a single-actuation system that reuses standard quadrotor motors for bidirectional ground motion via a passive belt-and-differential drivetrain. By integrating one-way bearings that decouple the propellers during reverse motor operation, the robot avoids prop-based rolling altogether and eliminates

extra wheel motors. We provide a detailed mechanical design, control method, and experimental validation in both flight and ground modes.

Experimental validation confirmed the effectiveness and practicality of our hybrid robot across various scenarios. Flight tests indicated minimal performance trade-offs, with only minor increases in energy consumption compared to a conventional quadrotor in the flight mode. Ground-mode experiments demonstrated impressive efficiency, successfully navigating steep slopes of up to 30° and performing agile turns with lateral accelerations close to $1g$, all while using significantly less energy than flying. The multi-terrain demo showcased the robot's smooth and rapid transitions between aerial and terrestrial modes, underscoring its real-world applicability for urban delivery and indoor navigation tasks.

In addition to the works listed above, I have also co-authored and contributed to two additional works that address other aspects of UAV performance. These studies will not be presented in full detail in this dissertation but are briefly summarized for completeness:

1. **Staging Energy Sources to Extend Flight Time of a Multirotor UAV.**

This work introduces the concept of *staging batteries* to extend flight time by partitioning the total battery mass into discrete segments that are discarded once depleted. By actively removing the dead weight during flight, the vehicle experiences lower overall mass and reduced power consumption. The paper develops a theoretical framework that quantifies the benefits of both discrete and continuous staging and explores the trade-offs inherent in each approach. Experimental validation on a two-stage quadcopter demonstrates an improvement of up to 19% in flight time under a fixed total battery mass budget, highlighting the potential of staging as a practical method for enhancing endurance in UAVs.

2. **Design and Control of a Midair-Reconfigurable Quadcopter using Unactuated Hinges.**

This paper presents a novel reconfigurable quadcopter design in which the vehicle's arms are attached to the central fuselage via unactuated hinges and cables. This configuration allows the quadcopter to passively change its shape midair by reversing the rotors to produce reverse thrusts, without the need for extra actuators. The reconfigurable geometry enables the vehicle to reduce its spatial footprint when navigating confined spaces—such as narrow corridors or windows—while maintaining stability and agility. Experimental results confirm that the design reliably adapts its configuration, thereby enhancing maneuverability and opening up new possibilities for mission-specific reconfiguration.

The materials in this thesis are based on the following papers:

- J. Tang, K. P. Jain and M. W. Mueller, "QUaRTM: A Quadcopter with Unactuated Rotor Tilting Mechanism Capable of Faster, More Agile, and More Efficient Flight". In: *Frontiers in Robotics and AI*, vol. 9, 2022.

- J. Tang and M. W. Mueller, "PairTilt: Design and Control of an Active Tilt-Rotor Quadcopter for Improved Efficiency and Agility". In: *Advanced Intelligent Systems*, Feb. 2025.
- J. Tang, R. Zhang, K. Beyduz, Y. Jiang, C. Wiebe, H. Zhang, O. Asoro, and M. W. Mueller, "Duawlfm: A Drone with Unified Actuation for Wheeled Locomotion and Flight Operation". To be submitted to: *IEEE/ASME Transactions on Mechatronics*
- K. P. Jain, J. Tang, K. Sreenath and M. W. Mueller, "Staging energy sources to extend flight time of a multirotor UAV". In: *2020 IEEE/RSJ International Conference on Intelligent Robots and Systems (IROS)*, 2020, pp. 1132-1139
- N. Bucki, J. Tang and M. W. Mueller, "Design and Control of a Midair-Reconfigurable Quadcopter Using Unactuated Hinges". In: *IEEE Transactions on Robotics*, vol. 39, no. 1, pp. 539-557, Feb. 2023

1.3 Dissertation Outline

Each of the following chapters corresponds to the main contributions listed above:

- **Chapter 2** provides a comprehensive literature survey covering tilt-rotor UAVs, morphing designs, fully actuated systems, and hybrid aerial-ground robots. This chapter situates the contributions of this dissertation in the broader research context.
- **Chapter 3** covers the QUaRTM system, which introduces an unactuated rotor tilting mechanism for enhanced high-speed performance.
- **Chapter 4** discusses the PairTilt design featuring an active tilt-rotor mechanism for improved efficiency and agility.
- **Chapter 5** presents Duawlfm, a dual-modal aerial-ground robot focusing on the unified actuation approach for seamless transitions between flight and ground driving.

1.4 Conclusion

In conclusion, this dissertation synthesizes research demonstrating that innovative mechanical architectures, coupled with tailored control strategies, can significantly broaden the operational capabilities of multirotor UAVs while preserving their fundamental simplicity. QUaRTM employs passive rotor tilting via spring-hinged arms to reduce drag, thereby enhancing maximum speed and cruise efficiency. PairTilt utilizes active paired-rotor tilting with minimal actuation to improve agility and efficiency, effectively decoupling key dynamics without the complexities of fully actuated systems. Duawlfm further extends versatility

through a unified actuation system enabling hybrid aerial-ground locomotion without additional motors. These primary works, alongside related research on battery staging and reconfigurability, highlight viable strategies for creating UAVs with improved speed, maneuverability, endurance, and adaptability for future mission requirements.

Chapter 2

Literature Survey

This chapter provides a comprehensive review of prior work related to multirotor UAV design, with a focus on addressing the challenges of aerodynamic efficiency, agility, and multi-modal operation. The surveyed literature spans both underactuated and fully actuated UAV systems, as well as hybrid aerial-ground robots. These bodies of work lay the foundation for the three systems developed in this dissertation: QUaRTM, PairTilt, and Duawlfm.

2.1 Quadcopters and the Need for Enhanced Efficiency

Quadcopters are among the most widely used UAV platforms due to their mechanical simplicity and vertical takeoff and landing (VTOL) capability [1]. They have found applications in surveillance [2], mapping [3], building inspection, delivery [4], and disaster management [5]. However, conventional quadcopters suffer from limited top speed and poor aerodynamic efficiency during fast flight due to their need to pitch the body forward to generate thrust. This body tilt increases drag area and load on the propellers, leading to higher power consumption and potential stall.

Several efforts have sought to improve endurance and flight efficiency. Wu et al. [6] presented a method for optimizing multicopter speed and sideslip angle. Jain et al. [7] explored endurance extension via battery-swapping docking vehicles, and [8] introduced battery staging to reduce onboard mass. Solar-powered UAVs, such as those studied by Reinhardt et al. [9], also represent promising avenues for long-duration missions.

2.2 Tilt-Rotor Designs for High-Speed Flight

To reduce drag while preserving lift, tilt-rotor architectures allow propellers to reorient toward the flight direction without requiring the main body to pitch. Early designs include the "Quad Tilt Rotor" prototype [10] and its associated flight mode control strategy [11]. Adap-

tive control approaches have also been applied to tilt-rotor vehicles, such as the constrained robust model reference adaptive controller presented in [12].

Some designs allow individual rotor tilting for full-state reachability [13], while others focus on omnidirectional control and wrench exertion in arbitrary directions [14]. These efforts underscore the potential of tilt mechanisms to enhance flight performance while also introducing challenges in mechanical complexity, control, and actuator requirements.

2.3 Innovations in Underactuated Tilt-Rotor UAVs

Recent studies have pushed the boundary of what is achievable within underactuated UAV designs. Panigrahi et al. [15] developed a hybrid VTOL system balancing rotorcraft and fixed-wing capabilities using thrust vectoring. Papachristos et al. [16] presented a quad-tiltrotor with predictive control for autonomous mode switching. Mikami and Uchiyama [17] applied dynamic inversion to ensure stability during tilt transitions.

More recent work explored morphing and tilting strategies that emphasize structural simplicity. Sakaguchi et al. [18] used a parallel link frame for tilting in a quadcopter. Mousaei et al. [19] incorporated actuator redundancy to maintain control in failure scenarios. Bucki et al. [20] and Falanga et al. [21] demonstrated morphing quadrotors capable of navigating narrow environments and adapting shape midair.

2.4 Fully Actuated UAV Platforms

Fully actuated systems expand control authority beyond the limitations of underactuated vehicles. Ryll et al. [22, 23] introduced quadrotors with independently tilting rotors to enable full six degrees of freedom (6DOF) control. The Voliro platform [24] and ODAR [25] offer omni-directional capabilities, enabling complex maneuvers such as vertical surface inspection and lateral disturbance rejection. Advanced configurations such as OmniMorph [26] and an eight-rotor NMPC-controlled UAV [27] further demonstrate the potential of these systems to achieve full pose tracking and robust agility, albeit with increased mechanical complexity. Control-focused work such as Li et al. [28] addressed servo dynamics within overactuated NMPC frameworks.

2.5 Hybrid Aerial-Ground Mobility

Multi-modal UAVs seek to extend operational efficiency by enabling terrestrial locomotion. However, integrating ground mobility usually requires additional actuators or repurposing of aerial propulsion systems—each with its own trade-offs.

2.5.1 Propeller-Based Ground Propulsion

Some hybrid vehicles use redirected or angled thrust for rolling. Page and Pounds [29] developed the Quadroller with low-friction wheels, while Sabet et al. [30] proposed Rollocopter, a spherical-shell UAV capable of terrain traversal. Premachandra et al. [31] retrofitted propellers for ground motion, and Sugihara et al. [32] demonstrated Delta, a deformable multi-rotor. Other designs like Skywalker [33], Zhang et al. [34], Lin et al. [35], and Qin et al. [36] explored passive or omnidirectional wheels combined with model predictive control. While mechanically simple, these systems often suffer from high power demand, safety concerns, and overheating due to continuous propeller use near the ground [37].

2.5.2 Dedicated Actuators for Ground Locomotion

Other hybrid designs opt for dedicated actuators for ground movement. Kalantari et al. [38] used spherical wheels on the Drivocopter. Morton and Papanikolopoulos [39] designed a transforming compact hybrid. Robotic platforms like SPIDAR [40], FlyHuman [41], MT-MUR [42], and M4 [43] demonstrate complex integration of aerial, wheeled, and legged locomotion, but at the cost of increased weight and system complexity.

2.6 Summary

The literature highlights an active research landscape focused on expanding UAV functionality across speed, agility, and operational modalities. The surveyed works span a spectrum from lightweight underactuated solutions to fully actuated, morphing, and multi-modal systems. The three UAV systems introduced in this dissertation—QUaRTM, PairTilt, and Duawlfín—seek to bridge critical gaps in this landscape. They contribute by offering new design paradigms that either minimize actuation (e.g., QUaRTM and Duawlfín) or strategically balance actuation and performance (e.g., PairTilt), enabling more efficient, agile, and versatile UAVs.

Chapter 3

QUaRTM: A Quadcopter with Unactuated Rotor Tilting Mechanism

We present QUaRTM – a novel quadcopter design capable of tilting the propellers into the forward flight direction, which reduces the drag area and therefore allows for faster, more agile, and more efficient flight. The vehicle can morph between two configurations in mid-air, including the untilted configuration and the tilted configuration. The vehicle in the untilted configuration has a higher pitch torque capacity and a smaller vertical dimension. The vehicle in the tilted configuration has a lower drag area, leading to a higher top speed, higher agility at high speed, and better flight efficiency. The morphing is accomplished without any additional actuators beyond the four motors of a quadcopter. The rigid connections between the quadcopter frame and the quadcopter arms are replaced with sprung hinges. This allows the propellers to be tilted when high thrusts are produced, and recover to the untilted configuration when the thrusts are brought low. The effectiveness of such a vehicle is demonstrated by running experiments on a prototype vehicle with a shape similar to a regular quadcopter. Through the use of tilting, the vehicle is shown to have a 12.5% higher maximum speed, better high-speed agility as the maximum crash-free cruise speed increased by 7.5%, and a better flight efficiency as the power consumption has dropped by more than 20% in the speed range of 15-20m s⁻¹.

The material in this chapter is based on the following work:

- J. Tang, K. P. Jain and M. W. Mueller, "QUaRTM: A Quadcopter with Unactuated Rotor Tilting Mechanism Capable of Faster, More Agile, and More Efficient Flight". In: *Frontiers in Robotics and AI*, vol. 9, 2022.

3.1 Introduction

Over the past decade, UAVs have become increasingly popular. One of the most common UAV designs is the quadcopter which is a multirotor device driven by four independently controlled propellers. The simplicity and agility of quadcopters as explained in [1] have

made them one of the preferred choices for a variety of applications, such as surveillance [2], mapping [3], building inspection, photography, delivery [4], and disaster management [5]. Nevertheless, conventional quadcopters are usually not able to achieve a high top speed, nor are they able to fly efficiently at a high speed. This is related to the fact that a quadcopter has to tilt its body toward the forward flight direction to counter the drag. However, tilting the quadcopter body means that a larger area is now subject to air resistance, which in turn increases the burden on the propellers. In addition to limiting the top speed, this also reduces the flight efficiency and might cause the quadcopter to stall. For tasks such as search and rescue and rapid package delivery that are both time and cost sensitive, and still require the vehicle to have high agility and vertical take-off capacity, we see a demand for a quadcopter platform that is capable of efficient high-speed flight [44, 45].

Some work has been done on increasing the flight efficiency and endurance of quadcopters. A method for finding the optimal speed and sideslip angle of a multicopter was presented in [6]. An approach to extending endurance and range by docking secondary quadcopters carrying replacement batteries is shown in [7]. An increase in flight time by using the battery in multiple stages has been demonstrated in [8]. Solar-powered UAVs, which can potentially fly large distances, have been explored in [9].

Since the limit on the top speed of a conventional quadcopter often has to do with its inherent aerodynamic properties, a more fundamental design change is often required to improve the efficiency and flight speed. A common design that can achieve the said goals is the tilt-rotor design. A tilt-rotor allows the propellers to be tilted toward the flight direction without the need for tilting the main body, thereby reducing the area subject to wind. Several tilt-rotor quadcopter designs have been explored. A convertible prototype "Quad Tilt Rotor" capable of vertical takeoffs like a quadcopter, and high-speed flight like a fixed-wing UAV was presented in [10]. A control scheme to handle the flight mode conversion from a helicopter to a fixed-wing "Quad-TiltRotors" was presented in [11]. A constrained robust model reference adaptive controller of an H-shaped tilt-rotor was presented in [12]. In addition to fusing a fixed-wing and a conventional quadcopter to enable the vehicle to travel at a high speed, several other tilt rotors designs have been explored. A tilt-rotor quadcopter capable of achieving any arbitrary desired state or configuration by tilting each rotor independently was presented in [13]. The design and optimal control of an omnidirectional micro aerial vehicle capable of exerting a wrench in any orientation while maintaining efficient flight configurations were presented in [14].

We propose a novel tilt-rotor vehicle design – a quadcopter with an unactuated rotor tilting mechanism (QUaRTM), capable of tilting the propellers into the forward flight direction without the use of any actuators beyond the four quadcopter motors. QUaRTM has two configurations: the untilted configuration with all propeller planes parallel to the central body, and the tilted configuration with all rotors tilted into the forward flight direction by an angle of 20 degrees. A photo of QUaRTM hovering in both configurations is shown in Figure 3.1. In contrast to a conventional quadcopter, the rigid connections between the quadcopter arms and the central body are replaced with hinges. This allows the propellers to tilt into the forward flight direction without having to tilt the central body. Springs are

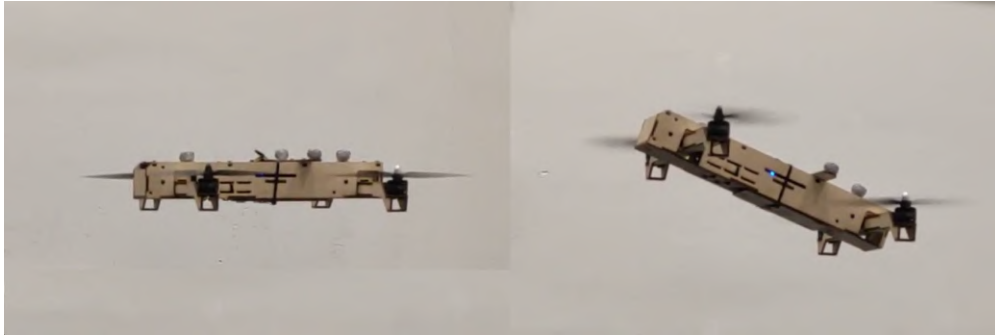


Figure 3.1: The experimental vehicle hovering in the untilted (left) and tilted (right) configurations.

added at the hinges to pull the arms into the untilted configuration. When the net propeller thrust is high enough to overcome the torque from the springs, the vehicle will transition into the tilted configuration. Then from the tilted configuration, when the net propeller thrust drops below a threshold, the arms will untilt and restore the vehicle to the untilted configuration. The spring torque acting on the arm is high in the untilted configuration and low in the tilted configuration. This creates a mechanical hysteresis that 1. prevents oscillations in the tilting behavior, 2. avoids unintended tilting or untilting, and 3. allows the propellers to produce a wider range of thrusts in both configurations. Figure 3.2 shows the internal architecture of the tilting mechanism.

QUARTM thus combines both the advantages of flying in the untilted configuration and flying in the tilted configuration with some trade-offs. When flying in the untilted configuration, the offset between the front and rear rotors' thrust axes is the largest, resulting in the highest pitch torque capacity at lower speed. In addition, since the propellers' plane is parallel to the quadcopter frame's top plane, the vertical dimension of the vehicle is small, which makes it theoretically possible for the vehicle to fly through narrower gaps. When flying in the tilted configuration, since the central body is not tilted toward the forward flight direction, the drag reflected on the vehicle is low. This allows the vehicle to achieve a higher top speed and a higher energy efficiency. In addition, the reduction in drag allows a greater portion of the vehicle's thrust capacity to be used for maneuvering instead of merely countering drag. This improves the high-speed agility of the vehicle. On the other hand, this vehicle has a slightly reduced range of thrust and torques. This is because to prevent unintended tilting and untilting, additional thrust constraints on the propellers need to be imposed. In addition, there is a slight increase in the mass and mechanical complexity of the vehicle due to the addition of the tilting mechanism.

Therefore, we argue that the proposed design is advantageous to existing solutions where the quadcopter is primarily expected to take off and land vertically, and fly at a high speed with high agility. Such applications are common when the targets are time-sensitive, e.g.

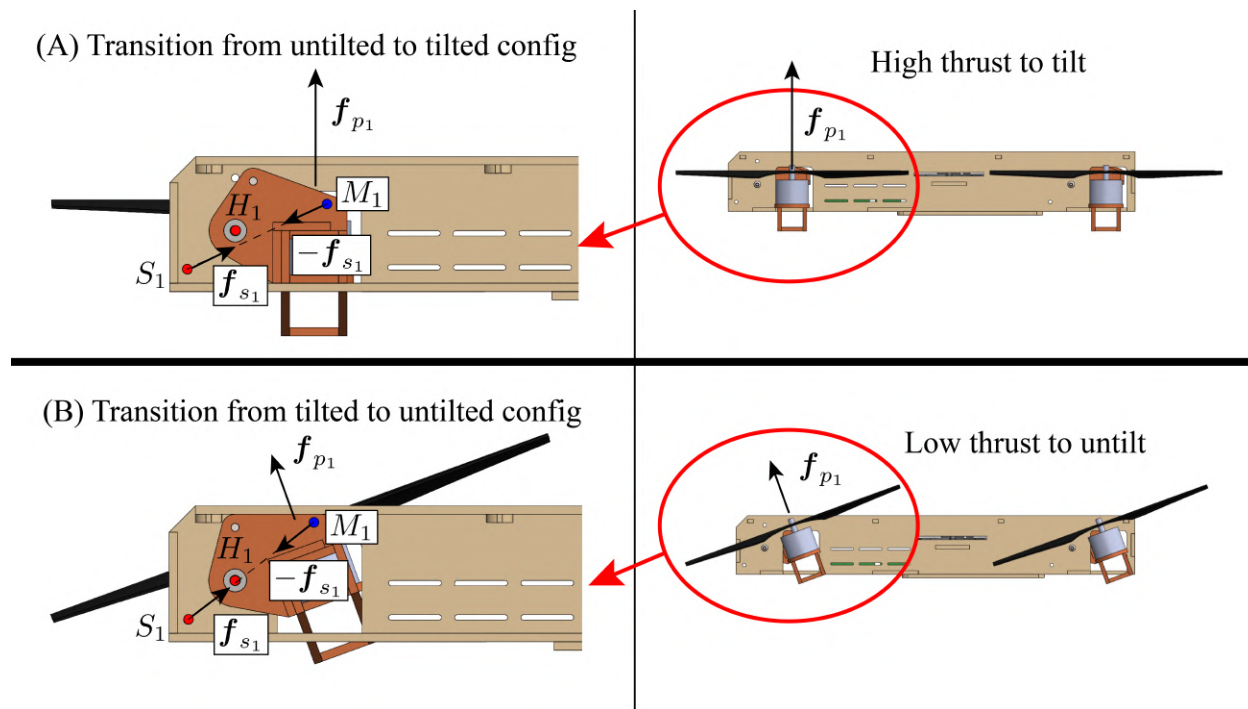


Figure 3.2: The vehicle viewing from the left side and the internal tilting mechanism for the front-right arm. (A) shows the vehicle in the untilted configuration, and (B) shows the vehicle in the tilted configuration. The fuselage is shown in beige. The arm shown in red orange is allowed to rotate around hinge H_1 . A spring is attached between point S_1 on the quadcopter central body and M_1 on the arm. The spring produces a torque on the arm around hinge H_1 that tries to keep the arm in the untilted configuration. The tensions in the spring are very close for the two configurations because the amount of extension is nearly identical. However, in the untilted configuration (A), the distance from hinge H_1 to line S_1M_1 is large, leading to a large moment arm and a large torque produced by the spring. Thus the arm will only tilt when a very high thrust is produced, allowing the vehicle in the untilted configuration to operate at a high maximum thrust. Once the spring torque is overcome by producing a high thrust, the arm will tilt and the vehicle will transition to the tilted configuration (B). The torque exerted by the spring will reduce because the moment arm has reduced. This ensures that the arm will not untilt so easily, allowing the vehicle in the tilted configuration to operate at a low minimum thrust.

long-distance package delivery, drone racing, search and rescue. This chapter will discuss the dynamics of the QUaRTM, the principles that govern the design of the vehicle, the experimental vehicle and its controller, and the experiments conducted to validate the design and its capabilities, including 1. the mid-air tilting and untilting transitions, 2. the improvements on the maximum vehicle speed and high-speed agility, and 3. the improvements on

flight efficiency when the vehicle travels at a high speed.

3.2 System Overview

In this section, we will provide an overview of the system. We will define the model of the vehicle and derive its dynamics. This will help us to 1. find the constraints on the propeller thrusts to prevent unintended tilting and untilting, and 2. design for the vehicle frame and the tilt angle.

3.2.1 Notation

We follow the notations in [46] for defining the model of the vehicle. Non-bold symbols like m represent scalars, lowercase bold symbols like \mathbf{g} represent vectors, and uppercase bold symbols like \mathbf{J} represent matrices. Subscripts such as m_C represent the body to which the symbol refers, and superscripts such as \mathbf{g}^E represent the frame in which the vector is expressed. A second subscript or superscript such as $\boldsymbol{\omega}_{CE}$ or \mathbf{R}^{CE} represents what the quantity is defined with respect to. However, the special superscript T represents the transpose of a matrix. To express a cross product, we use the skew-symmetric matrix form such that $\mathbf{a} \times \mathbf{b} = \mathbf{S}(\mathbf{a})\mathbf{b}$. The symbol \mathbf{d} represents a displacement, $\boldsymbol{\omega}$ represents an angular velocity, and \mathbf{R} represents a rotational matrix.

3.2.2 Model

First of all, we define a model of the vehicle which we will use for analysis. Figure 3.3 shows the quadcopter model as seen from the top. We model the system as 5 coupled rigid bodies, including the central body of the quadcopter and the 4 quadcopter arms with the rotors mounted. We denote the Earth frame as E , the central body frame as C , and the frame for each arm as A_i for $i \in \{1, 2, 3, 4\}$. The origin of any frame is defined to be at the center of mass of the corresponding body. For the central body frame, the x-axis \mathbf{x}_C points to the front of the vehicle, and the z-axis \mathbf{z}_C points upward from the body's top surface. The rotation matrix of central body frame C with respect to the Earth frame E is defined as \mathbf{R}^{CE} . For a vector expressed in the Earth frame \mathbf{v}^E , $\mathbf{v}^C = \mathbf{R}^{CE}\mathbf{v}^E$ represents its expression in the central body frame.

Each arm is allowed to tilt with respect to the central body frame C around the \mathbf{y}_C direction, and the fully tilted tilt angle is defined as β . Throughout this chapter, we will assume that all arms tilt at the same angle. We also define the combined arm frame A which has axes aligned with any arm i , and its origin located at the center of mass of the whole vehicle. When an arm is not tilted, all 3 axes point in the same directions as those of the central body frame, that $\mathbf{x}_C = \mathbf{x}_{A_i}$, $\mathbf{y}_C = \mathbf{y}_{A_i}$, $\mathbf{z}_C = \mathbf{z}_{A_i}$. Since tilting only happens in the $\mathbf{y}_C = \mathbf{y}_{A_i}$ direction, only \mathbf{z}_{A_i} and \mathbf{x}_{A_i} will change when the arm tilts. The rotation matrix

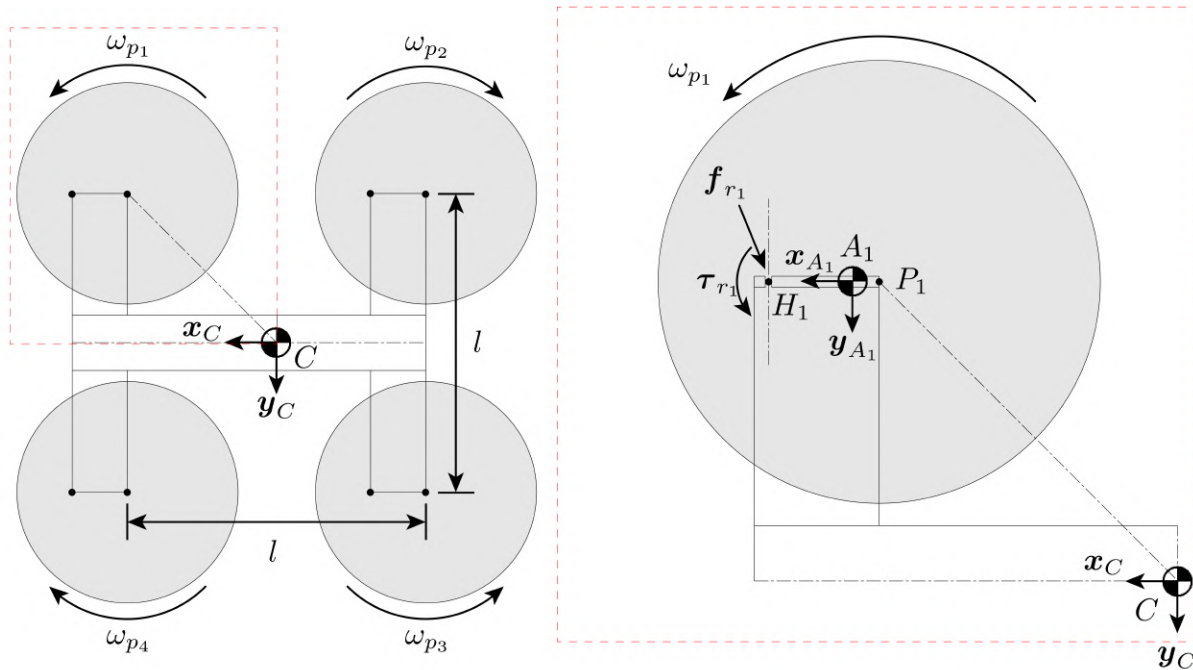


Figure 3.3: Top-down view of the vehicle model in the untilted configuration. The propellers are numbered 1, 2, 3, 4 in a clockwise manner. The right side shows the detailed view of rotor 1, where P_1 is the location of the rotor, A_1 is the COM of the arm that the rotor is attached to, and H_1 is the hinge that the arm can tilt about. Reaction force \mathbf{f}_{r_1} and torque τ_{r_1} act in opposite directions between each arm and the central body at the hinge H_1 .

of an arm with respect to the central body is thus a single degree of freedom rotation matrix defined as \mathbf{R}^{A_iC} .

Figure 3.4 shows forces and torques acting on arm 1. Note that while the figure shows only arm 1, the model can be generalized to all arms. To control the thrust at which the arm will tilt or untilt, a spring producing a force \mathbf{f}_{s_i} is connected between point S_i on the central body and point M_i on arm i . Note that spring is not the only option here but rather a design choice. Other widgets like magnets can be also used to produce such force. In addition to the spring force and the total acceleration force, arm i also sees the propeller force and torque ($\mathbf{f}_{p_i} = f_{p_i}\mathbf{z}_{p_i}$, $\tau_{p_i} = \tau_{p_i}\mathbf{z}_{p_i}$), and the hinge's reaction force and torque ($-\mathbf{f}_{r_i}$, $-\tau_{r_i}$). The mass and moment of inertia of the central body at its center of mass are denoted as m_C and \mathbf{J}_C respectively. Similarly, the mass and moment of inertia of any arm i at its center of mass are denoted as m_A and \mathbf{J}_A .

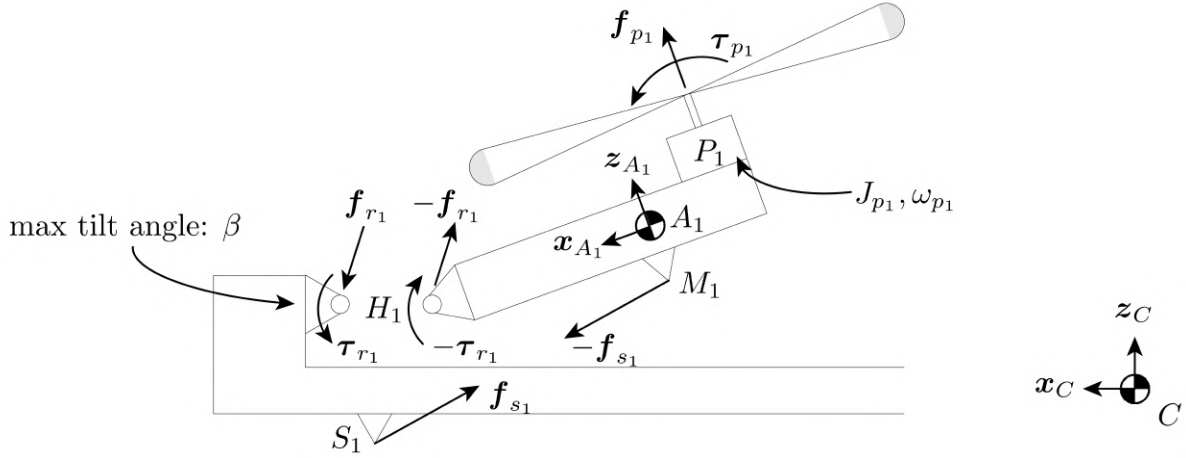


Figure 3.4: Free-body diagram showing the forces acting on arm 1 viewing from the left side. The length of the arm is exaggerated. A spring is attached between point S_1 on the quadcopter central body and M_1 on the arm. The spring exerts a torque that tries to keep the arm in the untilted configuration. The propeller produces a thrust force \mathbf{f}_{p_i} and a torque τ_{p_i} in the z_{A_1} direction. The momentum of inertia of the rotor around its axis is J_{p_1} , and the rotor rotates at a speed of ω_{p_1} .

3.2.3 Aerodynamics

Now, we model the aerodynamics of the vehicle. We will use these results to design for the tilt angle in Section 3.3. We express the aerodynamics of the quadcopter in the Earth frame E . Assuming that the quadcopter is cruising in the \mathbf{x}_E direction at a fixed height, the drag and lift forces are:

$$\mathbf{f}_D = -\frac{1}{2}C_D(\alpha)\rho Av^2\mathbf{x}_E \quad (3.1)$$

$$\mathbf{f}_L = \frac{1}{2}C_L(\alpha)\rho Av^2\mathbf{z}_E \quad (3.2)$$

Where α is the angle of attack, $C_D(\alpha)$ and $C_L(\alpha)$ are the angle-of-attack-dependent drag and lift coefficients, ρ is the density of air, v is the speed of the quadcopter, and A is the reference area which is the projection area of the vehicle onto its top surface. Figure 3.5 shows the breakdown of forces on the quadcopter when it is cruising. The force balance of the quadcopter can be expressed as:

$$f_\Sigma \sin(-\alpha + \beta) = \frac{1}{2}C_D(\alpha)\rho Av^2 \quad (3.3)$$

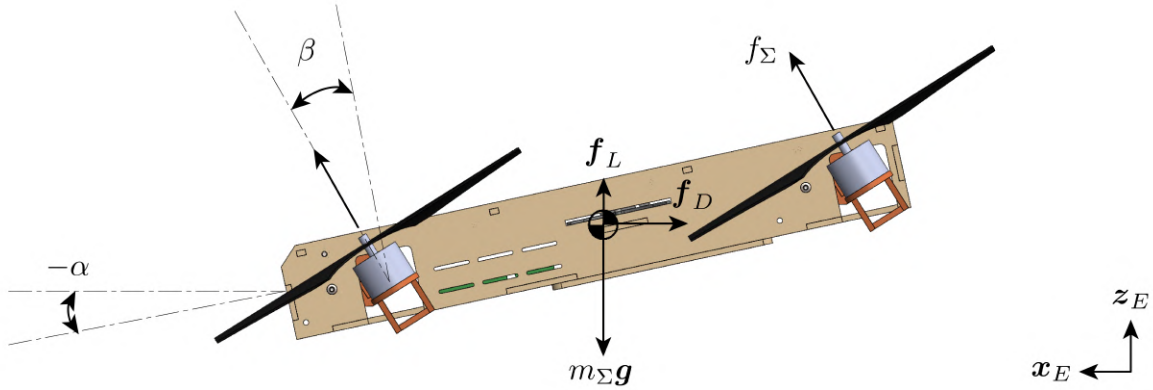


Figure 3.5: Free-body diagram of the vehicle when cruising. The tilt angle β is the angle between the arm and the central body, and the angle of attack α is the angle between the central body and the horizon.

$$f_{\Sigma} \cos(-\alpha + \beta) = m_{\Sigma}g - \frac{1}{2}C_L(\alpha)\rho Av^2 \quad (3.4)$$

Where $f_{\Sigma} := \sum_{i=1}^4 f_{p_i}$ is the total thrust from all 4 propellers, m_{Σ} is the total mass of the vehicle, and g is the gravitational acceleration. We will use the results here to design for the tilt angle in Section 3.3.

3.2.4 Rigid body dynamics

We derive the rigid body dynamics of the vehicle, especially those governing the tilting of the arms. We will use these results in Section 3.1 to design for the vehicle configuration, and in Section 4.1 to compute the bounds on the control to ensure that mid-air morphing happens in a controlled manner. Since tilting and untilting usually happen during the early and late stages of flight where the speed is low, we will not consider aerodynamic forces here. The translational and rotational dynamics of the vehicle can be computed using Newton's and Euler's laws of motion [47]. The translational dynamics of the central body expressed in the Earth frame E , and the rotational dynamics of the central body expressed in the central body frame C are:

$$m_C \ddot{\mathbf{d}}_{CE}^E = m_C \mathbf{g}^E + \mathbf{R}^{EC} \sum_{i=1}^4 (\mathbf{f}_{r_i}^C + \mathbf{f}_{s_i}^C) \quad (3.5)$$

$$\mathbf{J}_C^C \dot{\boldsymbol{\omega}}_{CE}^C + \mathbf{S}(\boldsymbol{\omega}_{CE}^C) \mathbf{J}_C^C \boldsymbol{\omega}_{CE}^C = \sum_{i=1}^4 (\boldsymbol{\tau}_{r_i}^C + \mathbf{S}(\mathbf{d}_{H_iC}^C) \mathbf{f}_{r_i}^C + \mathbf{S}(\mathbf{d}_{CS_i}^C) \mathbf{f}_{s_i}^C) \quad (3.6)$$

The translational and rotational dynamics of arm i expressed both in the corresponding arm frame are:

$$\begin{aligned} m_{A_i} \mathbf{R}^{A_iE} \ddot{\mathbf{d}}_{CE}^E &= -m_{A_i} \mathbf{R}^{A_iC} (\mathbf{S}(\mathbf{d}_{CH_i}^C) \dot{\boldsymbol{\omega}}_{CE}^C + \mathbf{S}(\boldsymbol{\omega}_{CE}^C) \mathbf{d}_{CH_i}^C \boldsymbol{\omega}_{CE}^C) \\ &\quad - m_{A_i} (\mathbf{S}(\mathbf{d}_{H_iA_i}^{A_i}) \dot{\boldsymbol{\omega}}_{A_iE}^{A_i} + \mathbf{S}(\boldsymbol{\omega}_{A_iE}^{A_i}) \mathbf{S}(\mathbf{d}_{H_iA_i}^{A_i}) \boldsymbol{\omega}_{A_iE}^{A_i}) \\ &\quad + \mathbf{z}_{A_i}^{A_i} f_{p_i} - \mathbf{f}_{r_i}^{A_i} - \mathbf{f}_{s_i}^{A_i} + m_{A_i} \mathbf{R}^{A_iE} \mathbf{g}^E \end{aligned} \quad (3.7)$$

$$\begin{aligned} \mathbf{J}_{A_i}^{A_i} \dot{\boldsymbol{\omega}}_{A_iE}^{A_i} + \mathbf{S}(\boldsymbol{\omega}_{A_iE}^{A_i}) \mathbf{J}_{A_i}^{A_i} \boldsymbol{\omega}_{A_iE}^{A_i} &= \mathbf{S}(\mathbf{d}_{P_iA_i}^{A_i}) \mathbf{z}_{A_i}^{A_i} f_{p_i} + \mathbf{z}_{A_i}^{A_i} \boldsymbol{\tau}_{p_i} - \boldsymbol{\tau}_{r_i}^{A_i} - \mathbf{S}(\mathbf{d}_{H_iA_i}^{A_i}) \mathbf{f}_{r_i}^{A_i} \\ &\quad - \mathbf{S}(\mathbf{d}_{M_iA_i}^{A_i}) \mathbf{f}_{s_i}^{A_i} - J_{p_i} \mathbf{S}(\boldsymbol{\omega}_{A_iE}^{A_i}) \omega_{p_i} \mathbf{z}_{A_i}^{A_i} \end{aligned} \quad (3.8)$$

Where J_{p_i} is the moment of inertia of the rotor, ω_{p_i} is the rotational speed of the propeller, and the last term $J_{p_i} \mathbf{S}(\boldsymbol{\omega}_{A_iE}^{A_i}) \omega_{p_i} \mathbf{z}_{A_i}^{A_i}$ indicates the gyroscopic torque produced by rotating the spinning rotor.

Now we consider the dynamics of the whole quadcopter. Its translational dynamics in the Earth frame E and rotational dynamics in the central body frame C are:

$$m_{\Sigma} \ddot{\mathbf{d}}_{CE}^E = m_{\Sigma} \mathbf{g}^E + \mathbf{R}^{EC} \mathbf{z}_{A_i}^C \sum_{i=1}^4 f_{p_i} = m_{\Sigma} \mathbf{g}^E + \mathbf{R}^{EC} \mathbf{z}_{A_i}^C f_{\Sigma} \quad (3.9)$$

$$\mathbf{J}_{\Sigma}^C \dot{\boldsymbol{\omega}}_{CE}^C + \mathbf{S}(\boldsymbol{\omega}_{CE}^C) \mathbf{J}_{\Sigma}^C \boldsymbol{\omega}_{CE}^C = \sum_{i=1}^4 \mathbf{S}(\mathbf{d}_{P_iC}^C) \mathbf{z}_{A_i}^C f_{p_i} + \mathbf{z}_{A_i}^C \boldsymbol{\tau}_{p_i} = \boldsymbol{\tau}_{\Sigma}^C \quad (3.10)$$

Where \mathbf{J}_{Σ} is the moment of inertia of the whole quadcopter, and $\boldsymbol{\tau}_{\Sigma}$ is the net torque produced by the 4 propellers on the quadcopter. We can use these equations to compute the linear and angular accelerations of the quadcopter:

$$\ddot{\mathbf{d}}_{CE}^E = \mathbf{g}^E + \frac{1}{m_{\Sigma}} \mathbf{R}^{EC} \mathbf{z}_{A_i}^C f_{\Sigma} \quad (3.11)$$

$$\dot{\boldsymbol{\omega}}_{CE}^C = \mathbf{J}_{\Sigma}^{C-1} \boldsymbol{\tau}_{\Sigma}^C - \mathbf{S}(\boldsymbol{\omega}_{CE}^C) \mathbf{J}_{\Sigma} \boldsymbol{\omega}_{CE}^C \quad (3.12)$$

Finally, plugging these equations back into the dynamics of the arm, we can find the reaction force $\mathbf{f}_{r_i}^{A_i}$ and torque $\boldsymbol{\tau}_{r_i}^{A_i}$ acting at the hinge:

$$\begin{aligned} \mathbf{f}_{r_i}^{A_i} &= m_A \left(\mathbf{R}^{A_iE} \left(\mathbf{g}^E - \ddot{\mathbf{d}}_{CE}^E \right) - \mathbf{S}(\mathbf{d}_{CA_i}^{A_i}) \mathbf{R}^{A_iC} \dot{\boldsymbol{\omega}}_{CE}^C \right. \\ &\quad \left. + \mathbf{R}^{A_iC} \left(\mathbf{S}(\boldsymbol{\omega}_{CE}^C) \mathbf{S}(\mathbf{d}_{CH_i}^C) \boldsymbol{\omega}_{CE}^C + \mathbf{S}(\boldsymbol{\omega}_{A_iE}^C) \mathbf{S}(\mathbf{d}_{H_iA_i}^C) \boldsymbol{\omega}_{A_iE}^C \right) \right) + \mathbf{z}_{A_i}^{A_i} f_{p_i} - \mathbf{f}_{s_i}^{A_i} \end{aligned} \quad (3.13)$$

$$\begin{aligned}
 \boldsymbol{\tau}_{r_i}^{A_i} = & \mathbf{R}^{A_i C} \boldsymbol{\tau}_{p_i}^C - \mathbf{S}(\mathbf{d}_{M_i A_i}^{A_i}) \mathbf{f}_{s_i}^{A_i} - \mathbf{S}(\mathbf{d}_{H_i A_i}^{A_i}) \mathbf{f}_{r_i}^{A_i} - \mathbf{J}_{A_i}^{A_i} \mathbf{R}^{A_i C} \dot{\boldsymbol{\omega}}_{CE}^C \\
 & - \mathbf{R}^{A_i C} \mathbf{S}(\boldsymbol{\omega}_{A_i E}^C) (\mathbf{R}^{A_i C})^T \mathbf{J}_{A_i}^{A_i} \mathbf{R}^{A_i C} \boldsymbol{\omega}_{A_i E}^C + J_{p_i} \mathbf{S}(\boldsymbol{\omega}_{A_i E}^{A_i}) \omega_{p_i} \mathbf{z}_{A_i}^{A_i}
 \end{aligned} \tag{3.14}$$

We note that for the arm to remain untilted, the hinge should only apply a negative reaction torque on the arm. Similarly, for the arm to remain tilted, the hinge should only apply a positive reaction torque on the arm. In math form, $\mathbf{y}_{A_i}^{A_i} \cdot \boldsymbol{\tau}_{r_i}^{A_i} \leq 0$ if the arm is to remain untilted, and $\mathbf{y}_{A_i}^{A_i} \cdot \boldsymbol{\tau}_{r_i}^{A_i} \geq 0$ if the arm is to remain tilted. We note that this constraint only holds when the arms tilt independently. However, the tilting of the arms could be coupled mechanically to relax the bounds. There are three arm coupling configurations. The first is the non-coupled configuration, where each arm tilts separately from one another. The second is the side-coupled configuration, where the two arms at the front are coupled and the two arms at the back are coupled, or the two arms on the left are coupled and the two arms on the right are coupled. The third is the all-coupled configuration, where all four arms are coupled to rotate together. The thrust bounds thus become:

$$\text{Non-coupled : } \mathbf{y}_{A_i}^{A_i} \cdot \boldsymbol{\tau}_{r_i}^{A_i} \leq 0, \text{ for } i \in \{1, 2, 3, 4\} \tag{3.15}$$

$$\text{Side-coupled : } \begin{cases} \mathbf{y}_{A_1}^{A_1} \cdot \boldsymbol{\tau}_{r_1}^{A_1} + \mathbf{y}_{A_4}^{A_4} \cdot \boldsymbol{\tau}_{r_4}^{A_4} \leq 0 \\ \mathbf{y}_{A_2}^{A_2} \cdot \boldsymbol{\tau}_{r_2}^{A_2} + \mathbf{y}_{A_3}^{A_3} \cdot \boldsymbol{\tau}_{r_3}^{A_3} \leq 0 \end{cases}, \text{ or } \begin{cases} \mathbf{y}_{A_1}^{A_1} \cdot \boldsymbol{\tau}_{r_1}^{A_1} + \mathbf{y}_{A_2}^{A_2} \cdot \boldsymbol{\tau}_{r_2}^{A_2} \leq 0 \\ \mathbf{y}_{A_3}^{A_3} \cdot \boldsymbol{\tau}_{r_3}^{A_3} + \mathbf{y}_{A_4}^{A_4} \cdot \boldsymbol{\tau}_{r_4}^{A_4} \leq 0 \end{cases} \tag{3.16}$$

$$\text{All-coupled : } \sum_{i=1}^4 \mathbf{y}_{A_i}^{A_i} \cdot \boldsymbol{\tau}_{r_i}^{A_i} \leq 0 \tag{3.17}$$

We will use the results here to evaluate the vehicle agility and choose the arm-coupling configuration in Section 3.1 and Section 3.2, and compute the bounds on the control inputs to ensure that mid-air morphing happens in a controlled manner in Section 4.1.

3.3 Design

In this section, we will discuss the design of the quadcopter. The key design parameters are the arm coupling configuration and the tilt angle. The arm coupling configuration affects vehicle agility. The tilt angle mainly affects the drag force, flight speed, and high-speed agility. We design our vehicle by first choosing an arm coupling configuration and designing an overall vehicle frame. Then, we will use the parameters of the vehicle frame to analyze the impact of the tilt angle on the vehicle performance and decide on the tilt angle.

3.3.1 Arm-coupling configuration and agility

For a conventional quadcopter, the only limits on the vehicle agility are the maximum and minimum thrusts and torques that a propeller can produce ($f_{min}, f_{max}, \tau_{min}, \tau_{max}$). For our vehicle, however, we need to impose additional bounds on the propeller thrusts to prevent

the arms from tilting and untilting when not commanded to. These bounds are governed by the spring forces \mathbf{f}_{s_i} and some other dynamics effects as shown in Section 2.4.

To get a more intuitive understanding of how these bounds affect the agility of the vehicle and what we can do about it, let us consider a simplified case where the quadcopter is initially hovering in the untilted configuration, the angular acceleration is small, and the angular speed is small. $\mathbf{R}^{A_i C}$ thus becomes identity, and all terms of vehicle angular acceleration and quadratic terms of vehicle angular velocity drop out. The reaction torque in the $\mathbf{y}_{A_i}^{A_i}$ direction from Equation 3.14 thus simplifies to:

$$\begin{aligned} \mathbf{y}_{A_i}^{A_i} \cdot \boldsymbol{\tau}_{r_i}^{A_i} &= -\mathbf{y}_{A_i}^{A_i} \cdot (\mathbf{S}(\mathbf{d}_{M_i A_i}^{A_i}) + \mathbf{S}(\mathbf{d}_{A_i H_i}^{A_i})) \mathbf{f}_{s_i}^{A_i} + d_{H_i A_i, x}^{A_i} \left(-m_A \frac{f_\Sigma}{m_\Sigma} + f_{p_i} \right) \\ &\quad + \mathbf{y}_{A_i}^{A_i} \cdot (J_{p_i} \mathbf{S}(\boldsymbol{\omega}_{A_i E}^{A_i}) \boldsymbol{\omega}_{p_i} \mathbf{z}_{A_i}^{A_i}) \end{aligned} \quad (3.18)$$

$$= d_{M_i H_i, x}^{A_i} f_{s_i, z}^{A_i} + d_{H_i A_i, x}^{A_i} \left(-m_A \frac{f_\Sigma}{m_\Sigma} + f_{p_i} \right) - J_{p_i} \boldsymbol{\omega}_{A_i E, x}^{A_i} \boldsymbol{\omega}_{p_i} \quad (3.19)$$

Where $d_{M_i H_i, x}^{A_i} f_{s_i, z}^{A_i}$ represents the torque that the spring applies on the arm in the $\mathbf{y}_{A_i}^{A_i}$ direction around the hinge, $d_{H_i A_i, x}^{A_i} \left(-m_A \frac{f_\Sigma}{m_\Sigma} + f_{p_i} \right)$ represents the net torque from the thrust of the propeller and the inertial force from accelerating the arm around the hinge, and $J_{p_i} \boldsymbol{\omega}_{A_i E, x}^{A_i} \boldsymbol{\omega}_{p_i}$ represents the gyroscopic torque from the rotor. The propeller thrust just enough to tilt the arm is thus:

$$f_{p_i, tilt} = m_A \frac{f_\Sigma}{m_\Sigma} - \frac{d_{M_i H_i, x}^{A_i}}{d_{H_i A_i, x}^{A_i}} f_{s_i, z}^{A_i} + \frac{J_{p_i} \boldsymbol{\omega}_{A_i E, x}^{A_i} \boldsymbol{\omega}_{p_i}}{d_{H_i A_i, x}^{A_i}} \quad (3.20)$$

The tilting behavior is thus determined by not only the spring-related parameters which the designer can decide, but also the roll motion of the vehicle due to the gyroscopic torque $J_{p_i} \boldsymbol{\omega}_{A_i E, x}^{A_i} \boldsymbol{\omega}_{p_i}$. It turns out that the gyroscopic torque has a major negative impact on the agility of the vehicle. This is because the momentum of the rotor $J_{p_i} \boldsymbol{\omega}_{p_i}$ is usually quite large due to the high rotational speed of the rotor, and its product with the roll speed of the quadcopter which gives the gyroscopic torque could easily exceed the torque from the spring that is holding the arm in place, which can result in unintended tilting and untilting. To reduce the impact of the gyroscopic torque on the tilting behavior, we will have to couple the rotations of two adjacent arms, and force them to tilt together. Since every two adjacent propellers spin in opposite directions, the net angular momentum will cancel out if the speeds are close, and will significantly reduce the gyroscopic torque reflected on the arms. The uncoupled configuration of Equation 3.15 is thus not physically meaningful for most vehicles, and coupling the arms is always required. Near hover, because all rotors have similar speeds, coupling the arms essentially makes the gyroscopic torque drop out from the force balance, which will then further simplify the thrust to tilt the arm to:

$$f_{p_i,tilt} = m_A \frac{4f_{p_i,tilt}}{m_\Sigma} - \frac{d_{M_i H_i, x}^{A_i}}{d_{H_i A_i, x}^{A_i}} f_{s_i, z}^{A_i} \quad (3.21)$$

The tilt thrust is now only related to the mechanical properties of the vehicle, and is thus a design parameter that we can choose. The same applies to the untilt thrust. Typically, we will want the tilt thrust to be large but smaller than the propeller’s maximum thrust, and the untilt thrust to be small but larger than the propeller’s minimum thrust. This will ensure a wide thrust range in either configuration and improves the agility of the vehicle. Near hover, the propeller thrust is thus bounded by $\{f_{min}, f_{p_i,tilt}\}$ when the arms are untilted, and $\{f_{p_i,untilt}, f_{max}\}$ when the arms are tilted. Once the desired tilt and untilt thrusts are set, the corresponding spring and anchoring points can be picked to generate the desired thrusts.

We do note that coupling the arms increases the complexity of the vehicle, as some external connecting rods may be required. However, we also note that the two arms at the front share the same axis for tilting, as well as the two arms at the back. Therefore, we can use a single arm to mount the two rotors at the front and at the back. Then we will only need to use one hinge and one spring to tilt each rotor pair. This will make the quadcopter H-shaped instead of X-shaped, and will eliminate the need for an external connecting rod.

Figure 3.6 shows an H-shaped vehicle and an X-shaped vehicle. While using the H-shaped frame increases the length of the quadcopter’s fuselage, having a longer fuselage makes the quadcopter more streamlined and thus more aerodynamically efficient. Considering the agility of the vehicle, it is recommended to use the side-coupled configuration for slow maneuvers, and use the all-coupled configuration for more agile maneuvers. An example of how a vehicle with the all-coupled configuration is more agile than a vehicle with the side-coupled configuration is provided later in Section 4.1. In addition, an H-shaped quadcopter frame is usually preferred in order to reduce mechanical complexity. Once the arm-coupling configuration is chosen, the overall vehicle frame can be designed. Next, the relevant parameters can be used to design for the tilt angle.

3.3.2 Experimental vehicle frame design

Following the ideas of Section 3.1, we decided to use the all-coupled configuration for our experimental vehicle, and developed an H-shaped vehicle frame. The properties of the experimental vehicle frame are given in Table 3.1. The overall size of the vehicle is designed to be similar to a commonly used quadcopter. The motors are the EMAX MT2208 brushless motors, and the propellers are 8’ 8045 ABS propellers. Both are commercially available. In order to avoid discharging the battery at a rate beyond the safety range, we set our cap on the individual propeller thrust at $f_{max} = 4.5\text{N}$. The drag and lift coefficients are determined experimentally by flying the vehicle at various constant speeds and curve-fitting the measured lift and drag forces. The rotations of all four arms are synchronized by using a four-bar mechanism that links the front arm to the rear arm. The four-bar mechanism can

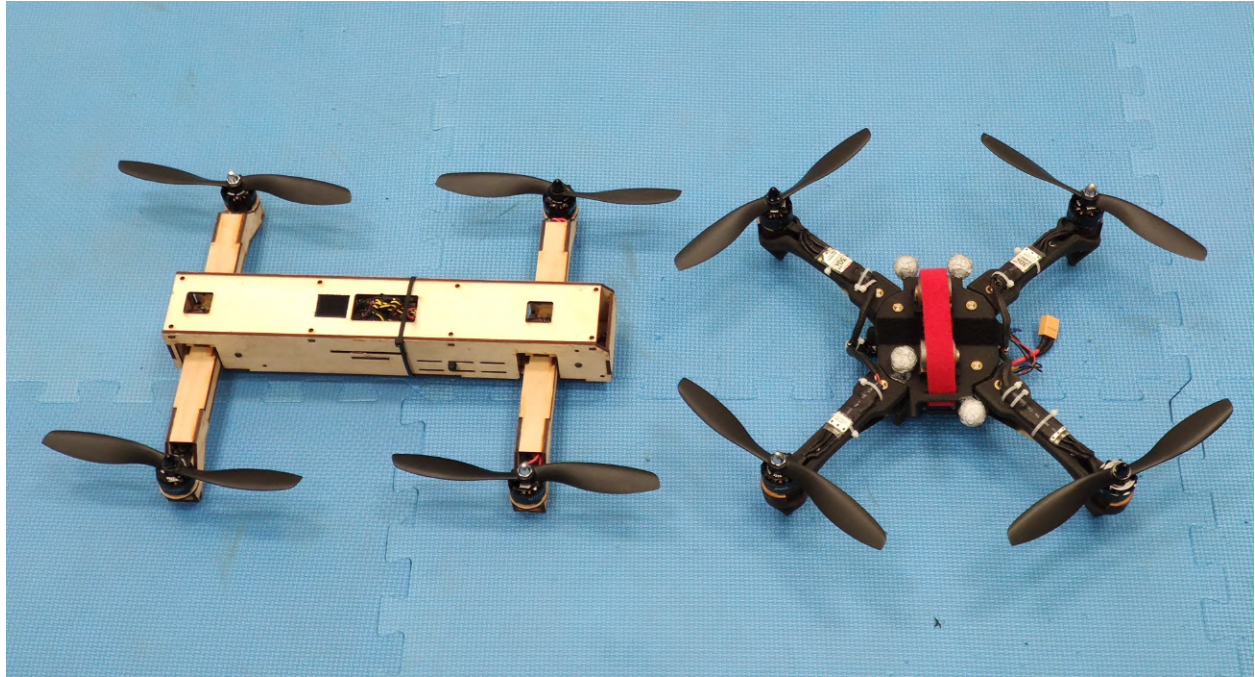


Figure 3.6: H-shaped (left) vs X-shaped (right) quadcopter frame. Using the H-shaped frame means that a single hinge and a single spring can be used to tilt two propellers at the same time, which reduces the mechanical complexity of the vehicle.

also be removed to convert the vehicle to the side-coupled configuration. While the mass of the springs can be different depending on the tilt angle, we can reasonably expect the entire tilting mechanism to add a mass of 50 grams, which is about 6 percent of the mass of the whole vehicle.

Figure 3.7 shows the experimental vehicle frame with the top cover plate taken off. We used laser-cut plywood to construct the overall frame because it allows for fast fabrication and provides high-enough precision. The plywood also shows high strength and rigidity which is desirable for aerial vehicles. The overall size of the vehicle frame is chosen to match the area span by the four propellers for compactness.

3.3.3 Tilt angle

Next, we need to choose a tilt angle. The tilt angle mainly affects 3 vehicle performance indicators, including the maximum flight speed, high-speed agility, and pitch agility. We will first formulate how we can compute these vehicle performance indicators using the aerodynamics model from Section 2.3. Then, we will use the experimental vehicle's frame parameters to evaluate the vehicle performance and decide the tilt angle and the remaining

Table 3.1: Experimental vehicle frame properties.

Symbol	Parameter	Value
m_{A_i}	Individual arm mass	75g
m_C	Central body mass	550g
m_Σ	Total vehicle mass	850g
m_T	Tilting mechanism mass	50g
A	Reference area	0.047m ²
C_D	Fitted drag coefficient equation	$0.773\alpha^2 + 0.543$
C_L	Fitted lift coefficient equation	1.264α
l	Distance between adjacent propellers	27cm
a	Tilt arm length	5cm
$\mathbf{d}_{P_i H_i}^{A_i}$	Position of the propeller with respect to the hinge	$[-a, 0, -1]^T$ cm
$f_{\Sigma, tilt}$	Total thrust to tilt the propellers at hover	13N
$f_{\Sigma, untilt}$	Total thrust to untilt the propellers at hover	2.5N
$f_{\Sigma, max}$	Maximum total thrust	18N
f_{max}	Maximum individual propeller thrust	4.5N
f_{min}	Minimum individual propeller thrust	0N

vehicle parameters in Section 3.4.

Maximum cruise speed

A regular quadcopter is usually not able to achieve a high top speed because it must tilt its body toward the forward flight direction, which increases the area subject to air resistance. This further increases the drag force and requires the propellers to produce even more thrust. However, our proposed vehicle is able to reduce the tilt angle of the central body and therefore could fly at a higher speed given the same hardware limit.

The relationship between the maximum speed and the corresponding designed tilt angle β can be solved given the limitation on the vehicle hardware performance. While the vehicle hardware performance can be limited by a range of factors, including the propeller structural strength, ESC current rating, etc., and is dependent on the vehicle speed and other external influences, we will assume that all of these can be generalized to a maximum total thrust of the vehicle $f_{\Sigma, max}$. The correlation between v_{max} and β can be solved by maximizing v_{max} under the following constraints:

$$\text{Cruise dynamics : } \begin{cases} f_\Sigma \sin(-\alpha + \beta) = \frac{1}{2}C_D(\alpha)\rho Av_{max}^2 \\ f_\Sigma \cos(-\alpha + \beta) = m_\Sigma g - \frac{1}{2}C_L(\alpha)\rho Av_{max}^2 \end{cases} \quad (3.22)$$

$$\text{Thrust limit : } \begin{cases} f_\Sigma \leq f_{\Sigma, max} \end{cases} \quad (3.23)$$

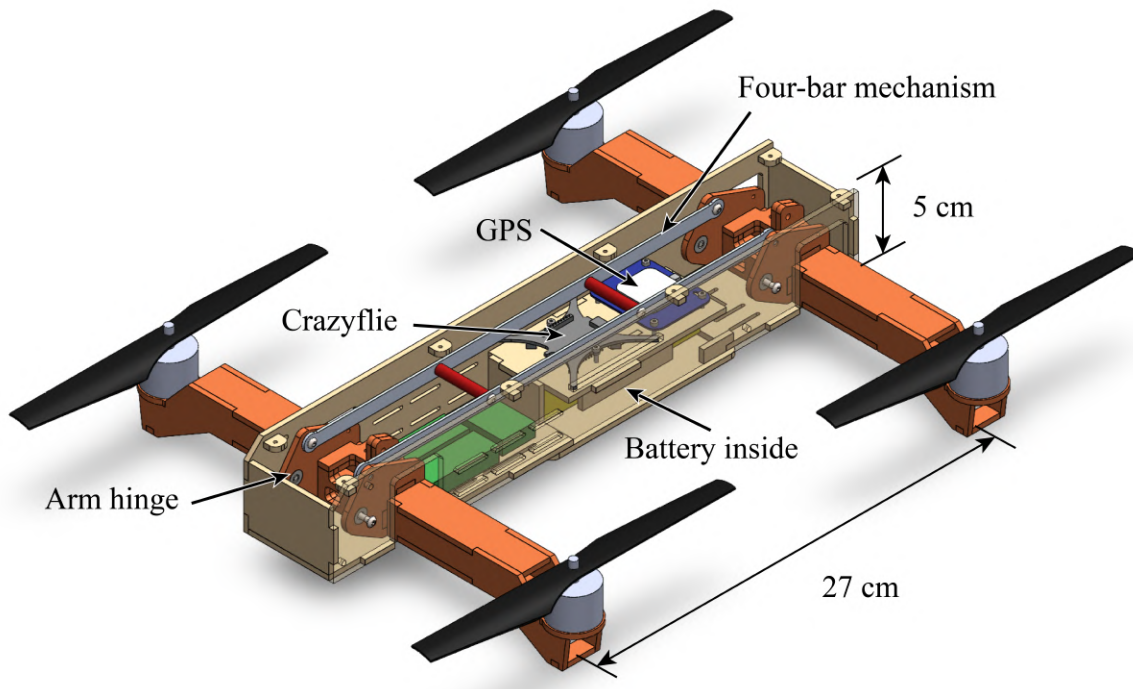


Figure 3.7: The experimental vehicle frame with the top cover plate taken off. The fuselage shown in beige is constructed with laser-cut wood. The arms shown in red orange are allowed to rotate around the arm hinges, and the rotations of the front and rear arms are coupled by a four-bar mechanism. Round stand-offs shown in red are installed on the long connecting rod of the four-bar mechanism to prevent buckling. Slots are cut on the fuselage for zip-tying wires and other electronics including the ESCs shown in green.

The solution to this problem for our experimental vehicle frame is provided in Section 3.4.

High-speed agility

When a quadcopter flies at the maximum cruise speed, all of the thrust capacity is used to counter the vehicle weight and the drag, meaning that it cannot maneuver in any other manner, e.g. accelerate laterally to avoid an obstacle, without falling and reducing its speed. However, if the propellers are allowed to tilt, due to the reduction in drag, the vehicle will no longer saturate its thrust at the same cruise speed. This enables a greater portion of the vehicle's thrust capacity to be used for maneuvering instead of merely countering drag at high speed, and will improve the high-speed agility of the vehicle. To quantify the agility of the proposed vehicle, we will consider an obstacle-avoidance example. For analysis, we will consider the following simplified maneuvers of the vehicle:

1. Cruise stage
 - a) Cruises at a maximum constant speed of v_{avoid} in the Earth x-direction \mathbf{x}_E ,
2. Turning stage
 - a) The vehicle detects an obstacle at a distance S in front of it, and starts a turning maneuver,
 - b) Constant maximum positive roll torque $\tau_{x,max}$ around the roll axis of the arm frame \mathbf{x}_A , and constant maximum pitch torque $\tau_{y,max}$ around the pitch axis of the arm frame \mathbf{y}_A for time Δt ,
 - c) Constant maximum negative roll torque $-\tau_{x,max}$ around the roll axis of the arm frame \mathbf{x}_A , and constant maximum pitch torque $-\tau_{y,max}$ around the pitch axis of the arm frame \mathbf{y}_A for time Δt ,
3. Lateral acceleration stage
 - a) The roll and pitch torques will change the orientation of the vehicle to allow it to accelerate laterally in the Earth y-direction to avoid the obstacle, while maintaining the height and x-direction speed of the vehicle.
 - b) By the time the x-coordinate of the vehicle reaches the obstacle, the vehicle makes a minimum of C y-direction clearance with the obstacle.

Figure 3.8 shows the example obstacle avoidance maneuver. The maximum crash-free cruise speed v_{avoid} thus reflects the high-speed agility of the vehicle. The faster a vehicle can travel without having to crash into the obstacle, the more agile it is. The correlation between v_{avoid} and β can be solved by maximizing v_{avoid} given the following constraints:

$$\text{Cruise dynamics : } \begin{cases} f_{\Sigma,-} \sin(-\alpha_- + \beta) = \frac{1}{2}C_D(\alpha_-)\rho A v_{avoid}^2 \\ f_{\Sigma,-} \cos(-\alpha_- + \beta) = m_{\Sigma}g - \frac{1}{2}C_L(\alpha_-)\rho A v_{avoid}^2 \end{cases} \quad (3.24)$$

$$\text{Turning dynamics : } \begin{cases} \phi = \frac{\tau_{x,max}}{I_{xx}} \cos \beta \Delta t^2 \\ \psi = -\frac{\tau_{x,max}}{I_{zz}} \sin \beta \Delta t^2 \\ \alpha_+ = \alpha_- - \frac{\tau_{y,max}}{I_{yy}} \Delta t^2 \end{cases} \quad (3.25)$$

$$\text{Fixed height \& speed : } \begin{cases} f_{\Sigma,+}(\sin(-\alpha_+ + \beta) \cos \phi \cos \psi + \sin \phi \sin \psi) = \frac{1}{2}C_D(\alpha_+)\rho A v_{avoid}^2 \\ f_{\Sigma,+}(\cos(-\alpha_+ + \beta) \cos \phi) = m_{\Sigma}g - \frac{1}{2}C_L(\alpha_+)\rho A v_{avoid}^2 \cos \phi \end{cases} \quad (3.26)$$

$$\text{Minimum clearance : } \left\{ s_y \left(t = \frac{S}{v_{max}} \right) \leq -C \right. \quad (3.27)$$

$$\text{Torque capacity limit : } \begin{cases} \tau_{y,max} = l\delta(4f_{max} - f_{\Sigma,+}) \cos \beta \\ \tau_{x,max} = l(1 - |\delta|)(4f_{max} - f_{\Sigma,+}) \end{cases} \quad (3.28)$$

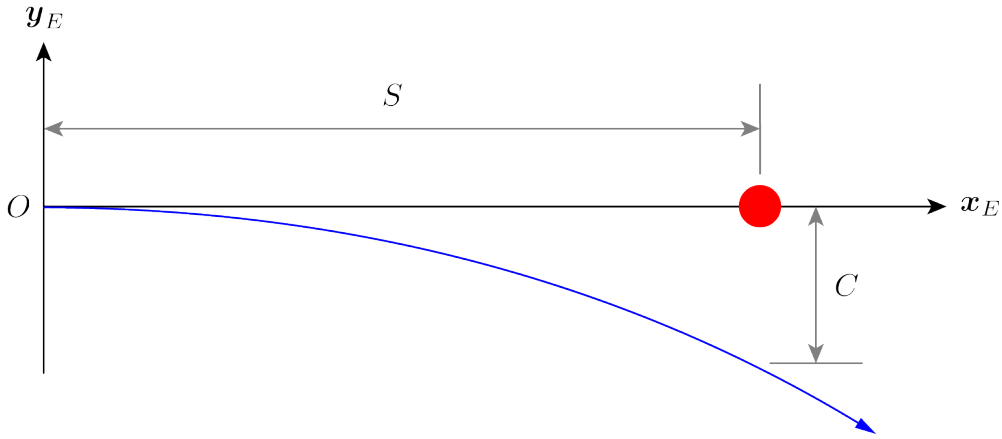


Figure 3.8: An example obstacle avoidance maneuver. The red dot represents the obstacle and the blue curve represents the flight path. The vehicle is initially flying toward the obstacle and starts an avoidance trajectory at O once it detects the obstacle. By the time the x -position of the vehicle reaches S , it must make a minimum of C y -direction clearance with the obstacle.

Where (ϕ, ψ) are the roll and yaw angles of the vehicle after the turning stage, $(f_{\Sigma,-}, f_{\Sigma,+})$ are the total vehicle thrusts before and after the turning stage, (α_-, α_+) are the angles of attack before and after the turning stage, and $\delta \in [0, 1]$ is the fraction of the vehicle's torque capacity used to produce a pitch torque. Note that although the vehicle produces a roll torque around the roll axis of the arm frame A , the yaw angle of the vehicle will also change. This is because the tilted propellers will produce a torque around the yaw axis of the central body frame C . For the given turning maneuver, the total thrust of the vehicle will monotonically increase from $f_{\Sigma,-}$ at $t = 0$, to $f_{\Sigma,+}$ at $t = 2\Delta t$, and stay at $f_{\Sigma,+}$ for the remainder of the flight. Throughout the turning stage, since the magnitudes of the desired roll and pitch torques are constant, the magnitude of the thrust shift across the four propellers to generate the desired roll and pitch torques are also constant. As a result, at $t = 2\Delta t$ where the total thrust is the highest, the thrust shift will result in one propeller having the peak thrust. We limit such peak thrust to f_{max} and with some algebraic manipulation, we can find the torque limit as shown by Equation 3.28. The solution to this problem is highly dependent on the vehicle's dynamic properties and is provided for our experimental vehicle frame in Section 3.4.

Pitch agility near hover

The change in tilt angle β changes the maximum pitch torque τ_y that the vehicle can generate. This is because when the arms tilt, the moment arm between the front rotors' thrust axes

and the rear rotors' thrust axes changes. Assuming that near hover, the maximum thrust difference between the front rotors and the rear rotors is Δf , the maximum pitch torque is thus $\tau_{y,max} = \Delta f l \cos \beta$. We note that this torque reduces as the tilt angle increases. Nevertheless, this problem can be mitigated by designing the rear rotors to be higher than the front rotors with respect to the central body. For a rotor height offset of Δh , the maximum pitch torque now becomes $\tau_{y,max} = \Delta f (l \cos \beta + \Delta h \sin \beta)$. However, this results in an increase in vehicle height, which restricts the vehicle's capability to maneuver in limited space. In addition, the drag area may also increase if the height offset is achieved by simply skewing the vehicle frame. Therefore, the designer will need to consider the application to find a balance between maximum pitch torque, the height of the vehicle, and the other vehicle performance indicators.

It is important to note that as the vehicle speed increases, the maximum thrust difference Δf will decrease due to additional drag on the vehicle. As discussed in the previous section, at high speed, because tilting the arms reduces the drag, Δf will be relatively larger when the arms are tilted, which can lead to a relatively higher maximum pitch torque. Therefore, while tilting the arms always reduce the pitch agility of the vehicle near hover, it does not necessarily reduce the pitch agility at higher speed.

3.3.4 Experimental vehicle tilt angle design

Using the parameters of the experimental vehicle frame in Table 3.1, we can solve for the correlations between the tilt angle β and the 3 vehicle performance indicators above. For quantifying the high-speed vehicle agility, we set the detection range to $S = 10\text{m}$ and clearance to $C = 1\text{m}$.

Figure 3.9 shows how the tilt angle changes the max linear speed v_{max} , the max crash-free speed v_{avoid} , and the remaining pitch torque capacity as compared to the torque at zero tilt angle. Increasing the tilt angle increases the maximum cruise speed of the vehicle with a decreasing marginal gain. The maximum speed that the vehicle can achieve is 33.28m s^{-1} at a designed tilt angle of 88.2° , which is a 64.8% increase from the maximum speed of 20.19m s^{-1} when the tilt angle is zero. The maximum crash-free cruise speed of the vehicle increases as the tilt angle increases, but is maxed out at $\beta = 68^\circ$. The maximum crash-free cruise speed that the vehicle can achieve is 21.56m s^{-1} at a designed tilt angle of 68° , which is a 24.3% increase from the maximum speed of 17.35m s^{-1} when the tilt angle is zero. However, increasing the tilt angle decreases the pitch torque capacity at hover monotonically.

In the end, we have chosen a tilt angle of $\beta = 20^\circ$ to preserve much of the pitch torque capacity, while creating enough differences to be observed in the maximum speed and maximum crash-free speed so that we can validate the analyses results with experiments. The 20° tilt angle is predicted to increase the maximum speed of the vehicle from 20.19m s^{-1} to 24.70m s^{-1} , and the maximum crash-free speed of the vehicle for the given trajectory from 17.35m s^{-1} to 19.24m s^{-1} . On the other side, the reduction in maximum pitch torque at hover is 6.03% in the tilted configuration.

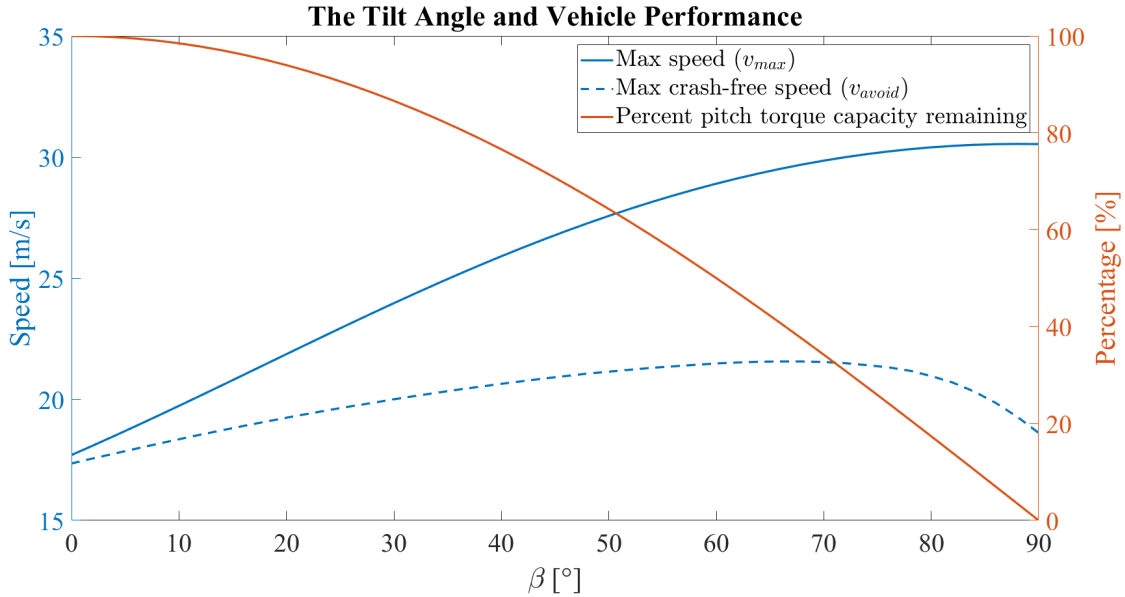


Figure 3.9: The correlation between the tilt angle and the vehicle performance for the experimental vehicle. Increasing the tilt angle increases the maximum cruise speed of the vehicle with a decreasing marginal gain. Increasing the tilt angle increases the maximum crash-free cruise speed of the vehicle up until $\beta = 68^\circ$. However, increasing the tilt angle decreases the pitch torque capacity.

Lastly, we will need to choose the spring and the anchoring points to produce the desired tilt and untilt thrusts. The spring force, anchoring points, and the desired tilt/untilt thrusts are correlated by Equation 3.21, and the standard spring equation $\mathbf{f}_{s_i} = -k (\|\mathbf{d}_{S_i M_i}\| - l_0) \frac{\mathbf{d}_{S_i M_i}}{\|\mathbf{d}_{S_i M_i}\|}$. We approach this problem by first experimentally determining the spring constants for a set of springs in stock that will fit in the vehicle frame. Then, we compute the exact anchoring points for all the springs by numerically solving the full equations with additional space constraints. Lastly, we choose the spring and the corresponding anchoring points that would minimize the size of the tilting mechanism. The vehicle's tilt angle and all other relevant properties are summarized in Table 3.2.

To ensure consistent configuration transition in actual flight, it is important to keep the springs under the limit of proportionality to prevent degradation. For long-term use, fatigue analysis on the springs is desired. In addition, because the wires powering the rotors will pass around the arm hinges, it is crucial to minimize the friction that wires introduce to the quadcopter arms by using softer wires, running cables properly, etc. It is also worth noting that the use of springs is rather a design choice but not the only option. In the end, our goal is to put a larger torque on the quadcopter arm in the untilted configuration, and a smaller torque on the quadcopter arm in the tilted configuration. Therefore, other solutions

Table 3.2: Experimental vehicle tilting-related properties.

Symbol	Parameter	Value
β	Tilt angle	20°
l_0	Spring rest length	1.75cm
k	Spring constant	8N cm^{-1}
$\mathbf{d}_{M_i H_i}^{A_i}$	Position of spring end 1 with respect to the hinge	$[-4, 0, 1]^T \text{cm}$
$\mathbf{d}_{S_i H_i}^{A_i}$	Position of spring end 2 with respect to the hinge	$[1.3, 0, -1]^T \text{cm}$

like using magnets of different strengths to attract the quadcopter arms can be applied, and may even offer a longer life cycle and smaller size.

With the design of the experimental vehicle finalized, we will now validate its capabilities with experiments.

3.4 Experimental Validation

In this section, we will use the experimental vehicle to validate the capabilities of the proposed design, including 1. the reliability of the tilting mechanism, 2. the improvement in the top linear speed, 3. the improvement in the high-speed agility, and 4. the increase in the energy efficiency.

3.4.1 Experiment setup

For all of our tests, we fly the vehicle outdoors in a flat grass field at the Richmond Field Station, Richmond. All the speed measurements are ground speeds, and while we do not specifically characterize the influence of wind, we strive to ensure consistency in the experiment results by: 1. conducting experiments only when the wind is low, 2. conducting experiments in short time frame to minimize wind variation, and 3. flying the vehicle consistently in the same direction.

The vehicle is localized by fusing readings from the following sensors:

- i Inertial measurement unit (accelerometer and rate-gyroscope) running at 500 Hz,
- ii 3-axis magnetometer running at 100 Hz,
- iii Global positioning system running at 5 Hz.

The sensor readings are fused via an off-the-shelf extended Kalman filter (EKF) algorithm taken from the open-source PX4 firmware [48]. The IMU and magnetometer are a part of the flight controller and the GPS is connected to the flight controller via a serial port (UART). The EKF is run on the flight controller at 500 Hz, predicting the states forward using the

IMU data, and using the GPS and magnetometer readings for the correction step of the EKF. The state estimates are then used by the flight controller for closed-loop control.

Data from the above sensors and the state estimates are logged via radio at 100 Hz for post-processing. Additionally, the voltage and current readings from the battery are measured using a power module and are also logged to calculate the power consumption of the quadcopter in the untilted and tilted configurations.

The quadcopter is controlled autonomously and tracks the desired position, velocity, acceleration, and yaw angle by using a cascaded position and attitude controller as shown in Figure 3.10.

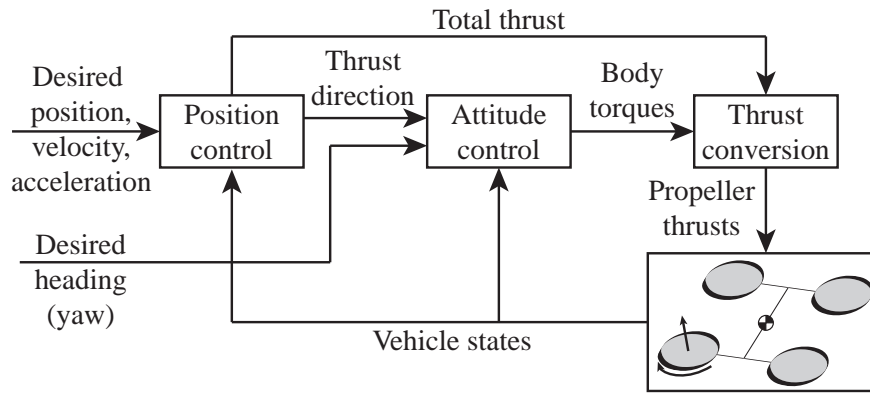


Figure 3.10: Block diagram of the quadcopter controller.

The position and attitude controller computes the desired body torques $\boldsymbol{\tau}^A = [\tau_x, \tau_y, \tau_z]^T$ and total thrust f_Σ in the combined arm A frame required to track the desired thrust direction and the desired yaw angle. Individual rotor thrusts $\mathbf{u} = [f_{p_1}, f_{p_2}, f_{p_3}, f_{p_4}]^T$ required to generate the desired total thrust and the desired body torques are then computed using the following mapping:

$$\mathbf{u} = \begin{bmatrix} f_{p_1} \\ f_{p_2} \\ f_{p_3} \\ f_{p_4} \end{bmatrix} = \begin{bmatrix} \mathbf{M}_{f_\Sigma} \\ \mathbf{M}_{\boldsymbol{\tau}^A} \end{bmatrix}^{-1} \begin{bmatrix} f_\Sigma \\ \tau_x \\ \tau_y \\ \tau_z \end{bmatrix} = \mathbf{M}^{-1} \begin{bmatrix} f_\Sigma \\ \boldsymbol{\tau}^A \end{bmatrix} \quad (3.29)$$

Where $\mathbf{M}_{f_\Sigma} \in \mathbb{R}^{1 \times 4}$ is the mapping from \mathbf{u} to f_Σ , $\mathbf{M}_{\boldsymbol{\tau}^A} \in \mathbb{R}^{3 \times 4}$ is the mapping from \mathbf{u} to $\boldsymbol{\tau}^A$, and $\mathbf{M} \in \mathbb{R}^{4 \times 4}$ is the combined mapping. The mapping is computed using the geometry of the vehicle and the torque τ_{p_i} from each propeller which correlates to the thrust f_{p_i} by $\tau_{p_i} = (-1)^i \kappa f_{p_i}$, where κ is the thrust to torque coefficient of the propeller. Since the body torques and the desired total thrust are in the combined arm frame A , the entries for the mapping matrices are given as:

$$\mathbf{M}_{f_\Sigma} = [1 \quad 1 \quad 1 \quad 1] \quad (3.30)$$

$$\mathbf{M}_{\tau^A}[:, i] = \mathbf{S}(\mathbf{R}^{AC} \mathbf{d}_{P_iC}^C) \mathbf{z}_A^A + (-1)^i \kappa \mathbf{z}_A^A \quad (3.31)$$

Lastly, we can compute the combined mapping matrix \mathbf{M} for the untilted and tilted configurations:

$$\mathbf{M}_{untilted} = \begin{bmatrix} 1 & 1 & 1 & 1 \\ -\frac{l}{2} & -\frac{l}{2} & \frac{l}{2} & \frac{l}{2} \\ -\frac{l}{2} & \frac{l}{2} & \frac{l}{2} & -\frac{l}{2} \\ -\kappa & \kappa & -\kappa & \kappa \end{bmatrix} \quad (3.32)$$

$$\mathbf{M}_{tilted} = \begin{bmatrix} 1 & 1 & 1 & 1 \\ -\frac{l}{2} & -\frac{l}{2} & \frac{l}{2} & \frac{l}{2} \\ -\cos \beta(a + \frac{l}{2}) + a & \cos \beta(a - \frac{l}{2}) + a & \cos \beta(a - \frac{l}{2}) + a & -\cos \beta(a + \frac{l}{2}) + a \\ -\kappa & \kappa & -\kappa & \kappa \end{bmatrix} \quad (3.33)$$

Combining this with the thrust bounds we computed in Section 2.4, we can find the limit on the total thrust and the desired body torques. The vehicle in the all-coupled configuration has the highest agility. The pitch torque capacity is higher, and the thrust bounds are almost not affected by the motion of the vehicle. The vehicle in the side-coupled has a lower maximum roll and yaw torque when the rolling speed is high. As an example, Figure 3.11 shows the limit on the roll torque and the total thrust that the vehicle can produce in the side-couple and all-coupled configurations for different rolling speeds, to prevent the arms from untilting in the tilted configuration.

As compared to a conventional quadcopter with the same vehicle parameters without the ability to tilt, the tilt-rotor has tighter bounds on the torque thrust and roll torque to prevent untilting. At zero rolling speed, the untilt bounds are identical for the all-coupled and side-coupled configurations. As the rolling speed increases, the gyroscopic torque discussed in Section 3.1 comes into play, and tightens the bounds for the vehicle in the side-coupled configuration. However, in the all-coupled configuration, the bounds are effectively not affected at all, and the vehicle maintains the same agility regardless of the maneuver. As a result, we have kept our vehicle in the all-coupled configuration, and we have found that the vehicle is able to maintain its configuration without any programmed tilt/untilt thrust and torque bounds.

3.4.2 Changing configuration test

The transition between the tilted and untilted configurations is tested. The transition from the untilted configuration to the tilted configuration is accomplished by commanding a high

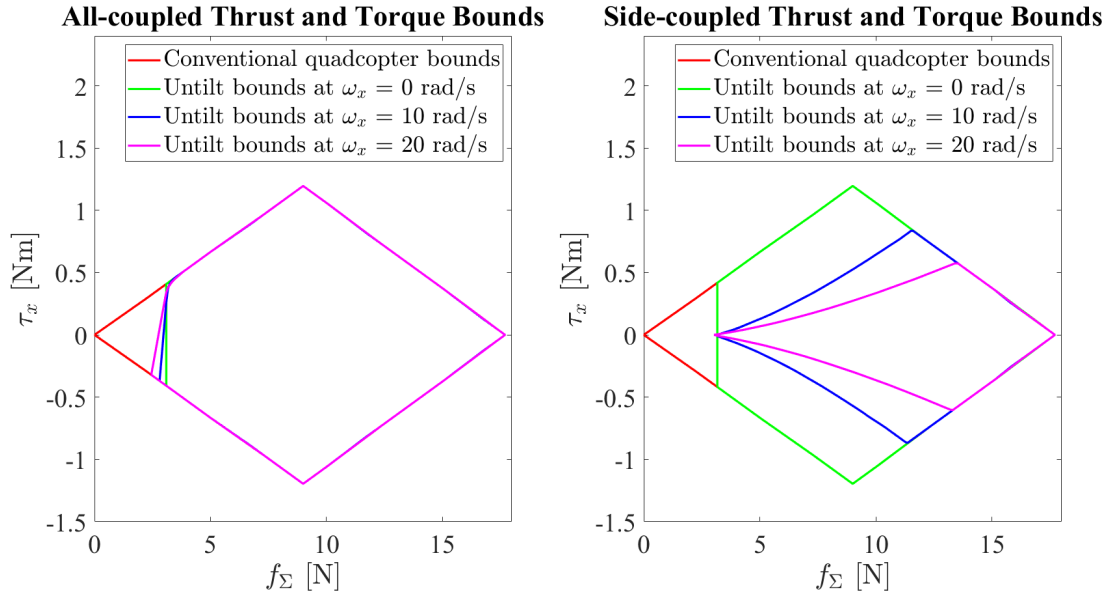


Figure 3.11: The limit on the roll torque and the total thrust that the vehicle can produce in the side-couple and all-coupled configurations for different rolling speeds, to prevent the arms from untilting in the tilted configuration.

total thrust for a fraction of a second. Right after the morphing, the same controller before the transition resumes to function but is updated to use the tilted mapping matrix M_{tilted} . To accommodate for the change in the vehicle position from suddenly producing a high thrust, we add an offset to the desired position right after the morphing. Figure 3.12 shows the vehicle switching from the untilted to the tilted configuration.

To switch back to the untilted configuration, we simply command a near zero thrust for a fraction of a second. Right after the morphing, the controller is switched back to use the untilted mapping matrix $M_{untilted}$. The sudden loss of thrust causes the vehicle to fall, so an opposite offset is added to the desired position to accommodate for the change in the vehicle position. The tilting and untilting are repeated 20 times and show no signs of failure. Figure 3.13 shows the vehicle commanded thrust and the measured accelerations for one tilt and untilt cycle.

3.4.3 Maximum linear speed tests

The maximum speed of the vehicle is tested by flying the vehicle in a straight line in the following manner:

1. Accelerate at a constant linear acceleration of a ,



Figure 3.12: The vehicle switches from the untilted to the tilted configuration. An offset is added to the desired position to accommodate for the change in the vehicle position due to the sudden high thrust.

2. Check if the maximum total thrust $f_{\Sigma,max}$ is reached, if so start decelerating until rest.
3. Record the maximum speed that the vehicle has reached v_{max} .

Since the maximum total thrust $f_{\Sigma,max}$ is above the tilt thrust $f_{\Sigma,tilt}$, we bolted the tilting mechanism in the untilted configuration to imitate a vehicle without the ability to tilt. In order to prevent the vehicle from flying beyond the flight space, we choose a to be 3.125 m s^{-2} . Adding the acceleration term to Equation 3.22, we can predict that the maximum speed in the untilted configuration is 17.70 m s^{-1} , and the maximum speed in the tilted configuration is 21.86 m s^{-1} . The actual experiment is repeated 3 times for each configuration. The experimental results are summarized in Table 3.3.

We can see that the average maximum speed of the vehicle in the tilted configuration is 12.5% higher than in the untilted configuration, and the results are repeatable. We do note that the vehicle in the untilted configuration is flying faster than the prediction. We suspect that this has to do with the fact that the lift model assumes that the angle of attack is in the linear region which will show a very high downward lift on the vehicle when the angle of attack is large. However, at this speed, we record that the angle of attack of the vehicle in the untilted configuration is almost -45° , which is beyond the linear region. As a result, the actual downward lift on the vehicle is smaller than the prediction, meaning that more of the vehicle thrust can be used to counteract the drag, thus allowing the vehicle in the untilted configuration to fly faster.

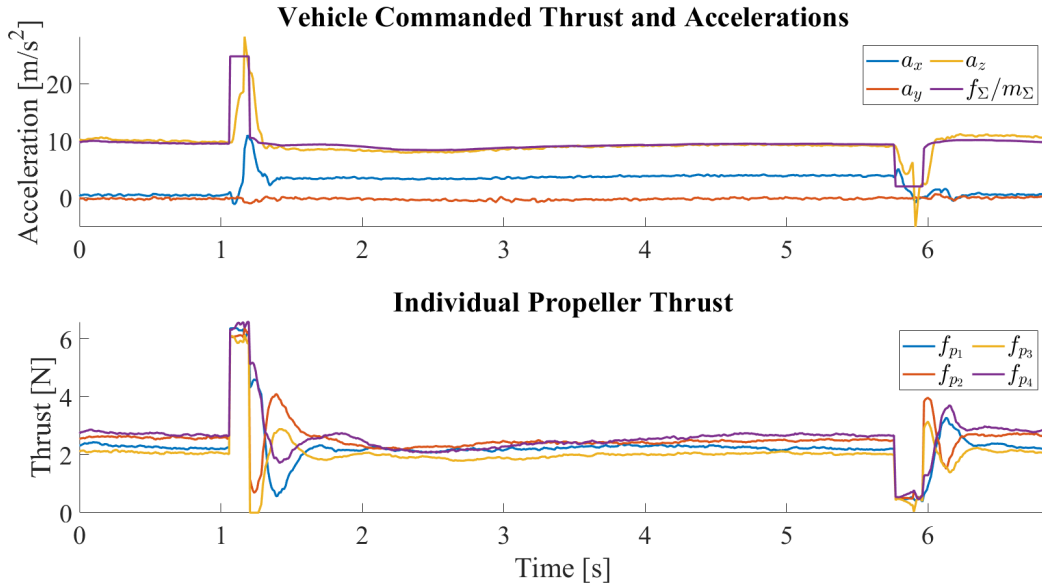


Figure 3.13: The vehicle commanded thrust normalized by the vehicle mass and the measured accelerations in the central body frame C for one tilt and untilt cycle. (a) In the tilting transition stage which starts at around $t = 1s$, the vehicle is commanded to tilt by producing a sudden high thrust. The surge in thrust is followed by a surge in the acceleration along z_C , which is then followed by an increase in the acceleration along x_C , meaning that the thrust axes of the propellers have been tilted forward. (b) In the tilted hover stage from around $t = 2s$ to $t = 5.7s$, the positive x_C acceleration indicates the 20° increase in the vehicle central frame’s pitch angle such that the propellers are pointing upward to keep the vehicle hovering. (c) In the untilting transition stage which starts at around $t = 5.7s$, the vehicle is commanded to untilt by producing a sudden low thrust. The drop in thrust is followed by a drop in the acceleration along z_C , which is then followed by a drop in the magnitude of acceleration along x_C , meaning that the thrust axes of the propellers have been restored. Despite the change in the mapping matrix, we can see that the individual propeller thrusts are very close once the vehicle has stabilized after the transition.

3.4.4 Obstacle avoidance tests

The high-speed agility of the vehicle is tested by having the vehicle track the obstacle avoidance trajectory discussed in Section 3.3.2. We create an imaginary obstacle on our path with $S = 10m$, and command the vehicle to cruise at the computed v_{max} and then turn to avoid the obstacle to achieve a clearance of $C = 1m$. We limit the individual propeller thrust at f_{max} , and compare the actual flight speed and clearance with the commanded ones to evaluate the real agility of the vehicle. The experimental results are summarized in Table 3.4.

Table 3.3: Maximum linear speed achieved by the vehicle and the associated angle of attack.

Trial	Untilted		Tilted	
	Max speed	Max AoA	Max speed	Max AoA
1	18.65m s ⁻¹	-41.47°	20.81m s ⁻¹	-25.79°
2	18.64m s ⁻¹	-45.20°	21.59m s ⁻¹	-16.05°
3	19.05m s ⁻¹	-39.73°	21.02m s ⁻¹	-26.59°
Average	18.77m s ⁻¹	-42.13°	21.14m s ⁻¹	-22.81°
Standard deviation	0.24m s ⁻¹	2.79°	0.40m s ⁻¹	5.87°

Table 3.4: The actual flight speed and clearance and the commanded flight speed and clearance.

Configuration	Cmd speed	Actual speed	Cmd clearance	Actual clearance
Untilted	17.35m s ⁻¹	17.70m s ⁻¹	1m	1.03m
Tilted	19.24m s ⁻¹	19.03m s ⁻¹	1m	1.24m

We can see that given the same thrust constraint, the vehicle is able to achieve the commanded clearance of $C = 1\text{m}$ in both the untitled and tilted configurations, and can reach a higher flight speed without crashing in the tilted configuration.

3.4.5 Aerodynamic performance tests

The reduction in drag allows less thrust to be produced to travel at the same speed, which increases the energy efficiency of the vehicle. To test the aerodynamic performance, the vehicle is flown at commanded horizontal speeds v_{des} of $\{10.0, 12.5, 15.0, 17.5, 20.0\}\text{m s}^{-1}$ in a straight line in the following manner:

1. Accelerate from rest to the cruising speed v_{des} over a specified acceleration distance s_{accel} ,
2. Cruise at v_{des} over a specified cruise distance s_{cruise} ,
3. Decelerate from cruising speed to rest over a specified deceleration distance s_{decel} .

Voltage and current data collected from the power module is evaluated over the steady state of the cruising portion of the trajectory, which is selected to last five seconds to get approximately 500 data points.

A sample plot of power and speed vs. time is shown in Figure 3.14. This specific plot is for the case of the quadcopter commanded to fly in the tilted configuration at 20m s^{-1} .

The plot of average power vs. average speed is shown in Figure 3.15. The power consumption is lower in the tilted configuration than in the untitled configuration at high speed.

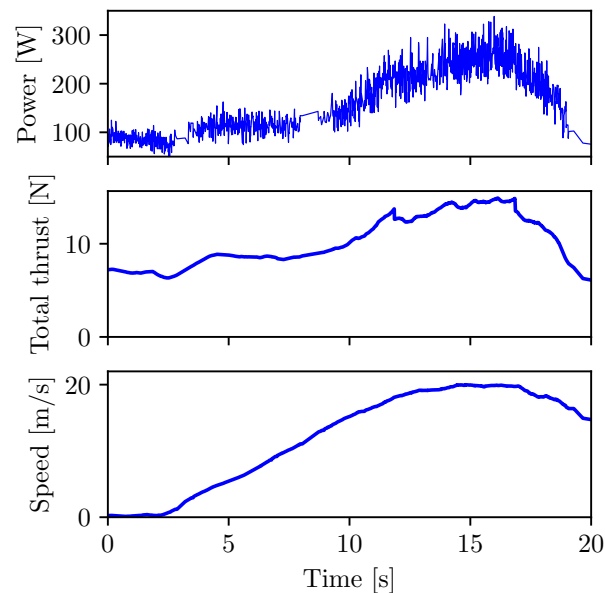


Figure 3.14: Power, total thrust, and speed vs. time for a single experiment. Data in this plot is from the experiment where the quadcopter is commanded to fly in the tilted configuration at 20 m s^{-1} .

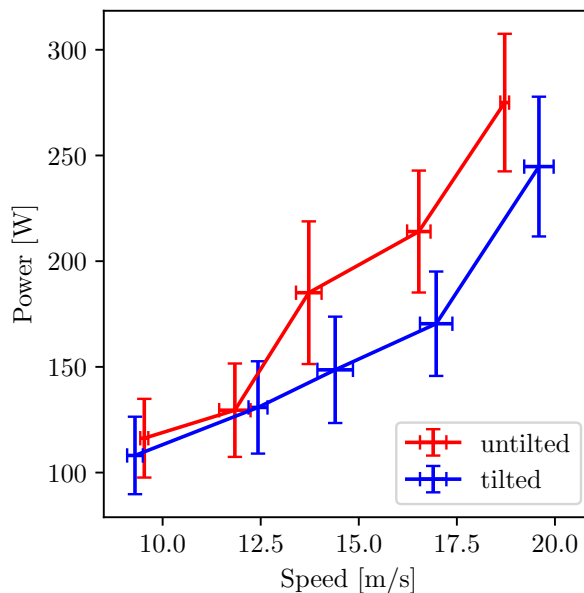


Figure 3.15: Power consumption vs. speed when flying in untitled and tilted configurations. The data points are the average values and the error bars represent one standard deviation in the data.

Figure 3.16: Comparison of power metrics in different flight configurations.

We can see that the power consumption in the tilted configuration in the speed range of $15 - 20 \text{ m s}^{-1}$ is more than 20% lower as compared to the untitled configuration.

3.5 Conclusion

In this chapter, we have presented a novel quadcopter design capable of tilting the propellers into the forward flight direction in mid-air to reduce the drag without the use of additional actuators. The reduction in drag allows the vehicle to fly at a higher top speed with higher agility, and improves the flight efficiency at high speed. Unlike the other multirotor-fixed-wing combo quadcopters, the proposed vehicle does not have wings. While this sacrifices the cruise efficiency, the vehicle has higher agility as the area subject to aerodynamic forces is kept small. Especially, the vehicle will not have high drag during rolling motion due to large wings paddling in the air like fixed-wing vehicles. By using simple sprung hinges instead of actuators or other complex mechanisms, the design is thus relatively less complicated than other aerial morphing vehicles. On the other side, the use of a passive tilting mechanism

means that the arms can only be tilted in one direction with a fixed tilting angle, and cannot achieve the arbitrary attitude of other actively tilted quadcopters.

The dynamics of such a vehicle were derived. Based on the dynamics, we discussed the key design parameters including the tilt angle and the vehicle configuration. The effects that these parameters have on the vehicle performance are presented, and the relevant design trade-offs are discussed. Analyses show that while the vehicle is always less agile near hover as compared to a conventional vehicle due to the introduction of additional thrust bounds, it does have a higher top speed and higher agility at high speed as lesser thrust capacity is used to counteract the aerodynamic forces in the tilted configuration.

An experimental vehicle with an overall size similar to a regular quadcopter is built to validate the analyses. Experiments are done to validate the capabilities of the vehicle. First, the vehicle is shown to transition between the tilted and untilted configurations reliably. Then, the vehicle is shown to have reached a higher maximum linear speed under the same thrust limit in the tilted configuration. Furthermore, the vehicle is shown to be more agile at high speed, as it can fly faster while avoiding a defined obstacle in the tilted configuration. Finally, the vehicle is shown to have a better energy efficiency than a conventional quadcopter at a higher speed.

The proposed design is thus able to fly at a higher top speed (by 12.5%), has higher high-speed agility (by 7.5%) and higher efficiency (20% lower power consumption for a speed range of 15-20m s⁻¹) with little trade-offs in mechanical complexity and low-speed agility. This can be useful for applications that are time-sensitive, such as package delivery and drone racing. In the future, the vehicle can be designed such that the tilt angle can be easily reconfigured, allowing it to fit a wide range of applications. The frame of the vehicle can also be designed to be more aerodynamically efficient, allowing for an even higher top speed and better high-speed agility. One approach to improve the aerodynamic efficiency of the vehicle frame is to reduce its vertical dimension, which can be achieved by reducing the size of the tilting mechanism through the use of shorter but stronger springs. In addition, the vehicle frame can be designed like an airfoil shape to reduce the drag coefficient, and even generate lift to counteract the vehicle weight.

Chapter 4

PairTilt: Design and Control of an Active Tilt-Rotor Quadcopter for Improved Efficiency and Agility

This chapter introduces PairTilt, a novel quadcopter design featuring two pairs of tiltable rotors, balancing the mechanical simplicity of conventional quadcopters with the enhanced agility of more complex tilt-rotor systems. While the system remains underactuated—specifically, the lateral translational degree of freedom is not directly controlled—this design choice is justified because it reduces complexity and minimizes energy use. The coupling of rotors reduces angular momentum issues, enhancing stability and efficiency without the challenges associated with tilting each motor individually, which would require higher servo torque due to significant gyroscopic torques.

PairTilt’s tiltable mechanism minimizes drag in high-speed flight, extending the operational range and making it well-suited for various aerial applications. Additionally, the design partially decouples translational and rotational dynamics, enabling agile maneuvers in confined spaces. The system’s dynamics are analyzed, and a cascaded controller is implemented to ensure stable flight across various scenarios. Through simulations and real-world experiments, we demonstrate the vehicle’s superior agility, compact hovering, sensor pointing ability, and energy efficiency at higher speeds compared to conventional quadcopters.

The primary contribution of this work lies in PairTilt’s distinctive design, which achieves a unique balance of simplicity, efficiency, and agility. This balance is made possible by the pairwise rotor coupling, which reduces complexity and gyroscopic torque effects, and the strategic prioritization of key degrees of freedom. This design approach opens new possibilities for aerial robotics applications requiring both maneuverability and efficient high-speed flight.

The material in this chapter is based on the following work:

- J. Tang and M. W. Mueller, "PairTilt: Design and Control of an Active Tilt-Rotor Quadcopter for Improved Efficiency and Agility". In: *Advanced Intelligent Systems*,

Feb. 2025.

4.1 Introduction

4.1.1 Background

Quadcopters, a type of unmanned aerial vehicle (UAV), are distinguished by their four rotors. This design allows for vertical take-off and landing (VTOL), making quadcopters highly versatile for a variety of applications. They are particularly noted for their mechanical simplicity and cost-effectiveness, which have contributed to their widespread adoption in both recreational and commercial contexts. The simplicity and ease of control offered by the standard quadcopter design [1, 49, 50] make it an excellent platform for a wide range of applications, including building inspection, photography, package delivery [4], and surveillance [2].

However, standard quadcopters also have significant limitations that affect their performance, especially in demanding environments such as urban areas. Although they excel in stability, their fixed rotor configuration restricts their speed and maneuverability, limiting their effectiveness in complex, obstacle-rich environments. Standard quadcopters also face inherent limitations in achieving high speeds efficiently. The design of quadcopters necessitates that they tilt forward to advance in the flight direction, which increases their frontal area exposed to air resistance. This increased drag not only burdens the propellers, but also limits the top speed and reduces overall energy efficiency. This inefficiency becomes particularly problematic when quadcopters are employed in tasks that require rapid movement such as search and rescue operations or fast package delivery, where efficiency and speed are crucial [51, 44].

Tilt-rotor UAVs present a promising alternative to standard quadcopters by addressing many of these limitations. By incorporating rotors that can tilt, these UAVs combine the VTOL capabilities of helicopters with the aerodynamic efficiency of fixed-wing aircraft. This design allows tilt-rotors to achieve higher speeds, better energy efficiency, and greater range compared to their quadcopter counterparts [15, 45].

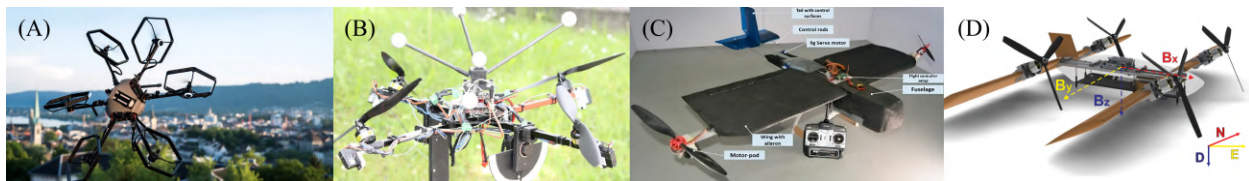


Figure 4.1: Examples of tilt-rotor vehicles in the literature: (A) and (B) are omni-directional UAVs with greater controllability [22, 24], (C) and (D) are hybrid VTOL tilt-rotors with greater endurance [15, 16].

4.1.2 Literature Review

Recent advancements in tilt-rotor UAVs have significantly improved the capabilities of underactuated systems. Panigrahi et al. [15] designed a hybrid VTOL UAV that optimizes endurance by integrating fixed-wing and rotorcraft features, using thrust vectoring for efficient transitions between vertical takeoff and horizontal flight. Similarly, Papachristos et al. [16] developed a quad-tiltrotor platform with a hybrid predictive control approach, enabling autonomous mode conversion between helicopter and fixed-wing modes while ensuring stability. Mikami and Uchiyama [17] implemented a control system for a quad tilt-wing UAV that maintains stability during transitions using a dynamic inversion method. Liang et al. [52] explored a composite tilt-rotor UAV, applying advanced aerodynamic modeling and control strategies to manage complex flight dynamics while remaining underactuated.

In addition, Sakaguchi et al. [18] proposed a quadcopter with a tilting frame using a parallel link mechanism, demonstrating its capability to perform stable maneuvers despite limited actuation. Tang et al. [51] introduced QUaRTM, a quadcopter with an unactuated rotor tilting mechanism that morphs between two configurations: untilted for higher pitch torque capacity and a smaller vertical dimension, and tilted for reduced drag area, higher top speed, and improved high-speed agility and efficiency. Mousaei et al. [19] introduced a tilt-rotor UAV that focuses on fault tolerance, utilizing actuator redundancy to maintain control under various failure scenarios. Bucki et al. [20] presented a passively morphing quadcopter with unactuated hinges that enable mid-air shape changes, allowing the vehicle to traverse narrow spaces and perform specific tasks without additional motors. Falanga et al. [21] developed a morphing quadrotor design capable of dynamically adapting its shape for navigating tight spaces and object manipulation, enhancing functionality within the constraints of underactuated systems. These studies illustrate how innovative designs and control strategies can maximize efficiency and maneuverability while operating within the inherent limitations of underactuated UAV systems.

In contrast, fully actuated systems aim to achieve full six degrees of freedom (6DOF) control by incorporating additional actuators beyond the conventional rotor setup. Ryll et al. [22, 23] developed quadrotor UAVs with tilting propellers, demonstrating how independent control of rotor orientation can provide complete maneuverability. Nemati et al. [13] expanded on this by using additional motors for rotor tilting, enhancing stability and control flexibility. The Voliro hexacopter platform by Kamel et al. [24] offered omni-directional control, allowing for complex maneuvers such as vertical surface inspection. Park et al. [25] designed an omni-directional aerial robot (ODAR) using bi-directional thrust generation for precise control under lateral disturbances. Brescianini and D’Andrea [27] introduced an eight-rotor configuration that maximizes agility, using decoupled control strategies for precise translational and rotational movement. Aboudorra et al. [26] presented the OmniMorph, a morphing UAV that optimizes energy use while ensuring full pose tracking with a single servomotor. Mousaei et al. [19] addressed actuator failure scenarios, developing robust control methods to maintain stability through configuration redundancy. Li et al. [28] integrated servo dynamics into nonlinear model predictive control (NMPC) for overac-

tuated systems, addressing nonlinearity and servo lag. Together, these works highlight how advanced actuation and control strategies in fully actuated systems overcome the limitations of underactuated designs, enhancing versatility and adaptability in complex environments.

4.1.3 Contribution

This chapter introduces PairTilt shown in Figure 4.2, a novel tilt-rotor UAV designed for enhanced aerial operations. PairTilt features an H-shaped frame with pairwise coupled tiltable rotors, driven by two servos. This configuration, unlike conventional quadcopter designs, minimizes frontal drag during high-speed flight, leading to improved aerodynamic efficiency and extended operational range. Furthermore, the actively tilting arms enable thrust vectoring in a 2D plane. This 2D thrust vectoring decouples forward translation and pitch rotation, allowing us to directly actuate 5 of the 6 DOFs of the quadcopter. This contrasts with conventional quadcopters, which typically actuate only 4 DOFs. This decoupling enhances agility and maneuverability, particularly in pitch rotation and forward translation, which are crucial for navigating complex environments. PairTilt prioritizes these key degrees of freedom for efficient flight, like most aircraft, which greatly improves simplicity. This capability distinguishes PairTilt from standard quadcopters with fixed rotors and offers a simpler alternative to omnidirectional designs that require complex actuation mechanisms for full 6-DoF control.

The primary contribution of this work lies in PairTilt’s unique design within the spectrum of tilt-rotor UAV configurations. By strategically balancing simplicity, efficiency, and agility, PairTilt achieves a distinctive combination of performance characteristics. This is achieved through:

- **Simplified Tilt Mechanism:** Pairwise rotor coupling reduces servo torque requirements and overall complexity compared to omnidirectional tilt-rotor designs by mounting two oppositely rotating rotors on each arm, effectively canceling out the gyroscopic torques that the servos must overcome.
- **Aerodynamic Efficiency:** The tilt-rotor configuration minimizes drag, leading to improved energy efficiency and extended flight times, surpassing the capabilities of standard quadcopters.
- **Enhanced Maneuverability:** The decoupling of forward translation and pitch rotation improves agility and allows for novel maneuvers, exceeding the capabilities of fixed-rotor designs while maintaining simplicity.

This design is validated through extensive testing focusing on agility, compact hovering capabilities, sensor pointing, and energy efficiency. The results demonstrate PairTilt’s practical effectiveness and its potential to significantly enhance various aerial operations, including search and rescue, package delivery, surveillance, inspection, and drone racing.

Furthermore, PairTilt contributes to the development of adaptive aerial robots by incorporating two internal DOFs, enabling in-flight reconfiguration of the rotor configuration. This dynamic shape adaptation, inspired by soft robotics, allows the drone to optimize performance for specific tasks or environmental conditions. PairTilt represents a compelling balance between mechanical complexity and meaningful morphological adaptation, opening new possibilities for versatile aerial robots operating in complex environments.

4.2 Overview

This section provides an overview of the system. Here, we introduce the notation that will be used throughout the document. We also present a dynamic model of PairTilt, with a detailed discussion of the design trade-offs in Section 3.

4.2.1 Notation

We follow the notation in [46] to define the vehicle model. Nonbold symbols like m represent scalars, lowercase bold symbols like \mathbf{g} represent vectors, and uppercase bold symbols like \mathbf{J} represent matrices. Subscripts such as m_C represent the body to which the symbol refers, and superscripts such as \mathbf{g}^E represent the frame in which the vector is expressed. A second subscript or superscript such as $\boldsymbol{\omega}_{CE}$ or \mathbf{R}^{CE} represents what the quantity is defined with respect to. However, the special superscript T represents the transpose of a matrix. To express a cross product, we use the form of a skew-symmetric matrix such that $\mathbf{a} \times \mathbf{b} = \mathbf{S}(\mathbf{a})\mathbf{b}$. The symbol \mathbf{d} represents a displacement, $\boldsymbol{\omega}$ represents an angular velocity, and \mathbf{R} represents a rotational matrix.

4.2.2 Vehicle Structure

Figure 4.2 illustrates the proposed vehicle. This vehicle is structured similarly to a standard quadcopter, but features an H-shaped frame with tiltable rotors. It consists of three coupled rigid bodies: the central body and two arms, each equipped with two rotors. The Earth frame is designated as E , and the central body frame as C , and the frame for each arm as A_i for $i \in \{1, 2, 3, 4\}$. In the central body frame, the x-axis \mathbf{x}_C points forward, and the z-axis \mathbf{z}_C extends upward from the body's top surface. In any arm frame A_i , the y-axis \mathbf{y}_{A_i} points in the same direction as \mathbf{y}_C , and the z-axis \mathbf{z}_{A_i} points along the rotor axis. The rotation matrix \mathbf{R}^{CE} transforms the vectors from the Earth frame E to the central body frame C , such that a vector in the Earth frame \mathbf{v}^E is represented in the central body frame as $\mathbf{v}^C = \mathbf{R}^{CE}\mathbf{v}^E$.

Each arm is able to tilt around the pitch axis \mathbf{y}_C of the central body frame C . The front arm controls the tilt for rotors 1 and 4, and the rear arm for rotors 2 and 3, with actuation provided by servos. The arms function independently and incorporate a total of six actuators: four propeller motors and two servos for rotor tilting.

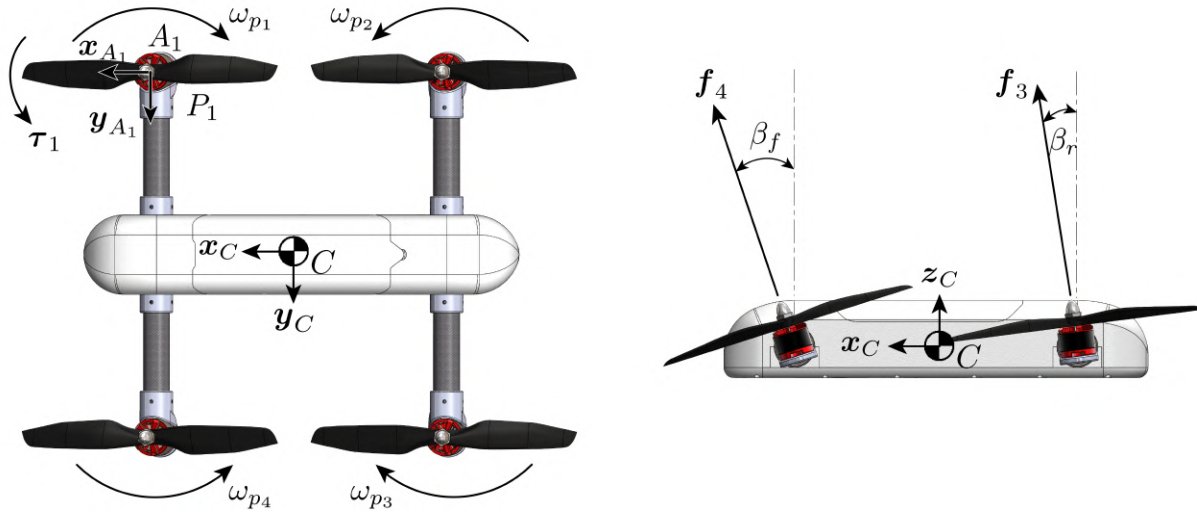


Figure 4.2: Top and left views of the vehicle. The white fuselage is defined as the central body. The black carbon fiber tubes with grey couplers, on which rotors are attached, are defined as the arms.

4.2.3 Rotor-tilting coupling

In our tilt-rotor UAV design, we opt to couple the two front rotors on a single arm and the two rear rotors on another, each driven by a single servo motor. This configuration reduces the complexity of the system compared to a design that uses four independent servos, one for each rotor. The reduction in complexity also extends to the torque requirement on the servos due to the gyroscopic effects experienced during maneuvers.

The gyroscopic torque of rotor i on a tilting arm is:

$$\boldsymbol{\tau}_{gyro} = J_{p_i} \mathbf{S}(\boldsymbol{\omega}_{A_i E}^{A_i}) \omega_{p_i} \mathbf{z}_{A_i}^{A_i} \quad (4.1)$$

where J_{p_i} represents the moment of inertia of a rotor around its axis of rotation, $\boldsymbol{\omega}_{A_i E}^{A_i}$ is the angular velocity of the arm in the tilting arm frame, ω_{p_i} is the propeller speed, and $\mathbf{z}_{A_i}^{A_i}$ is the rotor axis. Since the tilting arm is constrained to only rotate around the pitch axis, the torque reflected on the servo is thus:

$$\tau_{gyro,y} = J_{p_i} \omega_{A_i E,x}^{A_i} \omega_{p_i} \quad (4.2)$$

Fast maneuvers significantly increase gyroscopic torques as a result of the high rotational speeds of the rotors. The product of the rotor's momentum ($J_{p_i} \omega_{p_i}$) and the roll speed contributes to high gyroscopic torques, necessitating more powerful, heavier, and complex servo systems. To mitigate this, coupling the rotations of adjacent rotors that spin in opposite

directions effectively cancels out their net angular momentum since their speeds are similar, thus substantially reducing the resultant gyroscopic torque.

However, coupling rotors introduces complexity due to the need for mechanical linkages such as external connecting rods. To mitigate this, our vehicle adopts an H-shaped configuration, where each tiltable arm, front and rear, is equipped with two rotors and driven by a single servo. This configuration not only reduces structural complexity but also lessens the demand for high-torque servos, streamlining the overall design. Moreover, the H-shaped configuration can be aerodynamically optimized for forward flight, the preferred direction for most aerial vehicles, improving efficiency and extending range.

4.2.4 Dynamics

By coupling the rotors, the dynamics of the quadcopter become simpler. The system primarily involves three forces: the thrust produced, the resistive torque from that thrust, and a minimal torque from rotor acceleration (since rotors have small inertia). Additionally, the tilting arms have a low moment of inertia and slow acceleration, allowing us to neglect the torque involved in accelerating these arms. Consequently, the quadcopter behaves like a single rigid body, whose translational dynamics in the Earth frame E and rotational dynamics in the central body frame C can be simplified to:

$$\ddot{\mathbf{d}}_{CE}^E = \mathbf{g}^E + \frac{1}{m_\Sigma} \mathbf{R}^{EC} \mathbf{f}_\Sigma^C \quad (4.3)$$

$$\dot{\boldsymbol{\omega}}_{CE}^C = (\mathbf{J}_\Sigma^C)^{-1} (\boldsymbol{\tau}_\Sigma^C - \mathbf{S}(\boldsymbol{\omega}_{CE}^C) \mathbf{J}_\Sigma^C \boldsymbol{\omega}_{CE}^C) \quad (4.4)$$

Where \mathbf{J}_Σ represents the moment of inertia of the entire quadcopter, m_Σ denotes the mass of the whole vehicle, \mathbf{f}_Σ is the net force generated by the four rotors, and $\boldsymbol{\tau}_\Sigma$ is the net torque produced by the rotors. Assuming operation near hover, the dynamics simplify further: rotor thrust is considered only along its axis, and torque is assumed to act around its axis in the direction opposite to rotation. Since the rotor torque is proportional to the thrust and considering that the rotor axis direction is dictated by the tilt angles with tilting occurring around \mathbf{y}_C , the force and moment can be written as:

$$\mathbf{f}_\Sigma^C = (f_1 + f_4) \begin{bmatrix} s\beta_f \\ 0 \\ c\beta_f \end{bmatrix} + (f_2 + f_3) \begin{bmatrix} s\beta_r \\ 0 \\ c\beta_r \end{bmatrix} \quad (4.5)$$

$$\boldsymbol{\tau}_\Sigma^C = f_1 \begin{bmatrix} ks\beta_f - l_y c\beta_f \\ -l_x c\beta_f \\ kc\beta_f + l_y s\beta_f \end{bmatrix} + f_2 \begin{bmatrix} -ks\beta_r - l_y c\beta_r \\ l_x c\beta_r \\ -kc\beta_r + l_y s\beta_r \end{bmatrix} + f_3 \begin{bmatrix} ks\beta_r + l_y c\beta_r \\ l_x c\beta_r \\ kc\beta_r - l_y s\beta_r \end{bmatrix} + f_4 \begin{bmatrix} -ks\beta_f + l_y c\beta_f \\ -l_x c\beta_f \\ -kc\beta_f - l_y s\beta_f \end{bmatrix} \quad (4.6)$$

Where k is the propeller thrust to torque constant, with $k > 0$ indicating that rotor 1 spins clockwise. l_x is the distance between a rotor and the center of the vehicle frame along

the \mathbf{x}_C axis, and l_y is the distance between a rotor and the center of the vehicle frame along the \mathbf{y}_C axis. Additionally, β_f and β_r represent the tilting angles of the front and rear arms, respectively. These angles are defined as the angle between the rotor axis and \mathbf{z}_C , measured when the rotor is rotated around $\mathbf{y}_{A_i} = \mathbf{y}_C$, as shown in Figure 4.2. Consequently, the dynamics of PairTilt can be described using the six actuator inputs $\mathbf{u} = [\mathbf{f}; \boldsymbol{\beta}]$: the four rotor thrusts $\mathbf{f} = [f_1, f_2, f_3, f_4]^T$ and the two tilting angles $\boldsymbol{\beta} = [\beta_f, \beta_r]^T$.

4.3 Design Analysis

This section analyzes the design choices of PairTilt and compares its performance with existing UAV platforms. We begin with a multi-actuation analysis, examining the impact of PairTilt's unique tilting mechanism on its dynamic capabilities and robustness. We then delve into a detailed evaluation of PairTilt's agility, energy efficiency, and overall system performance, emphasizing its suitability for extended missions in complex environments. Finally, we compare PairTilt with other UAV designs, showcasing its balanced approach to simplicity, efficiency, and agility.

4.3.1 Robustness and Actuation Analysis

To assess the impact of the tiltable rotors on PairTilt's dynamic capabilities and controllability, we conducted a robustness and actuation analysis. This involved linearizing the system dynamics and evaluating both the rank of the input matrix \mathbf{B} and the system's response to disturbances using an \mathcal{H}_2 analysis. This provides insights into how the addition of two tilting servos affects the system's degrees of freedom and robustness across different operating conditions.

We begin by linearizing the system dynamics in Equations 4.5 and 4.6 around hover to obtain a state-space representation. First, we align the vehicle's body-fixed frame with the Earth frame, such that $\mathbf{x}_C = \mathbf{x}_E, \mathbf{y}_C = \mathbf{y}_E, \mathbf{z}_C = \mathbf{z}_E$. Then, we rotate the vehicle initially aligned with the Earth frame around \mathbf{y}_C by an angle θ' , defining a new intermediate frame E' as shown in Figure 4.3. Note that this intermediate frame is static and does not rotate with the vehicle in motion.

We incorporate the intermediate frame, E' , into the equations of motion. Considering the small angular rates associated with hovering, we neglect the term $\mathbf{S}(\boldsymbol{\omega}_{CE}^C) \mathbf{J}_\Sigma^C \boldsymbol{\omega}_{CE}^C$. Additionally, we introduce a wind disturbance force vector, $\mathbf{f}_d^E = [f_{d,x}, f_{d,y}, f_{d,z}]^T$, representing forces acting along the x, y, and z axes of the E frame. This yields the following dynamic equations:

$$\ddot{\mathbf{d}}_{CE}^E = \mathbf{g}^E + \frac{1}{m_\Sigma} \left(\mathbf{R}^{EE'} \mathbf{R}^{E'C} \mathbf{f}_\Sigma^C + \mathbf{f}_d^E \right) \quad (4.7)$$

$$\dot{\boldsymbol{\omega}}_{CE}^C = (\mathbf{J}_\Sigma^C)^{-1} \boldsymbol{\tau}_\Sigma^C \quad (4.8)$$

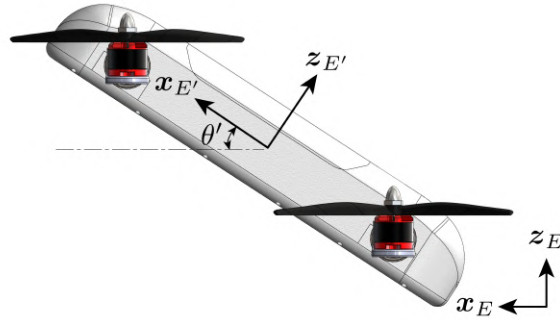


Figure 4.3: Left view of the vehicle and the rotated intermediate frame E' . Note that this intermediate frame is static and does not rotate with the vehicle in actual motion, it is defined to facilitate linearizing the dynamics of the vehicle when hovering near a pitch angle of θ' .

We now define the states, states derivatives, and inputs of the system for linearization:

$$\mathbf{x} = \begin{bmatrix} \mathbf{d}_{CE}^E \\ \dot{\mathbf{d}}_{CE}^E \\ \Delta\boldsymbol{\theta} \\ \boldsymbol{\omega}_{CE}^C \end{bmatrix} = \begin{bmatrix} \mathbf{s} \\ \mathbf{v} \\ \Delta\boldsymbol{\theta} \\ \boldsymbol{\omega} \end{bmatrix}, \quad \dot{\mathbf{x}} = \begin{bmatrix} \mathbf{v} \\ \ddot{\mathbf{d}}_{CE}^E \\ \boldsymbol{\omega} \\ \dot{\boldsymbol{\omega}}_{CE}^C \end{bmatrix}, \quad \mathbf{u} = \begin{bmatrix} \mathbf{f} \\ \boldsymbol{\beta} \end{bmatrix}, \quad \mathbf{d} = \mathbf{f}_d^E \quad (4.9)$$

Where $\Delta\boldsymbol{\theta} = [\Delta\phi, \Delta\theta, \Delta\psi]^T$ are the roll, pitch and yaw Euler angles of $\mathbf{R}^{E'C}$ with yaw-pitch-roll rotation sequence. We use Δ notations to distinguish this from the standard Euler representation relating frame C to frame E , which would encounter singularities at $\theta = \pm\frac{\pi}{2}$. The system can now be linearized around equilibrium to get the corresponding \mathbf{A} , \mathbf{B} and \mathbf{B}_d matrices, using $\mathbf{x}_{eq} = [0, 0, 0, 0, 0, 0, 0, 0, 0, 0, 0, 0]^T$, and $\mathbf{u}_{eq} = [\frac{m\Sigma g}{4}, \frac{m\Sigma g}{4}, \frac{m\Sigma g}{4}, \frac{m\Sigma g}{4}, -\theta', -\theta']^T$, based on the assumptions that each rotor produces equal thrust to balance the weight, and the servos rotate both arms to align with the vertical.

Our analysis shows that PairTilt's \mathbf{B} matrix has a rank of 5 regardless of the hover pitch angle θ' , which means there are 5 independent control directions available at any given moment. Notably, the row corresponding to \ddot{y} is all zeros in \mathbf{B} , signifying that \ddot{y} cannot be directly controlled. This limitation arises because the thrust vector can only vary within a 2D plane; achieving acceleration outside this plane necessitates changes in the drone's attitude, coupling attitude with lateral motion. However, the addition of the tiltable servos introduces an extra degree of freedom by decoupling pitch rotation from forward translation. While the system remains underactuated, the controllability matrix has a full rank of 12 regardless of the hover pitch angle θ' , confirming its controllability.

To further evaluate the system's robustness, we conducted an \mathcal{H}_2 analysis. This analysis focuses on how the vehicle's position responds to force disturbances \mathbf{d} , when hovering at

different pitch angles θ' . We define the performance vector \mathbf{z} as:

$$\mathbf{z} = \begin{bmatrix} \mathbf{s} \\ \gamma_1 \Delta\psi \\ \gamma_2 \mathbf{f} \\ \gamma_3 \boldsymbol{\beta} \end{bmatrix} \quad (4.10)$$

We select the scaling factors $\{\gamma_1 = 13.5 \text{ m/rad}, \gamma_2 = 0.5 \text{ m/N}, \gamma_3 = 1.2 \text{ m/rad}\}$ to align the LQR controller's behavior with that of the nonlinear controller presented later in this chapter. This choice reflects our objective of maintaining constant position and yaw. The corresponding \mathbf{C} and \mathbf{D} matrices are then determined based on the defined output vector \mathbf{z} . Using the relationships $\mathbf{Q} = \mathbf{C}^T \mathbf{C}$ and $\mathbf{R} = \mathbf{D}^T \mathbf{D}$, we compute the LQR controller gain matrix \mathbf{K} . Consequently, the closed-loop system dynamics can be expressed as $\dot{\mathbf{x}} = (\mathbf{A} - \mathbf{BK})\mathbf{x} + \mathbf{B}_d \mathbf{d}$.

Finally, we define \mathbf{C}_{H_2} and \mathbf{D}_{H_2} to focus on the position response, which lets us evaluate the system's \mathcal{H}_2 norm. This provides a measure of how sensitive the system is to wind disturbances, reflected in the deviation of its position. To make the comparisons clearer, we normalize these \mathcal{H}_2 norms against the baseline at $\theta' = 0^\circ$, giving us a relative sense of how well the system handles wind gusts under different configurations.

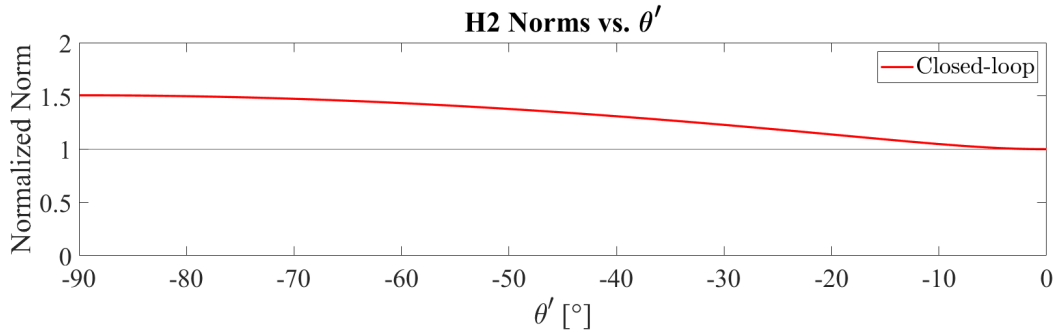


Figure 4.4: Normalized \mathcal{H}_2 norm variation with pitch angle θ' , representing the relative position response to force disturbances at different hover configurations. The \mathcal{H}_2 norm increases monotonically as the vehicle transitions from a flat hover ($\theta' = 0^\circ$) to a fully nose-up hover ($\theta' = -90^\circ$), indicating a gradual reduction in disturbance rejection. However, the system maintains acceptable robustness across the range of hover orientations.

Figure 4.4 illustrates the variation of the normalized \mathcal{H}_2 norm with respect to the hover pitch angle θ' . The plot reveals a monotonic increase in the \mathcal{H}_2 norm as the pitch angle decreases from 0° (flat hover) to -90° (fully nose-up hover), indicating a gradual reduction in disturbance rejection as the vehicle transitions towards a nose-up orientation. At $\theta' = -90^\circ$,

the normalized \mathcal{H}_2 norm is approximately 1.5 times greater than that at $\theta' = 0^\circ$. Nevertheless, the system maintains acceptable robustness across the range of hover orientations, demonstrating its capacity in mitigating the impact of wind disturbances.

4.3.2 Agility

PairTilt exhibits enhanced agility compared to conventional quadcopters, primarily due to the decoupling of its pitch rotational and forward translational dynamics through 2D thrust vectoring. This feature allows for independent control of pitch and forward translation, enabling rapid and agile maneuvers. These capabilities are particularly advantageous in complex environments, facilitating unique flight patterns like sustained nose-up hovering, which is useful for navigating confined spaces and performing specialized tasks.

Rapid Horizontal Motion

Conventional quadcopters achieve forward motion by pitching the entire aircraft, coupling rotational and translational dynamics. This results in less efficient maneuvers, especially when rapid adjustments are needed (e.g., obstacle avoidance). In contrast, PairTilt decouples forward translation from pitch rotation. By tilting the rotors, forward acceleration is achieved without altering the main body's orientation (Figure 4.5). This enables quicker position responses, crucial for navigating complex environments.

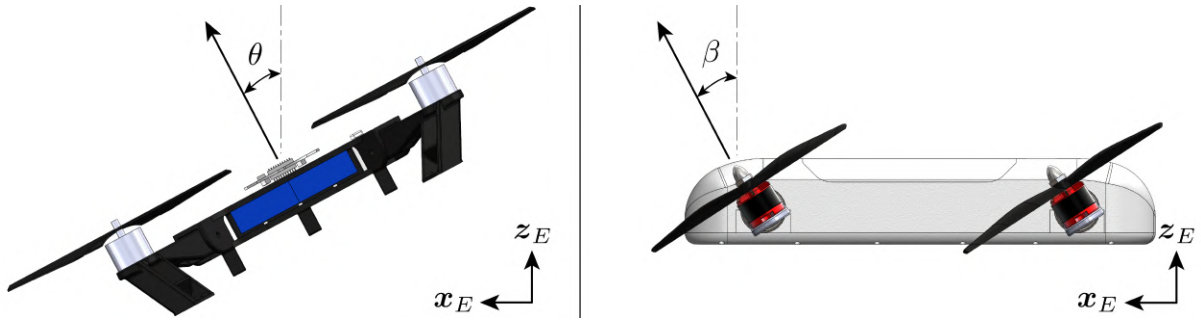


Figure 4.5: Horizontal thrust generation near hover. Left: Conventional quadcopter requires pitch change. Right: PairTilt tilts rotors while remaining level.

Linearizing the dynamics [53] reveals that a conventional quadcopter's forward acceleration \ddot{x} is proportional to its pitch angle θ : $\ddot{x} = g\theta$. Thus, faster pitch changes lead to faster acceleration. For a conventional quadcopter, the maximum pitch angular acceleration around hover is $\ddot{\theta}_{max} = mgl_x/I_{yy}$, where l_x is half the distance between the front and back rotors and I_{yy} is the moment of inertia of the vehicle around its \mathbf{y}_C . The maximum angular acceleration is limited by the maximum pitch torque that the propellers can produce without

the vehicle dropping in height, where the rear propellers generate a combined thrust equal to the vehicle’s weight, while the front propellers produce zero thrust.

Similarly, linearizing Equation 4.5 and assuming constant pitch while varying the rotor-tilt angle reveals that the linear acceleration in the roll-direction of the proposed tilt-rotor is given by $\ddot{x} = g\beta$. The rate of forward acceleration is primarily determined by the maximum angular acceleration of the tilting arms, $\ddot{\beta}_{max} = M_{servo}/I_{arm}$, where M_{servo} is the servo torque and I_{arm} is the arm’s moment of inertia. Importantly, this angular acceleration is independent of the vehicle’s mass, and I_{arm} is significantly smaller than I_{yy} , allowing for faster actuation. In our experimental vehicle, using small 12V servos resulted in a $\ddot{\beta}_{max}$ approximately 100 times greater than $\ddot{\theta}_{max}$, significantly enhancing agility.

In larger-scale applications, the scaling behaviors of these physical parameters become critical. Denoting L as the length scale of the vehicle, I_{yy} scales with L^5 , mass m scales with L^3 , and arm length l_x scales with L . Consequently, $\ddot{\theta}_{max}$ scales in reverse with L , suggesting a decrease in agility for conventional quadcopters as size increases, a limitation that cannot be easily overcome by simply employing more powerful motors due to inherent dynamic constraints. In contrast, the tilt-rotor design allows for the use of larger motors to compensate for increases in I_{arm} , maintaining comparable agility levels. It should be noted that these analyses assume instantaneous thrust changes in conventional quadcopters, which is unrealistic. Propeller dynamics further slow the response, a problem exacerbated in larger drones where propeller inertia scales with L^5 , which is why larger UAVs often incorporate variable-pitch propellers. As a result, the proposed tilt-rotor design should even be relatively more agile as the vehicle size scales up.

Although the agility of the proposed tilt-rotor vehicle can also be limited by the rate of the servo motors, our later experiments indicate that, even with these limitations, the tilt-rotor configuration can respond substantially faster. Further improvements can be made by adjusting the gear ratio, enhancing response times during directional changes since the servos are not continuously subject to high loads, allowing them to operate at higher speeds.

Independent Pitch Control

Unlike other tilt-rotor designs such as [51, 18], our proposed vehicle is equipped with rotors that are pairwise coupled on two separate arms, each designed to operate independently. This capability is primarily implemented to enhance pitch rotation agility, particularly when both arms are tilted forward.

Consider a tilt-rotor design where all rotors are coupled to tilt at the same angle. Let’s compare this ”all-coupled” configuration, hovering at a negative pitch angle, to our proposed vehicle as depicted in Figure 4.6. As the tilt angle β increases, the maximum achievable pitch torque $\tau_{y,max} = 2mgl_x \cos \beta$ decreases. At large tilt angles, achieving sufficient pitch torque in this configuration requires a significant thrust increase, reducing efficiency and potentially leading to instability. This is because the thrust vectors become less perpendicular to the body, requiring more thrust to generate the same torque. Furthermore, higher speeds inherently demand increased tilting to counteract aerodynamic drag. At these elevated speeds,

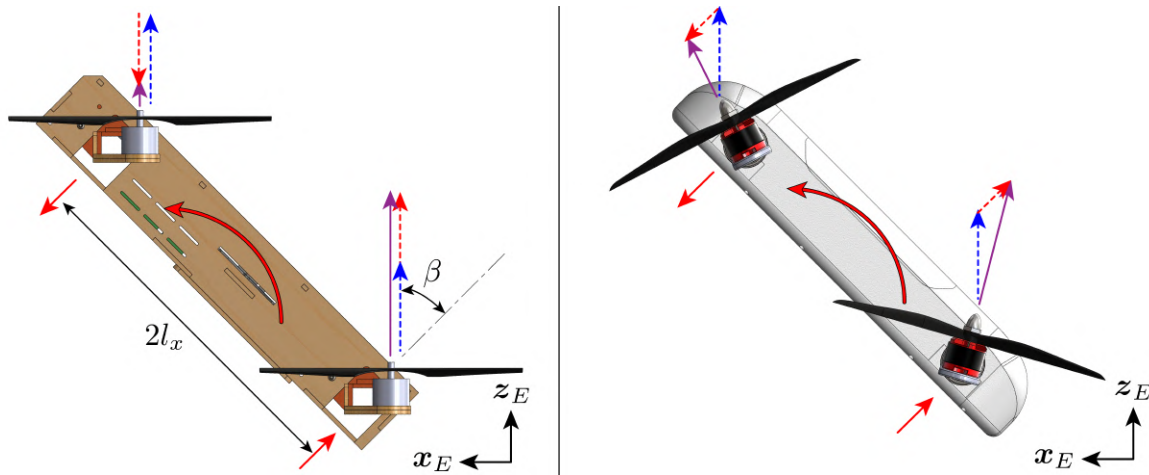


Figure 4.6: Comparison of pitch torque capabilities between all-coupled and independently-controlled tilt-rotor designs. The thrust required to hover (blue dashed arrows) is split equally across the front and rear rotors. The pitch torque (red solid curly arrow) is broken into a force couple (red solid straight arrows) at the front and rear arms. This force couple is converted to a new force couple that the vehicle can produce (red dashed arrows). The resultant thrust from adding the hover thrust and the vector thrust to generate pitch torque is shown as purple solid arrows. Left: the all-coupled tilt-rotor requires a larger change in thrust to produce equivalent pitch torque due to thrust vectors being less perpendicular to the vehicle body, decreasing efficiency and increasing stability challenges at higher speeds. Right: PairTilt allows effective pitch torque generation without significant thrust alteration by adjusting the relative rotor angles, enhancing agility and stability for novel flight maneuvers such as sustained nose-up hovering.

wind-induced disturbances also become more pronounced, posing challenges to the UAV's agility and stability. Notably, at a 90-degree tilt, this configuration completely loses pitch controllability.

In contrast, the proposed vehicle design features independently operating front and back arms, effectively allowing for thrust vectoring in the x - z plane. The independent arms can produce the required pitch torque by adjusting the relative angles of the rotors. Since the arms can rotate, it is possible to break down the required pitch torque into a force couple that is perpendicular to the vehicle body. These forces can then be added to the front and back rotor thrusts respectively, resulting in changes to the tilting angles and thrust magnitudes, as shown in Figure 4.6. Moreover, such changes in magnitude are the smallest possible because the forces are perpendicular to the vehicle body, thus improving efficiency.

Having demonstrated robust flight control at any hover pitch angle in Section 3.1, PairTilt can perform novel maneuvers that are essential for operations in urban and complex environments. One such maneuver includes the ability to fly with the nose pointing upward.

This capability significantly reduces the vehicle’s spatial footprint, as depicted in Figure 4.7, allowing for operation in confined spaces where traditional UAVs might not fit.

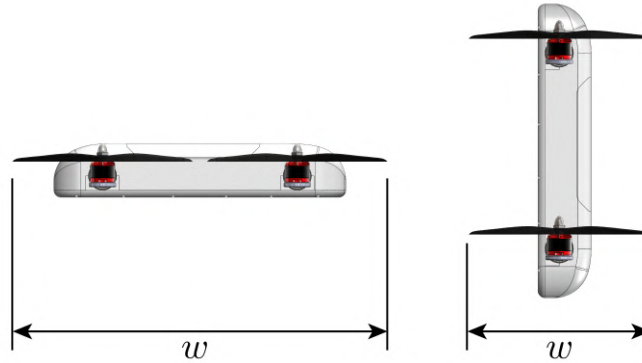


Figure 4.7: Comparison of vehicle footprint for the PairTilt vehicle during hover: (left) configured for conventional 0° pitch flight, (right) configured for -90° pitch flight. The width (w) in the conventional configuration must be at least twice the propeller diameter to accommodate propeller clearance, while the width is reduced to a single propeller diameter in the -90° pitch configuration.

The independent control of rotor pitch angles also enhances the UAV’s sensor pointing capabilities. By adjusting the pitch angle independently of the UAV’s flight path, sensors mounted on the UAV can maintain a fixed position on a target or scan an area more effectively, which is particularly advantageous for tasks requiring precise geolocation, surveillance, or environmental monitoring.

These maneuvers are not only indicative of the UAV’s agility but also enhance its functionality in diverse operating conditions, making it a versatile tool for both civilian and commercial applications.

4.3.3 Experimental Vehicle Design

The properties of the experimental vehicle are given in Table 4.1. The vehicle’s overall size is designed to be similar to a commonly used quadcopter. Each of the four rotors consists of an MT2208 BLDC motor and an 8” 8045 propeller. Each of the two tilting arms is driven by an HX-12H lightweight servo. The fuselage, inspired by high-speed rail trains, is aerodynamically designed for low drag during fast flight. Drag and lift coefficients were determined by simulating airflow in SolidWorks whose details will be discussed in the following section. The rotor tilting mechanism, including motors and bearings, adds approximately 65 grams, or 7%, to the vehicle’s mass.

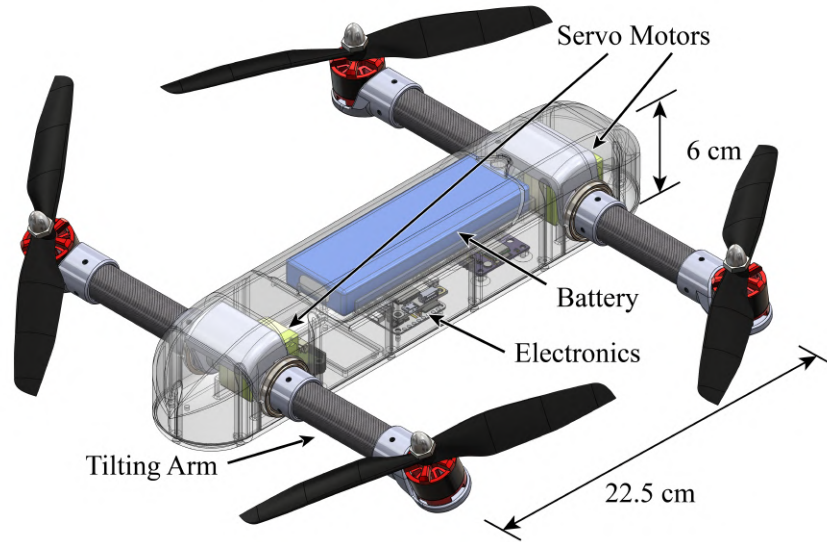


Figure 4.8: Isometric view of the experimental vehicle.

Symbol	Parameter	Value
m_T	Rotor-tilting mechanism mass	65 g
$m_{\Sigma,T}$	Vehicle mass with the tilting mechanism	1000 g
$m_{\Sigma,!T}$	Vehicle mass without the tilting mechanism	935 g
A	Reference area	0.05 m^2
C_D	Fitted drag coefficient equation	$-0.045\theta^3 + 0.21\theta^2 + 0.12\theta + 0.1$
C_L	Fitted lift coefficient equation	$0.081\theta^2 - 0.18\theta - 0.0086$
β_{max}	Maximum tilting angle	110°
β_{min}	Minimum tilting angle	-20°

Table 4.1: Experimental vehicle frame properties.

4.3.4 Energy Efficiency and Range

Rotor tilting allows the vehicle to maintain a reduced pitch angle during high-speed flight. This reduction in pitch angle not only lowers aerodynamic drag but also prevents the generation of counterproductive lift forces often associated with higher pitch angles, as demonstrated in Figure 4.9. While first-person view (FPV) drones commonly utilize an angled frame to minimize drag and lift during high-speed flight, this approach introduces challenges such as increased bulkiness, which affects storage, and reduced pitch rotation agility like discussed in Section 3.2.2. Additionally, although an airfoil-shaped frame could enhance lift and further decrease energy consumption, the PairTilt design prioritizes minimizing drag

and does not incorporate an airfoil.

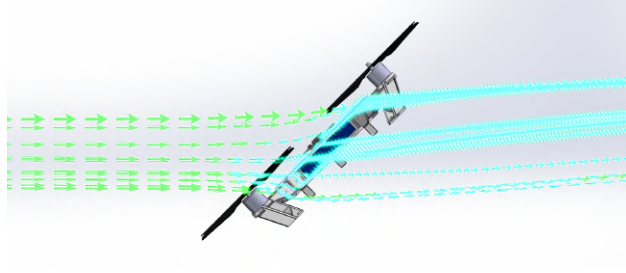


Figure 4.9: A conventional quadcopter would need to pitch forward to generate a forward thrust for high-speed flight. However, this creates a large drag area and induces downward lift on the vehicle, which limits its performance and efficiency for high-speed flight [51].

It is important to note that while the tilt-rotor configuration enhances aerodynamics, the mechanisms required for tilting add weight, increasing power consumption during hover or low-speed flight. This makes PairTilt suitable for missions requiring extended range, such as package delivery, but less suitable for tasks like monitoring where the vehicle is mostly hovering.

To assess the impact of these factors, we employ the following aerodynamic model for analysis where the vehicle is cruising in the horizontal direction at a fixed height. For a more straightforward comparison in our analysis, we assume that the front and back arms of PairTilt rotate at the same angle.

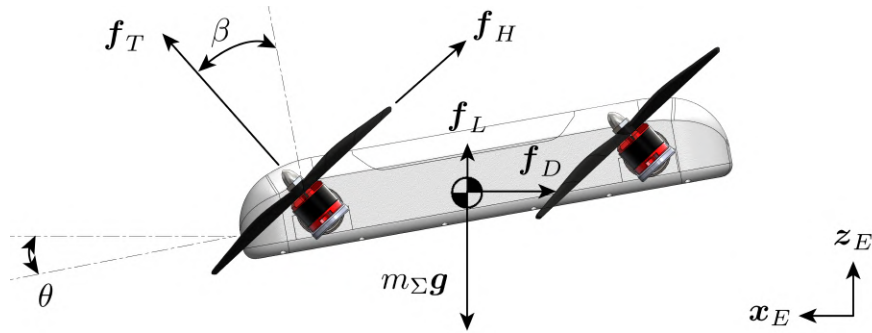


Figure 4.10: Free-body diagram of the vehicle when cruising. The tilting angle β is the angle between the arm and the central body, and the angle of attack θ is the pitch angle.

The force balance is thus:

$$\Sigma f_T \sin(\theta + \beta) - \Sigma f_H \cos(\theta + \beta) = \frac{1}{2} C_D(\theta) \rho A v^2 \quad (4.11)$$

$$\Sigma f_T \cos(\theta + \beta) + \Sigma f_H \sin(\theta + \beta) = m_{\Sigma}g - \frac{1}{2}C_L(\theta)\rho Av^2 \quad (4.12)$$

Where Σf_T is the total thrust force from the propellers, Σf_H is the total drag force from the propellers, θ is the pitch angle, β is the rotor tilt angle, $C_D(\theta)$ and $C_L(\theta)$ are the drag and lift coefficients, ρ is the density of air, v is the speed of the quadcopter, and A is the reference area which is the projection area of the vehicle onto its top surface. To determine the aerodynamic coefficients $C_D(\theta)$ and $C_L(\theta)$, we conducted a series of CFD simulations. The vehicle was initially designed in SolidWorks, and then the body model (excluding propellers) was imported into SolidWorks Flow Simulation. Within the Flow Simulation environment, we fixed the wind direction along the Earth x-axis and varied the vehicle's pitch angle (θ) to generate different airflow conditions. This allowed us to analyze the forces exerted on the airframe at various orientations to the oncoming wind. The resulting body forces from these simulations were then used to fit the drag and lift coefficients, $C_D(\theta)$ and $C_L(\theta)$, respectively. The files used for CFD with instructions on how to repeat the process can be found here: <https://drive.google.com/file/d/1FsD6KufTcDRzIooXxiEUGX9odgI79Qdw/view?usp=sharing>.

In addition, we acknowledge that propeller overlap might occur in the tilt-rotor configuration; however, we assume that this overlap does not significantly affect power consumption. This assumption is based on research findings which suggest that small overlap does not substantially alter power requirements [54]. Assuming that the center of the mass of the vehicle is at the midpoint of the two arm axes, and the moment on the vehicle is 0 Nm, the 4 rotors can be regarded to be producing the same amount of thrust and drawing the same amount of power. Finally, using the moving propeller model from [55], the force balance can be rewritten as:

$$4f_T(\omega, v, \theta + \beta) \sin(\theta + \beta) - 4f_H(\omega, v, \theta + \beta) \cos(\theta + \beta) = \frac{1}{2}C_D(\theta)\rho Av^2 \quad (4.13)$$

$$4f_T(\omega, v, \theta + \beta) \cos(\theta + \beta) + 4f_H(\omega, v, \theta + \beta) \sin(\theta + \beta) = m_{\Sigma}g - \frac{1}{2}C_L(\theta)\rho Av^2 \quad (4.14)$$

And the mechanical power required to drive the rotors is:

$$P = 4\tau_p(\omega, v, \theta + \beta)\omega \quad (4.15)$$

Where $\tau_p(\omega, v, \theta + \beta)$ is the yaw torque from the propeller. In the case of conventional quadcopters, the tilt angle β is always zero, and the vehicle adjusts its pitch angle θ to produce forward thrust. Conversely, for PairTilt, we maintain θ at zero while varying β to generate thrust. The above equations can be solved to find the energy. Utilizing parameters from the experimental vehicle, the above equations can be solved for and we can find the power required to fly at different speed for the 2 different types of vehicle. For a fair comparison, we will use the same vehicle frame parameters for the conventional quadcopter case, but reduces its weight by the weight entire rotor-tilting mechanism.

As depicted in Figure 4.11, the conventional quadcopter is more energy-efficient at hover due to its lower weight, optimal for tasks requiring minimal displacement. However, this

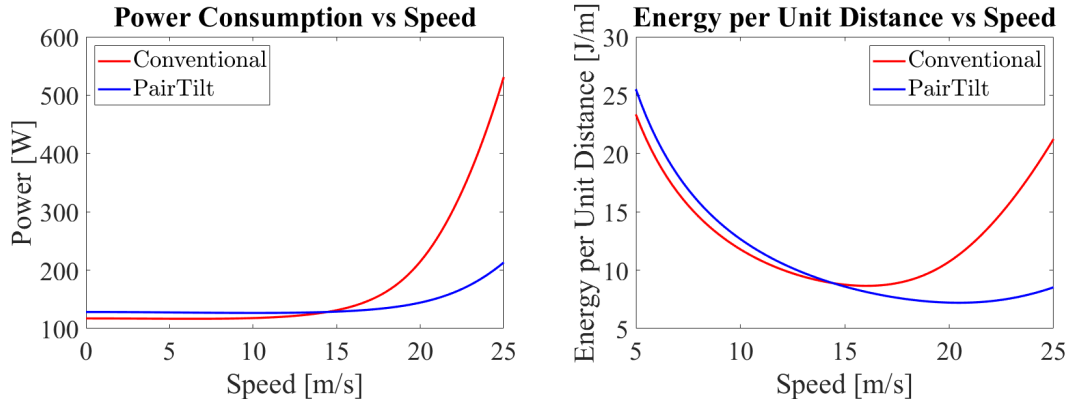


Figure 4.11: Comparison of electrical power consumption and energy efficiency between the tilt-rotor (PairTilt) and a conventional quadcopter. The results here account for motor efficiency in PairTilt. The left graph shows the power consumption, highlighting that the conventional quadcopter is more efficient at hover due to its lower weight. However, as speed increases, its efficiency declines, reaching parity with the tilt-rotor at approximately 14 m/s. The right graph illustrates energy per unit distance, showing the tilt-rotor’s superior range under the optimal cruise speed.

efficiency advantage declines as flight speed increases, reaching an equivalence with the tilt-rotor at around 14 m/s.

Beyond this point, PairTilt’s aerodynamic properties, which effectively minimize drag, allows it to surpass the conventional quadcopter in terms of power efficiency and maintain a longer range at optimal cruise speeds. For PairTilt, the lowest energy consumption achieved is 7.2 Joules per meter at a speed of 20 m/s. In contrast, the conventional quadcopter achieves its minimum energy usage of 8.7 Joules per meter at 16 m/s. This illustrates the tilt-rotor’s suitability for extended, high-speed missions, underscoring its potential utility in urban air mobility contexts where efficient travel over considerable distances is crucial.

4.3.5 Comparison with Other Designs

To effectively evaluate and compare PairTilt with different UAV designs, we use three key metrics: simplicity, efficiency, and agility. These metrics provide a comprehensive view of the strengths and trade-offs inherent in each design.

Simplicity Standard quadcopters are noted for their simplicity due to fewer moving parts and a straightforward control scheme [1]. In contrast, designs such as the hybrid quadcopters by Mikami and Uchiyama (2015) [17] introduce complexity that can complicate manufacturing and maintenance. However, passive tilt-rotor designs such as QUaRTM [51] offer lower

complexity by avoiding the use of additional actuators. On the other hand, PairTilt incorporates pairwise rotor tilting which, while moderately increasing complexity, does so less significantly than omnidirectional systems, which require many additional actuators for full 6DOF manipulation, impacting their practical simplicity and maintenance [22, 23, 13, 24]. In addition, by coupling the tilting arms, PairTilt requires lower servo torque and power compared to omnidirectional configurations due to the reduction in gyroscopic torque, as described in Equation 4.1. This also simplifies the complexity at the individual servo level.

Efficiency Efficiency in UAV designs varies widely. Standard quadcopters generally offer moderate efficiency and suffer from aerodynamic limitations [51]. Tilt-rotor and tilt-wing designs like those explored by Mikami and Uchiyama (2015) and Papachristos et al. (2013) [17, 16] enhance aerodynamic performance by allowing dynamic adjustments in rotor angles, which can outperform standard quads in terms of energy efficiency. PairTilt aims to further optimize this by ensuring that rotor adjustments enhance airflow and reduce drag without the extensive mechanical complexity seen in fully omnidirectional designs, which traditionally do not prioritize aerodynamic efficiency [22, 23, 13, 24].

Agility Agility is perhaps the most varied metric among UAV designs. Standard quads are limited by their fixed rotor configuration, while advanced systems like those studied by Ryll et al. (2012) and Nemati et al. (2016) offer great maneuverability with full 6DOF control [22, 23, 13, 24]. On the other hand, PairTilt enhances agility specifically in pitch rotation and forward translation - key aspects for operational effectiveness in preferred flight directions. This focus allows for improved response times and precise maneuverability in the most critical DOFs while maintaining a simpler and more robust system compared to fully omnidirectional configurations. Additionally, PairTilt reduces its mass by using less powerful servos, thanks to lower gyroscopic torque from arm coupling, thus enhancing agility. While PairTilt does not match the full agility of omni-directional UAVs, the trade-off in complexity for essential agility is justified given the operational scenarios most drones encounter.

As shown in Figure 4.12, each UAV design emphasizes different performance aspects. Standard quadcopters (grey) prioritize simplicity, while omnidirectional designs (yellow) achieve high agility at the expense of simplicity and efficiency. Underactuated wing VTOL designs (blue) focus on efficiency, but they compromise on simplicity and agility. PairTilt (red) stands out by balancing high agility and efficiency, while maintaining a simplicity level much closer to that of standard quadcopters.

By incorporating aspects of both traditional and advanced UAV designs, PairTilt strikes a balance, aiming for an optimal point where no single metric of performance is sacrificed for the gain of another, embodying the essence of Pareto efficiency in UAV design.

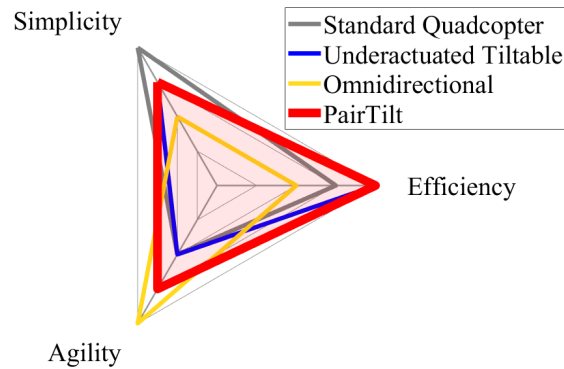


Figure 4.12: Radar plot comparing the performance metrics of various UAV designs. The plot includes three key metrics: simplicity, efficiency, and agility. The grey line represents the baseline standard quadcopter, which shows high simplicity but lower levels of agility and efficiency. The blue line indicates underactuated tilt-rotor/wing VTOL designs, which enhance efficiency but sacrifice simplicity and agility. The yellow line depicts omnidirectional designs, demonstrating high agility but at the cost of reduced simplicity and efficiency. The red line shows PairTilt, balancing high agility and efficiency while maintaining simplicity closer to that of standard quadcopters.

4.4 Control

We employ a model-based cascaded controller architecture for our tilt-rotor UAV, designed to enable autonomous tracking of desired position, velocity, acceleration, and orientation angles (yaw and pitch).

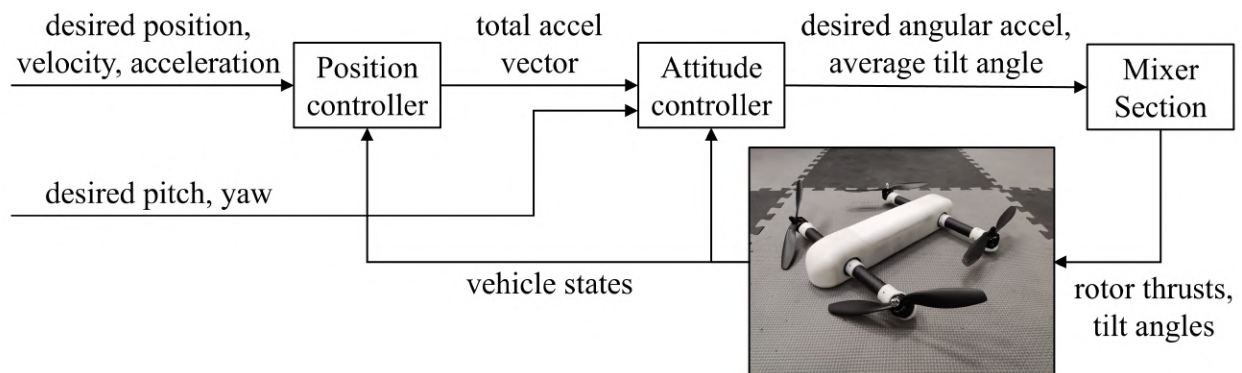


Figure 4.13: Block diagram of the quadcopter controller.

Position controller The position controller operates in the outermost loop of the control system. It takes the desired position, velocity, and acceleration as inputs, alongside the current states of position, velocity, and acceleration, to compute the desired acceleration. After calculating the desired acceleration, gravitational acceleration (\mathbf{g}) is added to determine the total acceleration vector that the vehicle should generate to achieve the desired trajectory.

$$\mathbf{a}_{des} = \omega_{nat}^2(\mathbf{p}_{des} - \mathbf{p}_{cur}) + 2\zeta\omega_{nat}(\mathbf{v}_{des} - \mathbf{v}_{cur}) + \mathbf{a}_{des,ff} \quad (4.16)$$

$$\mathbf{a}_{tot} = \mathbf{a}_{des} + \mathbf{g} \quad (4.17)$$

Attitude controller Following the position control loop, the attitude controller receives the total acceleration vector along with the desired pitch and yaw angles. Utilizing the current vehicle attitude as feedback, this controller outputs the necessary angular velocities and the average rotor tilt angle needed to align the vehicle's attitude with the total acceleration vector. Unlike controllers for conventional quadcopters, which align the x-component of total acceleration vector with propeller thrust by rotating the vehicle body, the PairTilt controller achieves this alignment by tilting the rotor arms. This results in a faster response, as discussed in Section 3.2. Desired angular acceleration is then computed based on these outputs and the current angular rates of the vehicle.

$$\hat{\mathbf{a}}_{tot} = \frac{\mathbf{a}_{tot}}{\|\mathbf{a}_{tot}\|} \quad (4.18)$$

$$\mathbf{n}_f = \hat{\mathbf{z}} \times \hat{\mathbf{a}}_{tot} \quad (4.19)$$

$$\beta_f = \arccos\left(\frac{\mathbf{a}_{tot}}{\|\mathbf{a}_{tot}\|} \cdot \hat{\mathbf{z}}\right) \quad (4.20)$$

$$\mathbf{R}_f = \text{axang2rotm}([\mathbf{n}_f/\|\mathbf{n}_f\|, \theta]) \cdot \text{axang2rotm}([0, 0, 1, \psi_{des}]) \quad (4.21)$$

$$\hat{\mathbf{x}}_0 = \frac{\mathbf{R}_f[:, 2] \times \hat{\mathbf{z}}}{\|\mathbf{R}_f[:, 2] \times \hat{\mathbf{z}}\|} \quad (4.22)$$

$$\hat{\mathbf{z}}_0 = \hat{\mathbf{x}}_0 \times \mathbf{R}_f[:, 2] \quad (4.23)$$

$$\mathbf{R}_0 = [\hat{\mathbf{x}}_0, \mathbf{R}_f[:, 2], \hat{\mathbf{z}}_0] \quad (4.24)$$

$$\mathbf{R}_{des} = \mathbf{R}_0 \cdot \text{axang2rotm}([0, 1, 0, \phi_{des}]) \quad (4.25)$$

$$\boldsymbol{\omega}_{des} = \boldsymbol{\tau}_{att} \oslash \text{rotmat2vec3d}(\mathbf{R}_{cur}^T \mathbf{R}_{des}) \quad (4.26)$$

$$\mathbf{n}_{tilt} = \mathbf{R}_{des}[:, 3] \times \mathbf{R}_f[:, 3] \quad (4.27)$$

$$\beta = \text{sign}(\mathbf{n}_{tilt} \cdot \mathbf{R}_f[:, 2]) \arccos(\mathbf{R}_{des}[:, 3] \cdot \mathbf{R}_f[:, 3]) \quad (4.28)$$

$$\mathbf{e}_\omega = \boldsymbol{\omega}_{des} - \boldsymbol{\omega}_{cur} \quad (4.29)$$

$$\boldsymbol{\alpha}_{des} = \boldsymbol{\tau}_\omega \oslash \mathbf{e}_\omega \quad (4.30)$$

Mixer section In the mixer section, the computed angular accelerations are used to derive the required body torques by multiplying them with the vehicle's moment of inertia. Initially, the total thrust is divided equally between the front and rear rotor arms. The mixer then processes the required pitch torque by breaking it down into a force couple, which is

perpendicular to the vehicle body. These forces are added to the front and back rotor thrusts, resulting in changes in tilting angles and thrust magnitudes. Given the changes in tilting angles, the geometric configuration of the vehicle is determined, allowing for the mapping of front arm total thrust, rear arm total thrust, roll torque, and yaw torque to the individual rotor thrusts.

$$\mathbf{f}_{tot} = m_{\Sigma} \|\mathbf{a}_{des}\| \quad (4.31)$$

$$\boldsymbol{\tau} = \mathbf{J}_{\Sigma}^C \boldsymbol{\alpha}_{des} \quad (4.32)$$

$$\Delta f_{pitch} = \frac{\boldsymbol{\tau}[2]}{2l_x} \quad (4.33)$$

$$\mathbf{f}_f = \left[\frac{f_{tot}}{2} \sin(\beta), \frac{f_{tot}}{2} \cos(\beta) - \Delta f_{pitch} \right] \quad (4.34)$$

$$\mathbf{f}_r = \left[\frac{f_{tot}}{2} \sin(\beta), \frac{f_{tot}}{2} \cos(\beta) + \Delta f_{pitch} \right] \quad (4.35)$$

$$\beta_f = \text{atan2}(\mathbf{f}_f[1], \mathbf{f}_f[2]) + \pi \cdot (\mathbf{f}_f[2] < 0) \quad (4.36)$$

$$\beta_r = \text{atan2}(\mathbf{f}_r[1], \mathbf{f}_r[2]) + \pi \cdot (\mathbf{f}_r[2] < 0) \quad (4.37)$$

$$D = \sin(\beta_f - \beta_r)k^2 + 2 \cos(\beta_f - \beta_r)kl_y - \sin(\beta_f - \beta_r)l_y^2 \quad (4.38)$$

$$\mathbf{M} = \begin{bmatrix} \frac{1}{2} & 0 & \frac{-(k \cos(\beta_r) + l_y \sin(\beta_r))}{2D} & \frac{-(l_y \cos(\beta_r) - k \sin(\beta_r))}{2D} \\ 0 & \frac{1}{2} & \frac{-(k \cos(\beta_f) - l_y \sin(\beta_f))}{2D} & \frac{(l_y \cos(\beta_f) + k \sin(\beta_f))}{2D} \\ 0 & \frac{1}{2} & \frac{(k \cos(\beta_f) - l_y \sin(\beta_f))}{2D} & \frac{-(l_y \cos(\beta_f) + k \sin(\beta_f))}{2D} \\ \frac{1}{2} & 0 & \frac{(k \cos(\beta_r) + l_y \sin(\beta_r))}{2D} & \frac{(l_y \cos(\beta_r) - k \sin(\beta_r))}{2D} \end{bmatrix} \quad (4.39)$$

$$\begin{bmatrix} f_1 \\ f_2 \\ f_3 \\ f_4 \end{bmatrix} = \mathbf{M} \begin{bmatrix} \|\mathbf{f}_f\| \\ \|\mathbf{f}_r\| \\ \boldsymbol{\tau}[1] \\ \boldsymbol{\tau}[3] \end{bmatrix} \quad (4.40)$$

$$\mathbf{u} = [f_1, f_2, f_3, f_4, \beta_f, \beta_r]^T \quad (4.41)$$

The resultant outputs, which include the thrust for each of the four rotors and the angles for the two servos, are converted into DShot and UART commands. These commands are subsequently sent to the motor controllers. It is important to note that while this controller configuration has proven sufficient for our experimental needs, it is not necessarily the optimal solution for all potential operational scenarios. Future work may explore alternative control strategies to improve performance and adaptability. Key controller parameters and mathematical function definitions are summarized in Tables 5.1 and 4.3, respectively.

4.5 Experimental Validation

To validate the theoretical advantages of the PairTilt design discussed in the previous sections, we conducted a series of simulations and experiments to assess its performance

Symbol	Parameter	Value
ω_{nat}	Position controller natural frequency	2 Hz (indoor), 1 Hz (outdoor)
ζ	Position controller damping ratio	1
τ_{att}	Attitude controller attitude time const	$[0.15, 0.15c\beta + 0.2s\beta, 0.15s\beta + 0.2c\beta]^T$ s
τ_ω	Attitude controller rates time const	$[0.05, 0.05c\beta + 0.1s\beta, 0.05s\beta + 0.1c\beta]^T$ s
l_x	1/2 rotor spacing (x-axis)	0.11 m
l_y	1/2 rotor spacing (y-axis)	0.138 m
k	Thrust-to-torque constant	0.014 m
\hat{z}	Unit vector (z-axis)	$[0, 0, 1]^T$

Table 4.2: Vehicle controller parameters. Here, $c\beta := \cos \beta$ and $s\beta := \sin \beta$.

Function	Definition
axang2rotm	converts axis-angle to rotation matrix
atan2	angle from x-axis to point (x, y)
rotmat2vec3d	converts rotation matrix to axis-angle vector

Table 4.3: Controller math functions definitions.

in various flight scenarios. These tests focused on evaluating compact hovering capabilities, sensor pointing capabilities, horizontal acceleration agility, and energy efficiency. A video showcasing the simulations and experiments conducted has been uploaded to: <https://youtu.be/dCXunBaXyjo>.

4.5.1 Compact Hover

The PairTilt vehicle’s ability to achieve a compact, nose-up hover configuration without losing controllability, as demonstrated in Table 4.4 and Figure 4.14, offers significant advantages for operating in confined or cluttered environments. By tilting its body to a -90° pitch angle, the vehicle effectively reduces its width from 420 mm to 200 mm, allowing it to navigate through narrow passages and gaps that would be inaccessible to conventional quadcopters or other tilt-rotor designs with fixed arm configurations. This capability is particularly valuable for tasks such as indoor inspection, search and rescue in collapsed structures, or navigating dense urban environments.

However, this compact configuration comes with a trade-off in power consumption. As shown in Table 4.4, the nose-up hover requires approximately 160 W of power, a 28% increase compared to the conventional 0° pitch hover. This increased power demand is primarily due to the aerodynamic interactions between the stacked propellers, where the lower propeller experiences the downwash from the upper propeller. This effect can be predicted to a very close magnitude using momentum theory, and is compensated for in the rotor control. Despite

this trade-off, the ability to significantly reduce the vehicle’s footprint and access otherwise unreachable areas makes the nose-up hover a valuable capability for specific applications where maneuverability in tight spaces is necessary.

Configuration	Position Ctrl	Attitude Ctrl	Hover Power	Width (w)
Flat (0° pitch)	Yes	Yes	125 W	420 mm
Nose up (-90° pitch)	Yes	Yes	160 W	200 mm

Table 4.4: Compact hover configuration comparison. The width w is defined in Figure 4.7.

In the experiment depicted in Figure 4.14, the PairTilt vehicle successfully navigated a narrow passage by transitioning into the nose-up hover configuration. This demonstrates the practical feasibility and potential real-world applications of this unique flight mode. The vehicle maintained stable flight and precise control throughout the maneuver, showcasing the effectiveness of the proposed control strategy in managing the increased power demands and unique dynamics of the nose-up configuration.

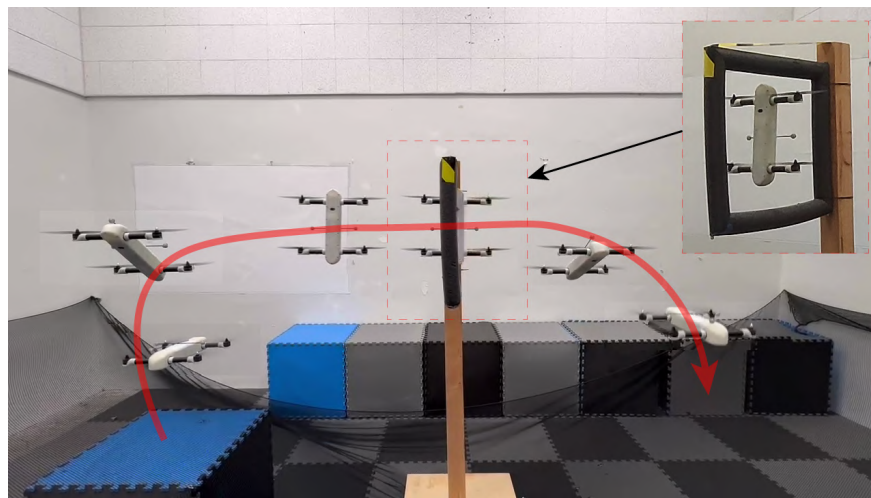


Figure 4.14: The flight path of PairTilt when traversing through a narrow passage. The passage is smaller than the width of the vehicle if the arms are not tilted like a conventional quadcopter. However, the ability of PairTilt to actively tilt the rotors in a pairwise manner allows for flight with nose pointing up, which drastically reduces the vehicle footprint, allowing it to maneuver through tighter spaces.

4.5.2 Sensor Pointing

PairTilt’s independent pitch control, facilitated by the two tilting arms, enables precise and versatile sensor pointing capabilities. Unlike conventional quadcopters which can only maintain arbitrary yaw at a fixed position, PairTilt can maintain arbitrary yaw and pitch angles within its mechanical limits. This allows onboard sensors, such as cameras or LiDAR, to be directed towards any desired position in space, independent of the vehicle’s flight path.

As demonstrated in Figure 4.15, the PairTilt vehicle can perform a camera scan of a room, directing the onboard camera towards different corners while maintaining a stable hover. This capability is particularly valuable for applications such as aerial surveillance, inspection, mapping, and object tracking, where the ability to precisely and dynamically control the sensor’s field of view is crucial.

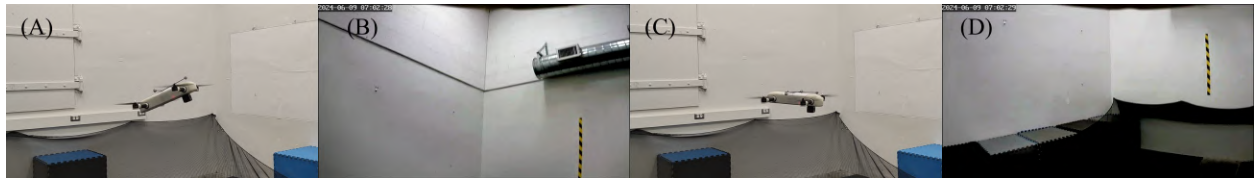


Figure 4.15: PairTilt doing a camera scan. (A) and (C) show the 3rd person views of the vehicle, (B) and (D) show the corresponding onboard camera footage. The left two photos (A) and (B) show the vehicle scanning the upper corner of the lab space, and the right two photos (C) and (D) show the vehicle scanning the bottom corner of the lab space. The vehicle is able to maintain arbitrary yaw and pitch angles within its mechanical limit, allowing onboard sensors to be pointed to any desired position in space.

PairTilt’s ability to maintain arbitrary yaw and pitch angles also simplifies the integration of heavier sensors. In conventional quadcopters, adding heavy sensors often requires complex and heavy gimbal mechanisms to stabilize the sensor’s orientation during flight. However, with PairTilt, these sensors can be mounted directly to the vehicle body, eliminating the need for additional stabilization mechanisms, as the body itself can be actuated to achieve arbitrary pitch and yaw orientations. This simplifies the overall system design, reduces weight, and potentially lowers costs.

4.5.3 Rapid Horizontal Motion

To validate the enhanced agility of PairTilt in rapid horizontal motion, we conducted high-fidelity simulations of an obstacle avoidance maneuver. High-fidelity simulations were used to evaluate the extreme limits of the vehicle’s agility, as these tests could potentially result in crashes in real-world experiments. The simulation are directly compared in real time with the same controller settings applied for both the conventional quadcopter and the tilt-rotor configurations. The simulation involved a step change in the desired x position of 0.1 m,

equivalent to one propeller radius, to mimic a sudden obstacle. We compared the PairTilt’s response to that of a conventional quadcopter with the same physical properties, except for the mass adjustment to account for the absence of the tilting mechanism. We increased the natural frequency (ω_{nat}) of the position controller in the x-direction until the system became unstable or exhibited excessive oscillations. The maximum achievable natural frequency for the conventional quadcopter was 4 Hz, while PairTilt achieved a significantly higher frequency of 11 Hz.

The simulation results, presented in Figure 4.16, demonstrate the PairTilt’s superior agility. The PairTilt vehicle achieved a significantly faster response, reaching 63.2% (1 time constant) of the desired position change in 0.21 seconds, compared to 0.46 seconds for the conventional quadcopter. This translates to a 55% reduction in response time. Additionally, the PairTilt vehicle reached a higher maximum speed of 0.52 m/s during the maneuver, a 73% increase compared to the conventional quadcopter’s 0.30 m/s. Even with the moderate-speed servos we selected (60° per second), the response remains significantly faster. Consequently, the overdesign of torque means that the response is not constrained by the power but rather the servo’s mechanical speed. Adjusting the gear ratio could further accelerate the response, providing even faster maneuverability, which is advantageous in rapid obstacle avoidance scenarios.

These results highlight the PairTilt’s ability to rapidly and precisely adjust its position, a critical capability for navigating cluttered environments and avoiding collisions. The enhanced agility of the PairTilt design is particularly valuable for applications such as drone racing, autonomous navigation in urban environments, and tasks requiring quick and precise movements in response to dynamic obstacles or changing conditions.

4.5.4 Energy Efficiency

To evaluate the energy efficiency of the PairTilt vehicle, we conducted outdoor flight tests at various speeds, starting at 12.5 m/s and increasing in 2.5 m/s increments up to 17.5 m/s. The flight path for the 12.5 m/s test was a 100 m straight line, divided into three equal 33.3 m segments for acceleration, cruising, and deceleration. For the tests at higher speeds, the flight path was extended to 150 m, maintaining the same three-segment structure with 50 m for each segment. Energy consumption data was collected during the constant speed cruise segments. The vehicle was flown in both conventional quadcopter mode (rotors fixed upright) and PairTilt mode (rotors tilted for better aerodynamics). To ensure a fair comparison, the weight of the conventional quadcopter was adjusted to account for the absence of the tilting mechanism. To mitigate potential inaccuracies stemming from the vehicle’s reliance on ground speed measurements, tests were conducted under carefully monitored, near-zero wind conditions using an anemometer.

The experimental results, as depicted in Figure 4.18, align with simulation predictions. As anticipated, the conventional quadcopter demonstrates superior efficiency during hover due to its lighter weight. However, the tilt-rotor design’s aerodynamic advantages become increasingly apparent as speed increases. Notably, the tilt-rotor surpasses the conventional

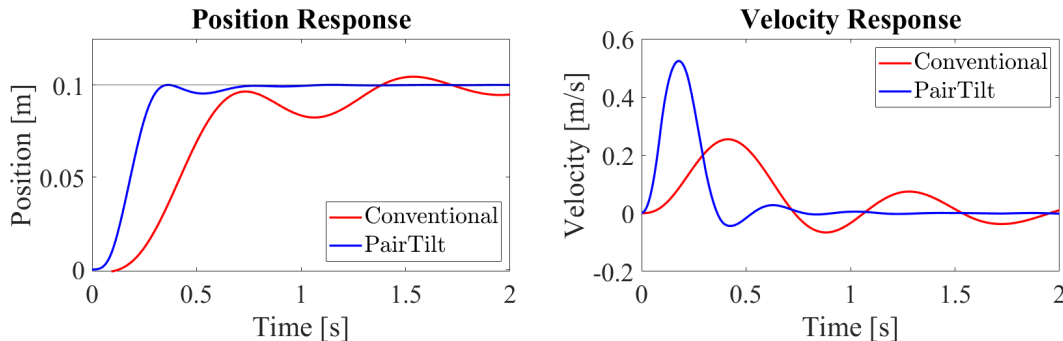


Figure 4.16: Simulated obstacle avoidance vehicle state variation. The vehicle hovers stably at $[0, 0, 1]^T$ m before 0 s. At 0 s, the desired x position is changed to 0.1 m to simulate an obstacle avoidance command. The graph shows the x position and velocity state changes of two vehicles after the maneuver onset. The conventional quadcopter shown in the graph shares the same physical properties as the PairTilt vehicle but has its mass adjusted to account for the absence of the rotor-tilting mechanism. The graph depicts the vehicles under the highest x natural frequency gain for position control that does not result in excessive oscillation or instability. The PairTilt vehicle converges to the new setpoint significantly faster, reaching 63.2% (1 time constant) of the new desired x position in 0.21 s compared to 0.46 s for the conventional quadcopter, a reduction of 55%. The maximum speed reached is also higher for the PairTilt vehicle, 0.52 m/s compared to 0.30 m/s for the conventional quadcopter, a 73% increase. In addition, PairTilt exhibited smaller oscillation, suggesting improved stability and control during rapid maneuvers.

quadcopter in efficiency even before the model-predicted 14 m/s threshold. We attribute this difference to the propeller pitching moment, which induces a slight negative pitch in the tilt-rotor, generating lift that partially counteracts the drone’s weight and reduces energy consumption.

In practice, the tilt-rotor design exhibits a longer range than the conventional quadcopter, reflected in a lower unit cost of transport. This finding underscores the tilt-rotor’s superior energy efficiency and range potential at higher speeds, making it an attractive option for applications such as long-range package delivery or aerial surveillance missions that demand extended flight durations. The strong agreement between our simulation and experimental results validates the tilt-rotor’s enhanced range and cost-effectiveness.

4.5.5 Discussion

The experimental results consistently align with the theoretical predictions and design expectations, validating the effectiveness of the PairTilt concept and its control framework. The compact hover tests showcased the vehicle’s unique ability to navigate confined spaces,



Figure 4.17: Outdoor flight footage of the drone operating in two different control modes. Left: conventional quadcopter mode, where the rotors are fixed upright to the vehicle body, and the vehicle pitches forward during forward flight. Right: PairTilt mode, where the vehicle body is commanded to remain level, and the rotors tilt forward to generate forward thrust. Both photos show the vehicle flying at 15 m/s. Despite the same speed, the conventional quadcopter mode exhibits a much larger pitch angle, resulting in higher air resistance and power consumption.

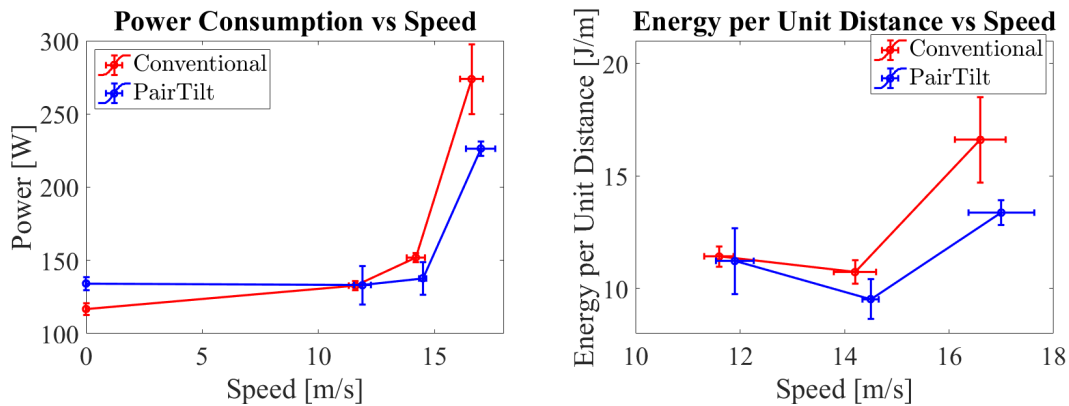


Figure 4.18: Comparison of electrical power consumption and energy efficiency between PairTilt and a conventional quadcopter. Center dots denote the mean, and error bars represent one standard deviation of the measurements collected over the specified time frame. The left graph displays power consumption as a function of airspeed, highlighting the conventional quadcopter’s higher efficiency at hover due to its lower weight. However, this efficiency decreases with increasing speed. The right graph depicts the energy per unit distance (a proxy for range) as a function of airspeed, demonstrating the tilt-rotor’s superior range potential, especially at higher cruise speed. The alignment of trends between simulation and experimental data underscores PairTilt’s benefits in extending range and reducing transportation costs.

a capability not achievable with conventional quadcopter designs. The sensor pointing experiments highlighted the versatility and precision of the PairTilt’s independent pitch control, enabling a wide range of potential applications in surveillance, inspection, and monitoring tasks. The agility simulations further confirmed the PairTilt’s superior maneuverability compared to traditional quadcopters, particularly in scenarios requiring rapid and precise movements. Finally, the energy efficiency tests demonstrated the tilt-rotor design’s advantages in long-range, high-speed flight, opening up possibilities for applications such as package delivery and extended surveillance missions.

These results validate the effectiveness of the PairTilt design and control framework, demonstrating its potential for various applications in aerial robotics. The enhanced agility, compact form factor, and energy efficiency of the PairTilt vehicle make it well-suited for tasks in complex environments. The successful validation of the theoretical predictions through experimental results suggests that this innovative design approach could be applied to future aerial robotic systems.

4.6 Conclusion

In this chapter, we introduced PairTilt, a novel tilt-rotor quadcopter design aimed at enhancing agility and efficiency for various aerial applications. The design’s core features include an H-shaped frame with pairwise-coupled tiltable rotors, striking a balance between mechanical simplicity and enhanced functionality. While slightly more complex than conventional quadcopters, the PairTilt design avoids the excessive complexity of fully omnidirectional tilt-rotor configurations, making it a more practical and maintainable solution. We developed a model-based cascaded controller that leverages the tilt-rotor configuration for faster response times and precise control.

Through extensive experimental validation, we demonstrated the PairTilt’s superior performance in various scenarios. The vehicle successfully achieved compact hovering, precise sensor pointing, and rapid horizontal motion, outperforming a conventional quadcopter in agility tests. Additionally, the tilt-rotor design proved to be more energy-efficient at higher speeds, leading to a longer range compared to the conventional quadcopter.

The PairTilt design and control framework presented in this chapter offer a potential pathway for advancements in tilt-rotor UAVs. The system’s modularity and adaptability lend themselves to integration with complementary technologies, such as vision-based navigation and obstacle avoidance. Further research into control strategies may yield even greater agility and efficiency, broadening the potential applications of tilt-rotor UAVs, particularly in challenging environments.

The successful validation of the PairTilt concept through both simulations and experiments highlights its potential to revolutionize aerial mobility. PairTilt merges the vertical takeoff and landing of quadcopters with the aerodynamic efficiency of tilt-rotor aircraft. This versatile platform shows potential for applications ranging from package delivery and

inspection to search and rescue, contributing to the advancement of air mobility in complex environments.

Chapter 5

Duawlfm: A Drone with Unified Actuation for Wheeled Locomotion and Flight Operation

This chapter presents Duawlfm, a drone with unified actuation for wheeled locomotion and flight operation that achieves efficient, bidirectional ground mobility. Unlike existing hybrid designs, Duawlfm eliminates the need for additional actuators or propeller-driven ground propulsion by leveraging only its standard quadrotor motors and introducing a differential drivetrain with one-way bearings. This innovation simplifies the mechanical system, significantly reduces energy usage, and prevents the disturbance caused by propellers spinning near the ground, such as dust interference with sensors. We provide a detailed mechanical design, present control strategies for rapid and smooth mode transitions, and validate the concept through extensive experimental testing. Flight-mode tests confirm stable aerial performance comparable to conventional quadcopters, while ground-mode experiments demonstrate efficient slope climbing (up to 30°) and agile turning maneuvers approaching $1g$ lateral acceleration. The seamless transitions between aerial and ground modes further underscore the practicality and effectiveness of our approach for applications like urban logistics and indoor navigation.

The material in this chapter is based on the following work:

- J. Tang, R. Zhang, K. Beyduz, Y. Jiang, C. Wiebe, H. Zhang, O. Asoro, and M. W. Mueller, "Duawlfm: A Drone with Unified Actuation for Wheeled Locomotion and Flight Operation". To be submitted to: *IEEE/ASME Transactions on Mechatronics*

5.1 Introduction

5.1.1 Background

Unmanned Aerial Vehicles (UAVs) exhibit notable advantages in terms of mobility and terrain adaptability. Due to their ability to operate in three-dimensional space [1, 50], UAVs possess superior maneuverability can traverse complex or unstructured environments—such as rugged terrain, dense vegetation, or urban obstacles—without the constraints imposed by ground contact. Such mobility makes UAVs especially suitable for tasks that require rapid deployment, flexible routing and access to otherwise inaccessible locations, like delivery, remote sensing, and infrastructure inspection and monitoring [56, 57, 58]. However, UAVs also suffer from several intrinsic limitations, which primarily stem from the aerodynamic and propulsion requirements associated with sustained flight. For instance, multirotor UAVs must constantly generate lift equal to their weight through high-speed rotation of propellers, resulting in significant energy expenditure even when hovering [?].

Ground mobility can alleviate some of these issues. By letting aerial robots roll or drive when airborne travel is not essential, energy consumption can be substantially reduced and safety hazards near the ground can be minimized [56]. However, achieving this aerial-ground versatility is non-trivial. Hybrid robots must incorporate additional hardware or specialized transmissions to enable terrestrial motion, typically adding weight, complexity, and potential failure points [38, 36, 32]. The goal, then, is to design a hybrid configuration, which can preserve the UAV’s agility and compactness while gaining the energy and functional benefits of ground locomotion.

5.1.2 Literature Review

Numerous hybrid aerial-ground vehicles have been proposed to strike a balance between flight capabilities and terrestrial efficiency. Existing designs can be broadly divided into two primary approaches based on how they achieve ground propulsion.

5.1.2.1 Propeller-driven ground propulsion

These UAV designs employ angled or redirected thrust from their existing propellers to achieve ground locomotion. Page and Pounds (2014) introduced the Quadroller, a quadrotor with low-friction wheels and skateboard steering trucks that rolls farther than it hovers despite minimal mass penalty [29]. Sabet et al. (2019) designed Rollocopter, a spherical-shell platform that rolls on extreme terrain and flies, balancing power via an energy-aware controller [30]. Premachandra et al. (2019) retrofitted a quadcopter’s propellers for ground motion and obstacle avoidance without extra actuators [31]. Sugihara et al. (2024) proposed Delta, a deformable multirotor that rolls with its entire body and seamlessly switches modes [32]. Pan et al. (2023) demonstrated Skywalker, which uses an omnidirectional wheel and differential-flatness control to achieve up to a speed of 5 m/s and 75.2% energy savings



Figure 5.1: Top: Duawlfm is in aerial mode. Bottom: Duawlfm is running on the sidewalk in ground mode.

on the ground [33]. Zhang et al. (2023) designed a quadcopter with passive wheel and leveraged nonlinear model predictive control (MPC) with maximum $3m/s$ ground velocity [34]. Similarly, Lin et al. (2024) proposed Skater, a bi-copter with passive wheels that leverages vectored thrust and MPC for robust terrain traversal and steering [35]. Qin et al. (2020) integrated a single passive wheel at a UAV's base, saving 77% battery during rolling [36].

Such an approach offers simplicity, as no additional actuators or motors are required. However, using propellers for ground propulsion generally requires higher power than dedicated wheel actuation, particularly during sustained or high-force maneuvers. Continuous

spinning of propellers near the ground may also stir up dust and debris, potentially interfering with onboard sensors and affecting other system components. Additionally, prolonged ground operation can increase thermal loads on motors, possibly reducing their service life [37], and the spinning propellers pose inherent safety concerns.

5.1.2.2 Additional actuators for ground motion

The second category equips the robot with dedicated actuators—usually motors driving wheels or legs. Kalantari et al. (2020) introduced Drivocopter, a UAV with four actuated spherical wheels for long-endurance hybrid mobility and propeller protection [38]. Morton and Papanikolopoulos (2017) developed a compact hybrid that transforms between ground and air modes, shielding flight hardware when grounded [39]. Zhao et al. (2023) introduced SPIDAR, a quadruped with distributed vectorable rotors for both walking and flight [40]. Sugihara et al. (2023) presented FlyHuman, a humanoid with wheels and a flight unit enabling aerial, legged, and wheeled locomotion under unified control [41]. Adarsh and Dharmana (2018) developed MTMUR, an amphibious robot using custom wheels and floats to navigate land, water, and air [42]. Sihite et al. (2023) introduced M4, which repurposes appendages into wheels, thrusters, and legs for eight distinct locomotion modes [43].

The advantage of this design lies in the use of two independent sets of actuators, which eliminates concerns about motor overload and allows each actuator to operate efficiently. Moreover, by decoupling the power sources for ground and aerial locomotion, the propellers are not engaged during ground movement, which enhances operational safety. These designs typically demonstrate robust ground maneuverability but at the expense of higher total mass which in turn reduced flight times. The greater complexity also increases cost and maintenance requirements.

5.1.3 Contribution

Despite the diversity of existing hybrid platforms, current designs typically rely either on propeller-driven rolling or on additional terrestrial actuators to enable ground mobility. The field thus remains open to exploring simpler and lighter solutions capable of bidirectional ground travel by leveraging only existing aerial motors, thereby minimizing mechanical complexity and energy use.

This chapter introduces Duawlfm (Figure 5.1), a drone with unified actuation for wheeled locomotion and flight operation that achieves efficient, bidirectional ground mobility without requiring additional actuators or relying on propeller thrust for terrestrial locomotion. Ground propulsion is achieved using a mechanical drivetrain powered by differential motor speeds, with one-way bearings that decouple propellers during terrestrial operation. This streamlined approach enables stable and energy-efficient terrestrial locomotion, avoids the complexity and mass associated with adding dedicated ground actuators, and preserves the full functionality of conventional quadrotor flight. Specifically, the contributions of this letter are:

- The proposed hybrid design achieves bidirectional ground mobility using the drone’s *existing* motors only, requires *no additional actuators* and avoids *propeller-based ground propulsion*.
- The proposed system integrates a lightweight drivetrain that enables efficient ground driving without energy loss during flight, supports seamless transitions between modes with no reconfiguration, and allows differential motor control for intuitive bidirectional steering on the ground.
- Comprehensive real-world tests demonstrate stable and agile flight, smooth ground locomotion, and robust aerial-ground transitions.

The remainder of this chapter is organized as follows: Section 5.2 provides a detailed description of the mechanical design of the hybrid robot, highlighting key structural features and the principles enabling dual-mode locomotion. Section 5.3 elaborates on the mode-switching control algorithm developed for hybrid mobility. Section 5.4 presents a comprehensive set of real-world experiments, analyses, and evaluations of the system. Finally, Section 5.5 concludes the chapter and discusses directions for future research.

5.2 Design

5.2.1 Design Objectives

The goal of this work is to develop a hybrid aerial-ground robot capable of both flying and driving using a single unified actuation system. To minimize hardware complexity and weight, the design reuses the drone’s existing motors for both flight and ground propulsion. A key requirement is to ensure that during ground operation, the propellers do not engage or consume energy, thereby avoiding unnecessary aerodynamic drag and power loss. All added components must be as lightweight and as compact as possible.

5.2.2 Key Insights

Multicopter UAVs typically employ brushless DC motors, which are electrically capable of bidirectional operation but mechanically constrained due to the aerodynamic design of their propellers. Propellers are usually optimized for thrust generation in only one direction, making reverse rotation highly inefficient in terms of thrust-to-power ratio.

This inherent directional asymmetry can be leveraged for passive mechanical decoupling. By mounting each propeller to its shaft through a one-way bearing, it becomes possible to engage the propeller only during forward motor rotation—the optimal direction for aerodynamic thrust—while allowing the propeller to disengage and freely rotate if the motor reverses direction. In such a configuration, reverse motor rotation could potentially be exploited to mechanically harvest torque without unnecessarily spinning the propellers, thus enabling efficient power transfer to a ground drivetrain.

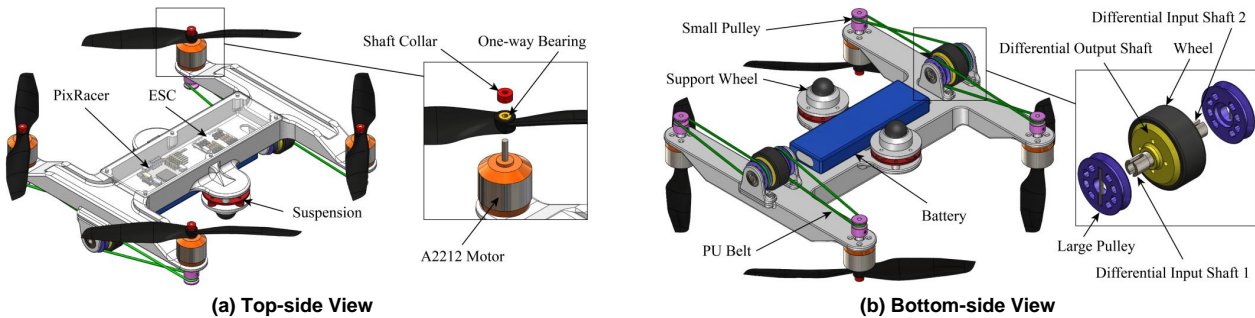


Figure 5.2: (a): Top-side view of Duawlfm. It shows its aerial propulsion system. The vehicle features four A2212 1400 kv motors driving 8-inch (8045) propellers. Each propeller is mounted via a one-way bearing and secured by a shaft collar, ensuring that in flight mode the bearings lock to generate thrust, while in ground mode the propellers freewheel. (b): Bottom-side view. It shows the ground drivetrain arrangement. Each motor shaft is equipped with a small pulley that drives a belt connected to a larger pulley on one of the differential’s input shafts. Two opposing motors feed their respective differentials, whose output shafts are directly connected to integrated wheels. Universal ball casters at the front and rear provide stable ground support.

Because motors would spin exclusively in reverse during ground mode, directly coupling each motor to a wheel could lead to unidirectional wheel rotation, severely limiting ground mobility. A differential mechanism, commonly used in automotive applications, can resolve this limitation by combining inputs from two opposing motors. By coupling these motors through pulleys to a central differential, wheel rotation becomes dependent on the relative motor speeds rather than absolute speeds. Equal speeds can yield stationary wheels, while slight speed variations between motors allow wheels to rotate either forward or backward, providing full bidirectional ground mobility. A schematic of the proposed architecture is shown in Figure 5.3

Furthermore, most drone motors are sensorless brushless DC types due to their simplicity and cost efficiency, but this inherently leads to poor startup behavior at very low speeds. A differential mechanism can alleviate this problem by enabling both motors to run at a nominal idle speed during ground operation. In this scenario, as long as motor speeds remain matched, the wheel does not rotate, effectively bypassing the problematic motor startup region. Adjusting relative motor speeds slightly from this nominal point can then produce smooth and controlled wheel motion, improving ground-mode drivability without the need for additional actuators or complex mechanical switching.

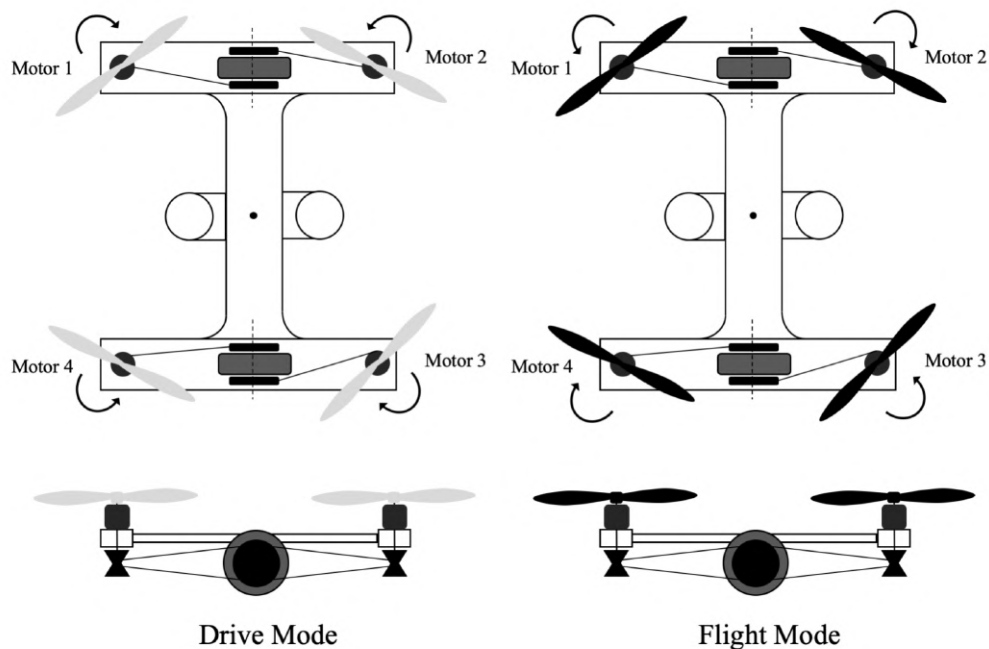


Figure 5.3: Motor directions for drive and flight modes. In the flight mode, the propellers are engaged with the one-way bearings that allow torques to be transmitted to generate thrust. In the drive mode, the motors reverse and decouple the propellers. The motor speed differences are manipulated to provide full bidirectional ground mobility through the differentials.

5.2.3 Experimental Vehicle Design

The hybrid UAV prototype was developed as a custom quadrotor platform that integrates both aerial and ground mobility into a single compact vehicle. The design is organized into two distinct parts: the aerial side (top side) and the ground side (bottom side).

The top side of the vehicle closely resembles a conventional quadcopter. It has four A2212 1400kv BLDC motors mounted symmetrically on a lightweight 3D-printed frame. Each motor drives an 8-inch (8045) propeller that has a one-way bearing press-fitted and glued into its mounting hole. A shaft collar is installed on the top of each motor shaft to constrain the propeller. In flight mode, the motors spin forward, and the one-way bearings lock the propellers, allowing them to generate thrust. When the motors reverse for ground operation, the bearings allow the propellers to freewheel, effectively disengaging them so that energy is not wasted through propeller drag.

The top side of the vehicle houses the ground drivetrain. For ground propulsion, each pair of opposing motors transmits torque via small pulleys attached to their extended shafts. These pulleys drive belts that connect to larger pulleys on the input shafts of miniature

differentials. Each differential then drives an integrated ground-contact wheel directly. The differential mechanism converts the relative speeds of the paired motors into bidirectional wheel rotation, enabling the vehicle to move forward, reverse, or execute turning maneuvers without additional actuators. To provide ground stability, two universal ball casters are mounted at the front and rear of the chassis.

This integrated configuration allows a quick transition between flight and ground modes through software-controlled reversal of motor rotation. In forward rotation (flight mode), the propellers are engaged to generate thrust, while in reverse rotation (ground mode) the propellers freewheel and the drivetrain—comprising the pulleys, belts, and differentials—provides efficient and bidirectional ground traction without extra actuators. The entire vehicle weighs only about 800 g, which is notably light for a system of this scale incorporating ground mobility mechanisms.

5.3 Control

The vehicle uses a mode-switched control framework (Figure 5.4), allowing the same four motors to power either the propellers for flight or the ground wheels for driving. Mechanically, the belt-driven differentials remain engaged at all times, but the propellers are decoupled by one-way bearings when motors spin in reverse.

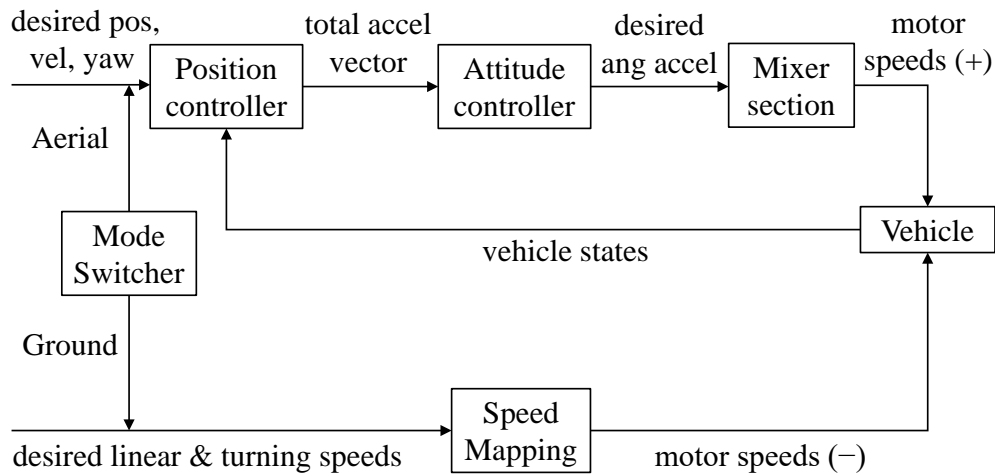


Figure 5.4: The diagram of the two-mode control framework. In aerial mode, a closed-loop cascaded controller manages acceleration, with inputs coming from either manual controls (for outdoor FPV flights) or an outer-loop position controller (for indoor Motion Capture flight). In ground mode, desired linear and rotational speeds are directly mapped to motor speed commands using factors such as gear ratio and wheel radius.

5.3.1 Flight Mode

In flight mode, the motors rotate forward and the one-way bearings allow the motor shafts to transmit torque to the propellers. Similar to many existing quadcopters, we employ a model-based cascaded controller architecture for Duawlfm in the flight mode. The controller enables autonomous tracking of desired position, velocity, and yaw. The controller can be decomposed into a position controller, an attitude controller, and a mixer section.

5.3.1.1 Position Controller

The position controller, in the outermost control loop, uses the desired and current positions and velocities to compute the desired acceleration. It then adds gravitational acceleration (\mathbf{g}) to produce the total acceleration needed to follow the trajectory.

$$\begin{aligned}\mathbf{a}_{des} &= \omega_{nat}^2(\mathbf{p}_{des} - \mathbf{p}_{cur}) + 2\zeta\omega_{nat}(\mathbf{v}_{des} - \mathbf{v}_{cur}) \\ \mathbf{a}_{tot} &= \mathbf{a}_{des} + \mathbf{g}\end{aligned}\tag{5.1}$$

5.3.1.2 Attitude Controller

The attitude controller aligns the thrust direction with the desired total acceleration vector and applies the desired yaw. It computes the desired orientation, then derives the desired angular velocity and desired angular acceleration using current state feedback. The control law is as follows:

$$\hat{\mathbf{a}}_{tot} = \frac{\mathbf{a}_{tot}}{\|\mathbf{a}_{tot}\|}\tag{5.2}$$

$$\mathbf{n}_f = \hat{\mathbf{z}} \times \hat{\mathbf{a}}_{tot}\tag{5.3}$$

$$\beta_f = \arccos(\hat{\mathbf{a}}_{tot} \cdot \hat{\mathbf{z}})\tag{5.4}$$

$$\mathbf{R}_f = \mathcal{R}_{\mathcal{M}}([\mathbf{n}_f/\|\mathbf{n}_f\|, \beta_f])\tag{5.5}$$

$$\mathbf{R}_{des} = \mathbf{R}_f \begin{bmatrix} \cos \psi_{des} & -\sin \psi_{des} & 0 \\ \sin \psi_{des} & \cos \psi_{des} & 0 \\ 0 & 0 & 1 \end{bmatrix}\tag{5.6}$$

$$\boldsymbol{\omega}_{des} = \boldsymbol{\tau}_{att} \oslash \mathcal{V}(\mathbf{R}_{cur}^T \mathbf{R}_{des})\tag{5.7}$$

$$\mathbf{e}_{\omega} = \boldsymbol{\omega}_{des} - \boldsymbol{\omega}_{cur}\tag{5.8}$$

$$\boldsymbol{\alpha}_{des} = \boldsymbol{\tau}_{\omega} \oslash \mathbf{e}_{\omega}\tag{5.9}$$

Where $\mathcal{R}_{\mathcal{M}}$ is a function that converts an axis-angle representation to rotation matrix form, and \mathcal{V} is a function that converts a rotation matrix to a 3D rotation vector.

5.3.1.3 Mixer Section

Given the vehicle's geometry, mass, moment of inertia, and motor constants, the mixer computes the individual rotor thrusts based on the total desired thrust and body torques.

The outputs are then converted into motor speeds using propeller characteristics and sent as DShot signals to the ESC. Key controller parameters are summarized in Table 5.1.

$$f_{tot} = m \|\mathbf{a}_{tot}\| \quad (5.10)$$

$$\boldsymbol{\tau} = \mathbf{J} \boldsymbol{\alpha}_{des} \quad (5.11)$$

$$\begin{bmatrix} f_1 \\ f_2 \\ f_3 \\ f_4 \end{bmatrix} = \frac{1}{4} \begin{bmatrix} -1/l & -1/l & -1/k & 1 \\ -1/l & 1/l & 1/k & 1 \\ 1/l & 1/l & -1/k & 1 \\ 1/l & -1/l & 1/k & 1 \end{bmatrix} \begin{bmatrix} \tau_x \\ \tau_y \\ \tau_z \\ f_{tot} \end{bmatrix} \quad (5.12)$$

Table 5.1: Vehicle controller parameters.

Symbol	Parameter	Value
ω_{nat}	Natural frequency	2 Hz
ζ	Damping ratio	1
$\boldsymbol{\tau}_{att}$	Attitude time constant	[0.2, 0.2, 0.5] s
$\boldsymbol{\tau}_{\omega}$	Rates time constant	[0.05, 0.05, 0.2] s
l	Adjacent rotor spacing	0.22 m
k	Propeller thrust to torque constant	0.014 m

5.3.2 Ground Mode

In ground mode, the UAV's desired linear speed v_x (m/s) and angular speed ω_z (rad/s) from user inputs are used to compute the individual wheel speeds. The vehicle's right and left wheel speeds, w_r and w_l respectively, are defined as:

$$w_r = k_1 (v_x + k_2 \omega_z), \quad w_l = k_1 (v_x - k_2 \omega_z) \quad (5.13)$$

where k_1 is the inverse of the wheel radius and k_2 is the lateral offset of the wheels from the vehicle center. Motor commands for ground mode are derived from the calculated wheel speeds. Let w_i denote the idle motor speed, and let $\omega_1, \omega_2, \omega_3$, and ω_4 represent the commanded motor speeds for the four motors in their reverse directions. These are computed as follows:

$$\begin{aligned} \omega_1 &= -k_3 w_r + w_i, & \omega_2 &= k_3 w_r + w_i, \\ \omega_3 &= k_3 w_l + w_i, & \omega_4 &= -k_3 w_l + w_i \end{aligned} \quad (5.14)$$

where w_r and w_l are the right and left wheel speeds defined in Equation (5.13), and k_3 is the reduction ratio of the pulley-belt transmission. For robust ground operation, the motors

are maintained above the nominal idle speed, and the minimum commanded speed is defined as

$$\omega_{\min} = w_i \quad (5.15)$$

If any computed motor command ω_i falls below ω_{\min} , that command is raised to ω_{\min} and the paired motor's command is increased by the same amount to maintain the required speed differential. For example, if for a pair of motors the computed commands are ω_1 and ω_2 and $\omega_1 < \omega_{\min}$, then the adjustments are performed as follows:

$$\omega_1 \leftarrow \omega_{\min} \quad \text{and} \quad \omega_2 \leftarrow \omega_2 + (\omega_{\min} - \omega_1) \quad (5.16)$$

This ensures that the intended speed difference $\omega_2 - \omega_1$ is maintained while avoiding operation in the low-performance startup region of sensorless brushless motors.

To illustrate ground-mode behavior, we plot motor speeds for a simple square-path driving test. As shown in Figure 5.5, when the vehicle is moving in a straight line between every two waypoints, the rear motors on each side spin faster than the front motors, which remain at the minimum speed ω_i : $|\omega_2| > |\omega_1| = |\omega_i|$ and $|\omega_3| > |\omega_4| = |\omega_i|$, causing both wheels to move forward. When the vehicle is turning around itself at a waypoint, the speed relationship becomes $|\omega_2| > |\omega_1| = |\omega_i|$ and $|\omega_4| > |\omega_3| = |\omega_i|$, so the right wheel continues to advance while the left wheel reverses, making the vehicle turn counterclockwise.

Mode switching does not require any physical reconfiguration beyond reversing motor spin directions. The high-level autonomy stack (or a user command) selects flight or drive mode, causing the controller to generate motor speed setpoints for either aerial thrust (forward rotation) or ground travel (reverse rotation). This unified approach enables rapid transitions with minimal mechanical complexity while preserving the vehicle's standard quadrotor functionality in flight.

5.4 Experimental Validation

The proposed hybrid UAV was evaluated in four sets of experiments that test its performance in both flight and ground modes, as well as its ability to transition seamlessly between these modes. Below, we present the key experiments along with discussions that highlight the performance trade-offs, advantages, and implications of the design.

5.4.1 Circular Motion Experiment

To evaluate maneuverability and efficiency during tight turning motions, circular paths with a radius of 1 meter were tested in both flight and ground modes at speeds ranging from 1.0 to 2.0 m/s. Figure 5.6 (A, B) shows the experiment footage. Table 5.2 summarizes the average power consumption for 5 seconds and the lateral acceleration experienced in each scenario.

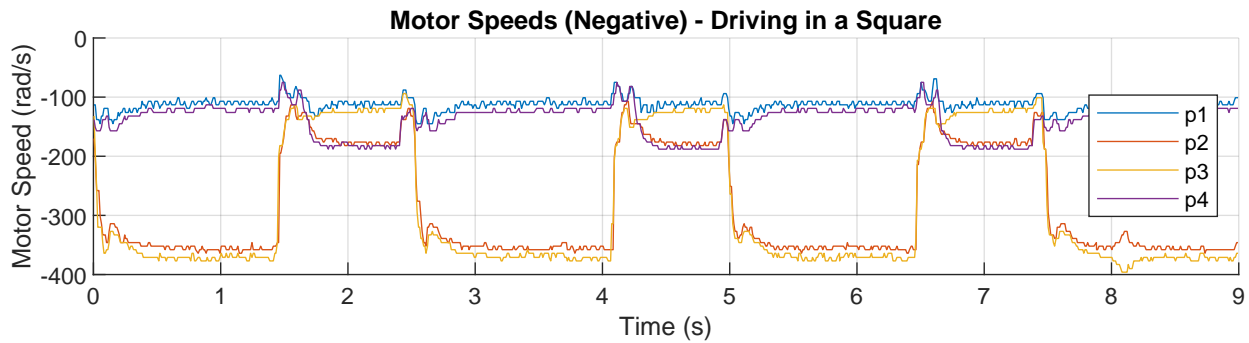
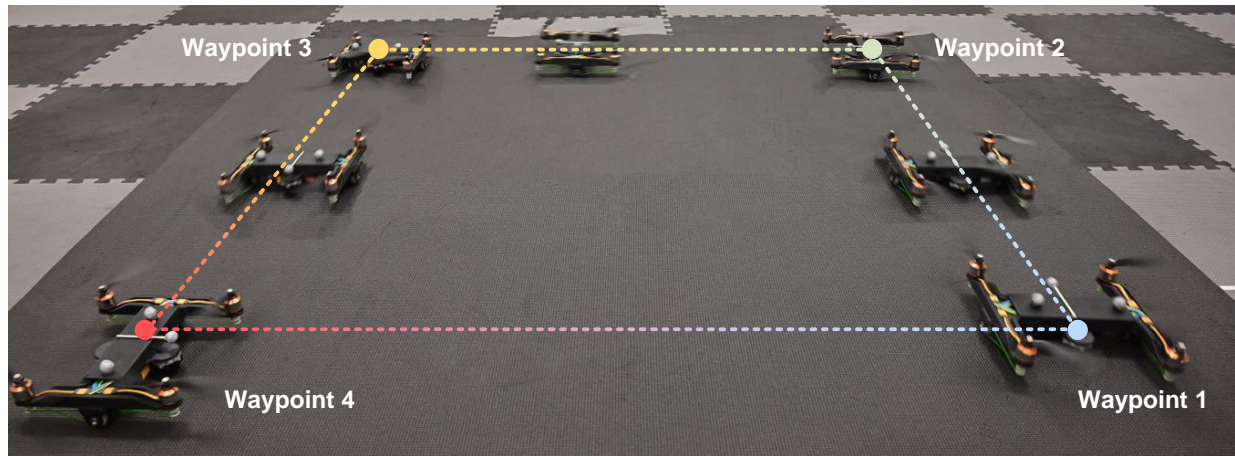


Figure 5.5: Motor speed profiles for a complete square-path maneuver in the ground mode. The vehicle departs waypoint 1 and reaches waypoint 2 at $t = 1.5$ s, then performs a 90° in-place rotation from $t = 1.5$ s to 2.5 s. It travels to waypoint 3, arriving at $t = 4.0$ s, executes a second 90° turn from $t = 4.0$ s to 5.0 s, then moves to waypoint 4, arriving at $t = 6.5$ s. At waypoint 4 it performs a third 90° rotation between $t = 6.5$ s and 7.5 s before returning toward waypoint 1 to complete the square.

Table 5.2: Average power consumption during circular motion (1-meter diameter) at various speeds in flight and ground modes.

Speed (m/s)	Lateral G-force (g)	Fly Power (W)	Drive Power (W)
1.0	0.20	124.6	3.9
1.5	0.46	140.6	8.2
2.0	0.82	188.8	14.9

The results clearly demonstrate that for rapid turning maneuvers, the ground mode significantly outperforms flight mode in terms of energy efficiency. At 1.0 m/s, ground-mode

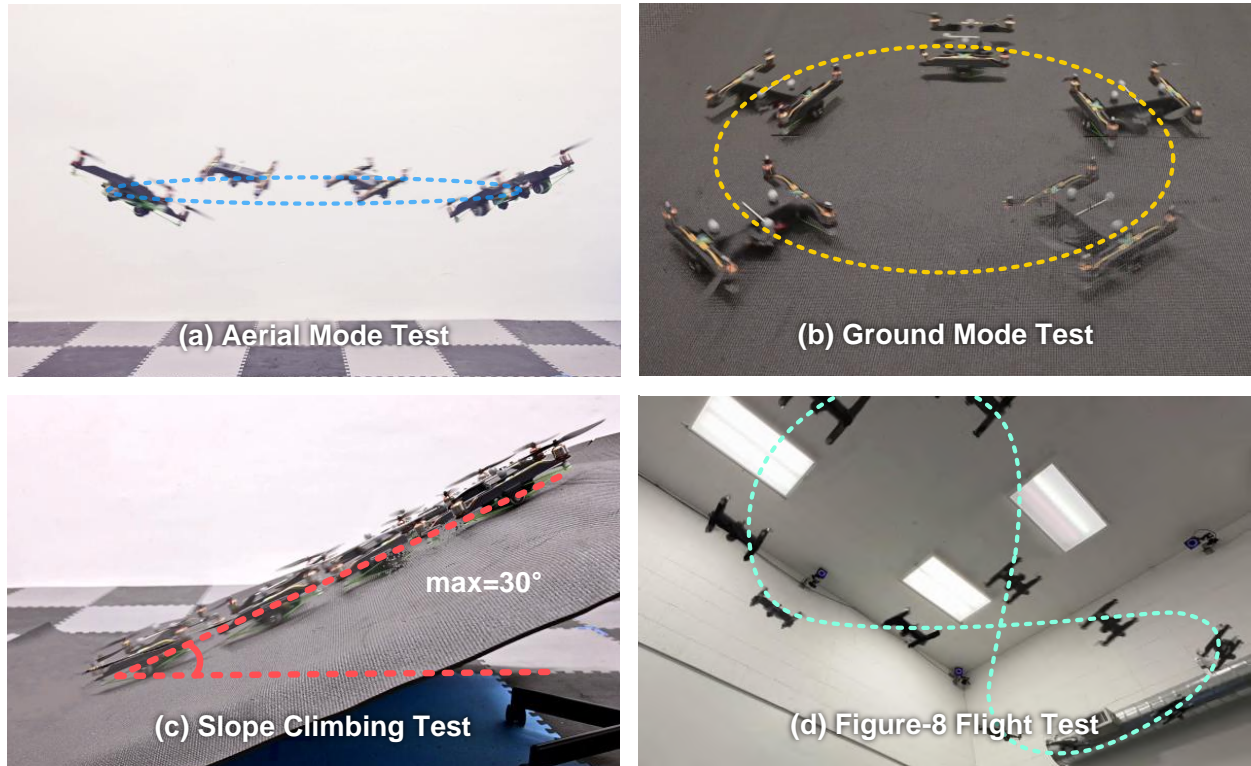


Figure 5.6: Time-lapse pictures of experiments. To test the power consumption and lateral acceleration under two different modes, we test and record the data when (a) Duawlfm flying in a circle. (b) Duawlfm driving in a circle. To explore the maximum sloop-climbing capability, we let (c) Duawlfm drives up a ramp up to 30° . To test the performance of proposed controller, we make (d) Duawlfm fly along the figure-8 trajectory.

operation consumes only 3.9 W, whereas flight mode requires 124.6 W, which is over 30 times higher. Even at increased speeds of up to 2.0 m/s, ground mode maintains drastically lower power demands compared to flight mode (14.9 W vs. 188.8 W). This substantial difference arises primarily because ground mode leverages tire-ground frictional forces, significantly reducing the power needed for directional control compared to aerodynamic maneuvering in flight.

Additionally, ground-mode operation exhibits exceptional agility, comfortably handling maneuvers that generate lateral accelerations approaching 1g (0.82g at 2.0 m/s). This indicates that the hybrid vehicle is not only energy-efficient but also highly capable of rapid directional changes in confined spaces, making it especially suitable for dynamic urban and indoor environments where tight maneuvering is frequently required.

In summary, the data confirms that ground-mode operation provides a marked advantage in energy efficiency and agility for short-range, rapid-turning maneuvers, enhancing the overall practicality and versatility of the hybrid UAV in realistic deployment scenarios.

5.4.2 Slope Climbing Ability

Table 5.3: Measured energy consumption per unit height climbed on different slope angles.

Slope Angle (°)	Mean Power (W)	Energy / Height (J/m)
5	4.0	50.9
10	4.6	37.9
15	4.5	27.5
20	4.5	24.8
25	5.0	25.9
30	5.4	26.5

To assess the ground-mode capability of the Duawlfm, climbing experiments as shown in Figure 5.6 (C) were conducted with slope inclines ranging from 5° to 30° at a fixed forward speed of 0.5 m/s. The average power consumption and energy expenditure per unit height climbed were measured and summarized in Table 5.3.

The experimental results highlight several important aspects of Duawlfm’s ground performance. First, the power requirements for slope climbing remain consistently low, averaging between 4.0 W to 5.4 W across all tested angles, demonstrating high drivetrain efficiency. The data indicate that climbing is inherently energy-efficient, particularly on steeper slopes where the energy required per unit height actually decreases due to reduced traversal distance, reaching as low as 24.8 J/m at 20°. This trend shows the system’s effectiveness at converting energy into vertical displacement.

Additionally, the vehicle demonstrates robust climbing capabilities, successfully managing steep inclines up to 30°, at which point tire slippage begins to occur. Notably, a 30° incline already represents a significantly challenging gradient far exceeding typical accessibility ramps mandated by ADA standards (maximum 4.76°). Thus, the UAV’s climbing performance comfortably surpasses real-world urban navigation requirements, including indoor environments and common building terrains. These findings confirm that the differential drivetrain provides consistent, efficient, and reliable performance even on steep slopes, making the UAV highly suitable for versatile deployment scenarios involving varied terrain conditions.

5.4.3 Figure-8 Flight Test

The addition of one-way bearings and an integrated ground drivetrain alters Duawlfm’s rotor dynamics compared to a conventional quadcopter. Because the one-way bearings block reverse torque transmission, active propeller braking is no longer possible. Moreover, the ground drivetrain remains engaged even in flight, so each rotor must accelerate the pulleys, belt, and differential—adding inertia and introducing frictional losses.

Table 5.4: Hover and Figure-8 Flight Performance

Vehicle	Hover Power (W)	Fig.-8 RMSE (cm)	Fig.-8 Power (W)
Baseline	120.7	3.4	134.7
Duawlfm	124.4	2.8	138.5

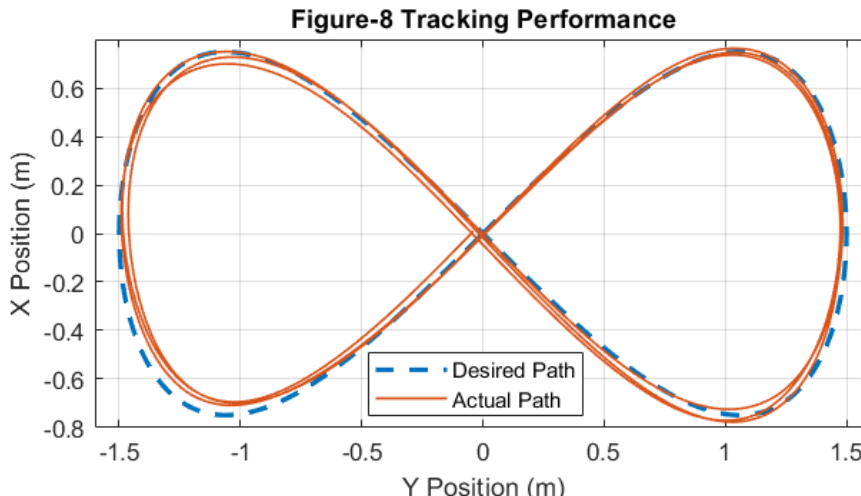


Figure 5.7: Figure-8 flight test: the actual path (solid) of Duawlfm closely follows the desired trajectory (dashed), despite the additional inertial load of the ground drivetrain.

We argue that, despite these extra loads, the effects on performance are minimal. Propeller drag alone suffices to slow the rotors at an acceptable rate in the absence of active braking, as is common in many drones where the ESCs do not employ active braking. Additionally, the drivetrain components—such as plastic pulleys—are lightweight, resulting in only a small increase in total rotor inertia.

To investigate these effects, we executed a 3-cycle figure-8 trajectory tracking flight on Duawlfm and a baseline vehicle. The figure-8 trajectory is of 1.5 m major diameter with the vehicle flying at a speed of 2 m/s as shown in Figure 5.6 (D). The baseline vehicle is a modified Duawlfm with the same propellers but without the one-way bearings and with its ground drivetrain disconnected; all other parameters remain identical.

Figure 5.7 overlays the desired (dashed) and actual (solid) flight paths of Duawlfm, and Table 5.4 summarizes the quantitative results of Duawlfm and the baseline vehicle in both hover flights and figure-8 trajectory tracking.

The data indicate that Duawlfm’s trajectory tracking root-mean-squared error (RMSE) is small and comparable to the baseline, demonstrating that the added drivetrain components have virtually no effect on tracking performance. Both hover power and figure-8 trajectory tracking power are only about 3% higher than those of the baseline, so the ground drivetrain imposes only a minor penalty on energy efficiency due to friction losses. These results confirm

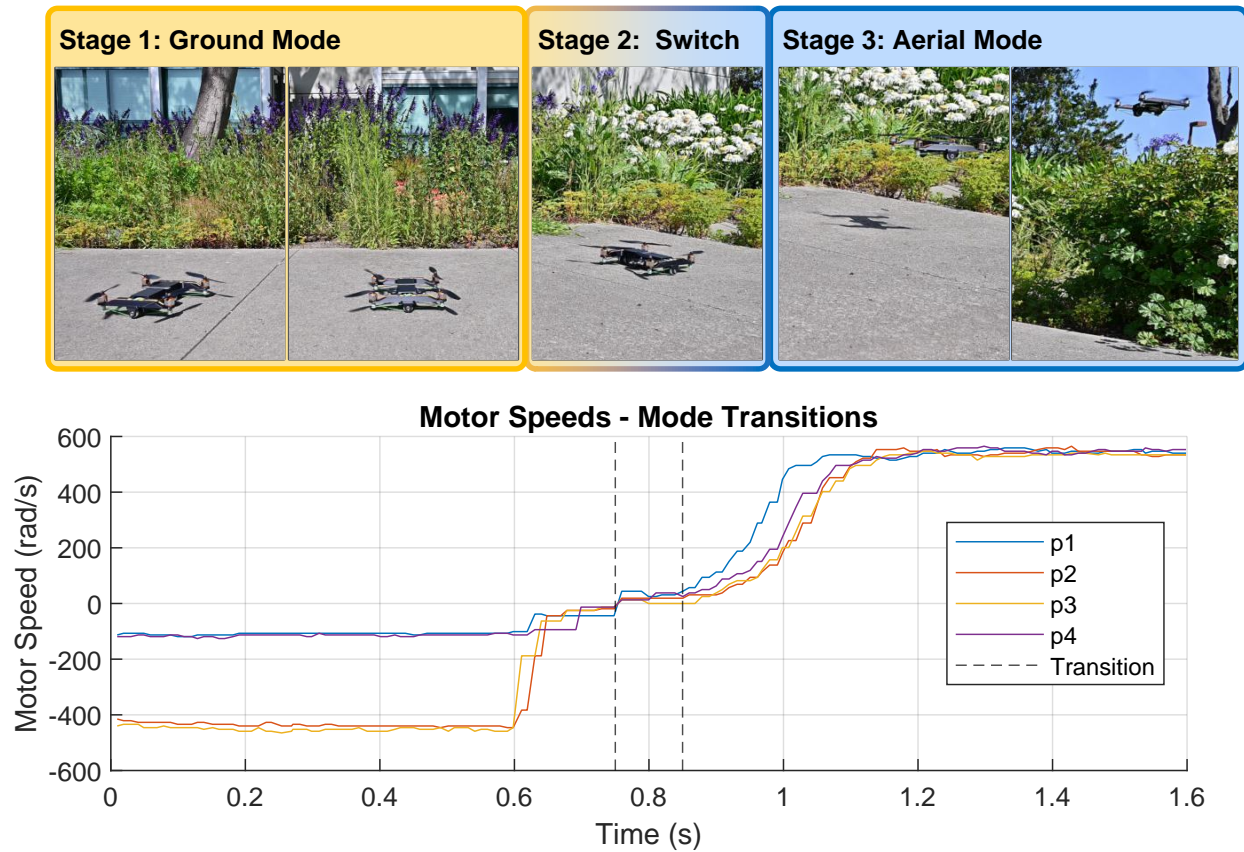


Figure 5.8: The demonstration of outdoor multi-terrain test. Stage 1: Duawlfín is running on the sidewalk. Stage 2: Duawlfín switches from its ground mode into aerial mode. The entire mode switch process is completed with 0.1 seconds since it only relies on reversing the directions of motor rotations. Stage 3: Duawlfín takes off and flies over the bush. With the complex terrain where the wheel locomotion cannot handle, the motors actuate propellers directly and enables the robot fly over it.

that the design modifications preserve robust aerial performance suitable for real-world UAV applications.

In theory, active propeller braking and complete drivetrain disengagement in flight could still be implemented—e.g. either actively with servos or passively with clutches that engage when thrust is applied. However, the results presented here represent the most conservative case (drivetrain always engaged and no active braking), and even under these conditions the vehicle performs well.

5.4.4 Outdoor Multi-Terrain Test

We performed a multi-terrain demonstration to showcase Duawlfín’s ability to transition between air and ground modes in a simulated delivery scenario. Specifically, we simulated a package delivery task from one building to another. For brevity and analytical clarity, only the initial phase—taking off and transitioning from ground to air outside the origin building—is presented here. Unlike all the other experiments, the flight mode controller in this part does not involve the position controller, and the vehicle is controlled manually with joystick-controlled acceleration instead. Figure 5.8 presents the results, with the top panel showing a time-lapse of the vehicle’s path as it takes off from ground mode and transitions into flying, and the bottom panel displaying motor speeds and power consumption over time.

The vehicle data plot illustrates how quickly the vehicle can switch the operational mode by having the motors switch direction—from negative (driving the wheels) to positive (generating lift)—with minimal delay. This quick reversal of motor direction confirms that Duawlfín’s transition mechanism is both mechanically simple and dynamically responsive, enabling efficient deployment for delivery tasks requiring frequent mode changes.

Overall, this demonstration highlights the UAV’s practical suitability for real-world urban logistics, showcasing its fast, stable, and energy-efficient transitions between aerial and ground operation modes.

5.5 Conclusion

We introduced Duawlfín, a drone with unified actuation for wheeled locomotion and flight operation that achieves efficient, bidirectional ground mobility without requiring additional actuators or relying on propeller thrust for terrestrial propulsion. The design employs one-way bearings and a differential system to repurpose existing quadrotor motors for both aerial flight and ground driving. This streamlined approach significantly reduces mechanical complexity, system weight, and energy usage while ensuring robust multimodal functionality.

Experimental validation confirmed the effectiveness and practicality of our hybrid robot across various scenarios. Flight tests indicated minimal performance trade-offs, with only minor increases in energy consumption compared to a conventional quadrotor in the flight mode. Ground-mode experiments demonstrated impressive efficiency, successfully navigating steep slopes of up to 30° and performing agile turns with lateral accelerations close to $1g$, all while using significantly less energy than flying. The multi-terrain demo showcased the robot’s smooth and rapid transitions between aerial and terrestrial modes, underscoring its real-world applicability for urban delivery and indoor navigation tasks.

Overall, Duawlfín provides a compelling alternative to existing hybrid UAV designs, offering substantial benefits in terms of efficiency, simplicity, and versatility. Future work will focus on further optimization of the mechanical drivetrain and integrating advanced autonomy to fully exploit the hybrid vehicle’s capabilities in complex operational environments.

Chapter 6

Conclusion and Future Directions

6.1 Conclusion

This thesis has demonstrated that rethinking the mechanical architecture of conventional multirotor UAVs can overcome many of their long-standing limitations. By combining simple, hardware-centric modifications with tailored control strategies, this work has achieved notable improvements in flight endurance, aerodynamic efficiency, agility, and multi-modal operation. Central to this effort are three key innovations: an unactuated rotor tilting mechanism (QUaRTM), an active tilt-rotor design (PairTilt), and a dual-modal aerial-ground approach using unified actuation (Duawlfm).

The QUaRTM system enables a quadcopter to morph between untilted and tilted configurations mid-flight passively, reducing frontal drag at higher speeds. This results in an increased top speed, improved high-speed agility, and lower power consumption without requiring additional actuators. Building on the idea of rotor tilting, the PairTilt design introduces active tilt-rotor control combined with pairwise rotor coupling. By decoupling forward translation from pitch rotation, the system offers a balanced approach to energy efficiency and maneuverability, particularly in environments demanding agile, high-speed flight. Lastly, the dual-modal aerial-ground concept Duawlfm leverages standard quadcopter motors to drive a passive belt-and-differential drivetrain, seamlessly integrating flight with efficient ground driving. Such a hybrid platform broadens the operational scope, making long-endurance missions and urban navigation more feasible.

Additionally, the thesis references two co-authored works that underscore the broader context of UAV mechanical innovations. The first investigates a battery-staging technique to discard depleted battery segments, yielding up to a 19% improvement in flight duration. The second introduces a midair-reconfigurable quadcopter design employing unactuated hinges, allowing the vehicle to passively alter its configuration in flight for enhanced maneuverability in confined spaces. Taken together, these contributions outline a comprehensive exploration of hardware-driven strategies that incrementally push the envelope of performance, efficiency, and versatility in modern UAVs.

The collective contributions of this work illustrate that straightforward, hardware-driven design changes can address fundamental limitations of conventional UAVs. Rather than relying solely on complex software-based control or heavy additional hardware, the innovations presented here achieve enhanced performance by carefully reengineering the vehicle’s structure and leveraging inherent mechanical advantages. While the proposed designs maintain the simplicity that has made quadcopters so popular, they push the envelope in terms of efficiency, speed, and agility.

6.2 Future Directions

Looking ahead, the prototypes in this thesis should be viewed as starting points rather than finished products. The obvious next step is to transform today’s hand-tuned concepts into tomorrow’s automatically designed, virtually tested, and self-adapting machines. With that goal in mind, the following research directions outline how future works can push these ideas from proof of concept to mission-ready reality:

- **Generative and Automated Design Pipelines**

Costly, trial-and-error fabrication cycles were a major bottleneck during this research. The next step is to build an end-to-end, *generative design* framework that couples multi-physics simulation with evolutionary or reinforcement-learning search. Such a pipeline would automatically explore hinge stiffness, actuator placement, drivetrain ratios, and structural topologies, returning manufacturable CAD files with performance guarantees before a single prototype is built.

- **Virtual Testbeds and Digital Twins**

A high-fidelity virtual environment—combining CFD for aerodynamics, MBD (multi-body dynamics) for mechanisms, and battery/thermal models—would allow rapid iteration and regression testing of design changes. Linking this simulator to a real-time digital twin of each prototype would enable hardware-in-the-loop experiments and accelerate fault-diagnosis and controller tuning.

- **Learning-Based Control for Novel Morphologies**

Passive or sparsely actuated morphing introduces complex, configuration-dependent dynamics that challenge classical gain-scheduled controllers. Model-based RL, imitation learning from aerobatic pilots, or hybrid adaptive-MPC schemes can be investigated to exploit the full agility of morphing frames while maintaining stability margins.

- **Co-Design of Structure, Actuation, and Control**

As UAV architectures grow more adaptive, the vehicle’s geometry, actuation strategy, and control logic should be conceived as a single, integrated design problem rather than independent stages. Future work can investigate high-level optimisation frameworks that jointly balance mechanical simplicity, energy efficiency, and closed-loop performance while respecting weight, cost, and manufacturability constraints.

In conclusion, while the innovations presented in this thesis provide an important step toward more efficient and versatile UAVs, they represent only a foundation upon which further improvements can be built. By pairing automated generative design, virtual testing, and learning-based control, the next iteration of research can deliver truly adaptive aerial systems—high-speed, long-range, and capable of intelligent self-reconfiguration in response to task demands and environmental uncertainty. These directions promise not only incremental gains but a paradigm shift toward *co-evolved* hardware and intelligence, bringing multifunctional UAVs from laboratory prototypes to robust, field-ready tools.

Bibliography

- [1] M. W. Mueller, S. J. Lee, and R. D'Andrea, "Design and control of drones," *Annual Review of Control, Robotics, and Autonomous Systems*, vol. 5, no. 1, pp. 161–177, 2022. [Online]. Available: <https://doi.org/10.1146/annurev-control-042920-012045>
- [2] A. Jaimes, S. Kota, and J. Gomez, "An approach to surveillance an area using swarm of fixed wing and quad-rotor unmanned aerial vehicles UAV(s)," in *2008 IEEE International Conference on System of Systems Engineering*. IEEE, 2008, pp. 1–6.
- [3] S. Siebert and J. Teizer, "Mobile 3D mapping for surveying earthwork projects using an unmanned aerial vehicle (UAV) system," *Automation in construction*, vol. 41, pp. 1–14, 2014.
- [4] C. A. Thiels, J. M. Aho, S. P. Zietlow, and D. H. Jenkins, "Use of unmanned aerial vehicles for medical product transport," *Air medical journal*, vol. 34, no. 2, pp. 104–108, 2015.
- [5] M. Erdelj, E. Natalizio, K. R. Chowdhury, and I. F. Akyildiz, "Help from the sky: Leveraging UAVs for disaster management," *IEEE Pervasive Computing*, vol. 16, no. 1, pp. 24–32, 2017.
- [6] X. Wu, J. Zeng, A. Tagliabue, and M. W. Mueller, "Model-free online motion adaptation for energy-efficient flight of multicopters," *IEEE Access*, 2022.
- [7] K. P. Jain, M. Park, and M. W. Mueller, "Docking two multirotors in midair using relative vision measurements," *arXiv preprint arXiv:2011.05565*, 2020.
- [8] K. P. Jain, J. Tang, K. Sreenath, and M. W. Mueller, "Staging energy sources to extend flight time of a multirotor uav," in *2020 IEEE/RSJ International Conference on Intelligent Robots and Systems (IROS)*. IEEE, 2020, pp. 1132–1139.
- [9] K. C. Reinhardt, T. R. Lamp, J. W. Geis, and A. J. Colozza, "Solar-powered unmanned aerial vehicles," in *IECEC 96. Proceedings of the 31st Intersociety Energy Conversion Engineering Conference*, vol. 1. IEEE, 1996, pp. 41–46.

- [10] Q. Lin, Z. Cai, J. Yang, Y. Sang, and Y. Wang, "Trajectory tracking control for hovering and acceleration maneuver of quad tilt rotor uav," in *Proceedings of the 33rd Chinese Control Conference*, 2014, pp. 2052–2057.
- [11] C. Papachristos, K. Alexis, and A. Tzes, "Hybrid model predictive flight mode conversion control of unmanned quad-tiltrotors," in *2013 European Control Conference (ECC)*, 2013, pp. 1793–1798.
- [12] R. B. Anderson, J. A. Marshall, and A. L’Afflitto, "Constrained robust model reference adaptive control of a tilt-rotor quadcopter pulling an unmodeled cart," *IEEE Transactions on Aerospace and Electronic Systems*, vol. 57, no. 1, pp. 39–54, 2021.
- [13] A. Nemati, N. Soni, M. Sarim, and M. Kumar, "Design, fabrication and control of a tilt rotor quadcopter:," 10 2016.
- [14] M. Allenspach, K. Bodie, M. Brunner, L. Rinsoz, Z. Taylor, M. Kamel, R. Siegwart, and J. Nieto, "Design and optimal control of a tiltrotor micro-aerial vehicle for efficient omnidirectional flight," *The International Journal of Robotics Research*, vol. 39, no. 10-11, pp. 1305–1325, 2020.
- [15] S. Panigrahi, Y. S. S. Krishna, and A. Thondiyath, "Design, analysis, and testing of a hybrid vtol tilt-rotor uav for increased endurance," *Sensors*, vol. 21, no. 18, 2021. [Online]. Available: <https://www.mdpi.com/1424-8220/21/18/5987>
- [16] C. Papachristos, K. Alexis, and A. Tzes, "Hybrid model predictive flight mode conversion control of unmanned quad-tiltrotors," in *2013 European Control Conference (ECC)*, 2013, pp. 1793–1798.
- [17] T. Mikami and K. Uchiyama, "Design of flight control system for quad tilt-wing uav," *2015 International Conference on Unmanned Aircraft Systems, ICUAS 2015*, pp. 801–805, 07 2015.
- [18] A. Sakaguchi, T. Takimoto, and T. Ushio, "A novel quadcopter with a tilting frame using parallel link mechanism," 06 2019, pp. 674–683.
- [19] M. Mousaei, J. Geng, A. Keipour, D. Bai, and S. Scherer, "Design, modeling and control for a tilt-rotor vtol uav in the presence of actuator failure," 05 2022.
- [20] N. Bucki, J. Tang, and M. W. Mueller, "Design and control of a midair-reconfigurable quadcopter using unactuated hinges," *IEEE Transactions on Robotics*, vol. 39, no. 1, pp. 539–557, 2023.
- [21] D. Falanga, K. Kleber, S. Mintchev, D. Floreano, and D. Scaramuzza, "The foldable drone: A morphing quadrotor that can squeeze and fly," *IEEE Robotics and Automation Letters*, vol. 4, no. 2, pp. 209–216, 2019.

- [22] M. Ryll, H. Bühlhoff, and P. Giordano, “Modeling and control of a quadrotor uav with tilting propellers,” 05 2012, pp. 4606–4613.
- [23] —, “First flight tests for a quadrotor uav with tilting propellers,” 05 2013, pp. 295–302.
- [24] M. S. Kamel, S. Verling, O. Elkhatib, C. Sprecher, P. Wulkop, Z. Taylor, R. Siegwart, and I. Gilitschenski, “Voliro: An omnidirectional hexacopter with tilttable rotors,” 01 2018.
- [25] S. Park, J. Her, J. Kim, and D. Lee, “Design, modeling and control of omni-directional aerial robot,” in *2016 IEEE/RSJ International Conference on Intelligent Robots and Systems (IROS)*, 2016, pp. 1570–1575.
- [26] Y. Aboudorra, C. Gabellieri, R. Brantjes, Q. Sablé, and A. Franchi, “Modelling, analysis, and control of omnimorph: an omnidirectional morphing multi-rotor uav,” *Journal of Intelligent & Robotic Systems*, vol. 110, 01 2024.
- [27] D. Brescianini and R. D’Andrea, “Design, modeling and control of an omni-directional aerial vehicle,” 05 2016, pp. 3261–3266.
- [28] J. Li, J. Sugihara, and M. Zhao, “Servo integrated nonlinear model predictive control for overactuated tilttable-quadrotors,” *IEEE Robotics and Automation Letters*, vol. 9, no. 10, pp. 8770–8777, 2024.
- [29] J. R. Page and P. E. I. Pounds, “The quadroller: Modeling of a uav/ugv hybrid quadrotor,” in *2014 IEEE/RSJ International Conference on Intelligent Robots and Systems*, 2014, pp. 4834–4841.
- [30] S. Sabet, A.-A. Agha-Mohammadi, A. Tagliabue, D. S. Elliott, and P. E. Nikravesh, “Rollocopter: An energy-aware hybrid aerial-ground mobility for extreme terrains,” in *2019 IEEE Aerospace Conference*, 2019, pp. 1–8.
- [31] C. Premachandra, M. Otsuka, R. Gohara, T. Ninomiya, and K. Kato, “A study on development of a hybrid aerial / terrestrial robot system for avoiding ground obstacles by flight,” *IEEE/CAA Journal of Automatica Sinica*, vol. 6, no. 1, pp. 327–336, 2019.
- [32] K. Sugihara, M. Zhao, T. Nishio, K. Okada, and M. Inaba, “Design and control of delta: Deformable multilinked multirotor with rolling locomotion ability in terrestrial domain,” *arXiv preprint arXiv:2403.06636*, 2024.
- [33] N. Pan, J. Jiang, R. Zhang, C. Xu, and F. Gao, “Skywalker: A compact and agile air-ground omnidirectional vehicle,” *IEEE Robotics and Automation Letters*, vol. 8, no. 5, pp. 2534–2541, 2023.

- [34] R. Zhang, J. Lin, Y. Wu, Y. Gao, C. Wang, C. Xu, Y. Cao, and F. Gao, "Model-based planning and control for terrestrial-aerial bimodal vehicles with passive wheels," in *2023 IEEE/RSJ International Conference on Intelligent Robots and Systems (IROS)*, 2023, pp. 1070–1077.
- [35] J. Lin, R. Zhang, N. Pan, C. Xu, and F. Gao, "Skater: A novel bi-modal bi-copter robot for adaptive locomotion in air and diverse terrain," *IEEE Robotics and Automation Letters*, vol. 9, no. 7, pp. 6392–6399, 2024.
- [36] Y. Qin, Y. Li, X. Wei, and F. Zhang, "Hybrid aerial-ground locomotion with a single passive wheel," in *2020 IEEE/RSJ International Conference on Intelligent Robots and Systems (IROS)*, 2020, pp. 1371–1376.
- [37] F. Saemi, A. Whitson, and M. Benedict, "Heat transfer models and measurements of brushless dc motors for small uass," *Aerospace*, vol. 11, no. 5, p. 401, 2024.
- [38] A. Kalantari, T. Touma, L. Kim, R. Jitosh, K. Strickland, B. T. Lopez, and A.-A. Agha-Mohammadi, "Drivocopter: A concept hybrid aerial/ground vehicle for long-endurance mobility," in *Proceedings of the 2020 IEEE Aerospace Conference*, 2020, pp. 1–10.
- [39] S. Morton and N. Papanikolopoulos, "A small hybrid ground-air vehicle concept," in *2017 IEEE/RSJ International Conference on Intelligent Robots and Systems (IROS)*, 2017, pp. 5149–5154.
- [40] M. Zhao, T. Anzai, and T. Nishio, "Design, modeling, and control of a quadruped robot spidar: Spherically vectorable and distributed rotors assisted air-ground quadruped robot," *IEEE Robotics and Automation Letters*, vol. 8, no. 7, pp. 3923–3930, 2023.
- [41] K. Sugihara, M. Zhao, T. Nishio, T. Makabe, K. Okada, and M. Inaba, "Design and control of a small humanoid equipped with flight unit and wheels for multimodal locomotion," *IEEE Robotics and Automation Letters*, vol. 8, no. 9, pp. 5608–5615, 2023.
- [42] A. R S and m. m. Dharmana, "Multi-terrain multi-utility robot," *Procedia Computer Science*, vol. 133, pp. 651–659, 01 2018.
- [43] E. Sihite, A. Kalantari, R. Nemovi, A. Ramezani, and M. Gharib, "Multi-modal mobility morphobot (m4) with appendage repurposing for locomotion plasticity enhancement," *Nature communications*, vol. 14, no. 1, p. 3323, 2023.
- [44] E. Frachtenberg, "Practical drone delivery," *Computer*, vol. 52, no. 12, pp. 53–57, 2019.
- [45] S. Poikonen and J. Campbell, "Future directions in drone routing research," *Networks*, vol. 77, 09 2020.

- [46] N. Bucki and M. W. Mueller, "Design and control of a passively morphing quadcopter," in *2019 International Conference on Robotics and Automation (ICRA)*, 2019, pp. 9116–9122.
- [47] P. H. Zipfel, *Modeling and Simulation of Aerospace Vehicle Dynamics, 2nd ed.* Reston, VA: American Institute of Aeronautics and Astronautics, 2007.
- [48] L. Meier, D. Honegger, and M. Pollefeys, "Px4: A node-based multithreaded open source robotics framework for deeply embedded platforms," in *2015 IEEE international conference on robotics and automation (ICRA)*. IEEE, 2015, pp. 6235–6240.
- [49] S. Norouzi Ghazbi, Y. Aghli, M. Alimohammadi, and A. A. Akbari, "Quadrotors unmanned aerial vehicles: A review," *International Journal on Smart Sensing and Intelligent Systems*, vol. 9, pp. 309–333, 03 2016.
- [50] R. Thusoo, S. Jain, and S. Bangia, "Quadrotors in the present era: a review," *Information Technology in Industry*, vol. 9, no. 1, pp. 164–178, 2021.
- [51] J. Tang, K. P. Jain, and M. W. Mueller, "Quartm: A quadcopter with unactuated rotor tilting mechanism capable of faster, more agile, and more efficient flight," *Frontiers in Robotics and AI*, vol. 9, 2022. [Online]. Available: <https://www.frontiersin.org/articles/10.3389/frobt.2022.1033715>
- [52] Z. Liang, L. Fan, G. Wen, and Z. Xu, "Design, modeling, and control of a composite tilt-rotor unmanned aerial vehicle," *Drones*, vol. 8, p. 102, 03 2024.
- [53] P. Wang, Z. Man, Z. Cao, J. Zheng, and Y. Zhao, "Dynamics modelling and linear control of quadcopter," in *2016 International Conference on Advanced Mechatronic Systems (ICAMechS)*, 2016, pp. 498–503.
- [54] A. Weishaupl and S. Prior, "Influence of propeller overlap on large scale tandem uav performance," *Unmanned Systems*, vol. 7, 05 2019.
- [55] R. Gill and R. D'Andrea, "Computationally efficient force and moment models for propellers in uav forward flight applications," *Drones*, vol. 3, p. 77, 10 2019.
- [56] F. Samouh, V. Gluza, S. Djavadian, S. Meshkani, and B. Farooq, "Multimodal autonomous last-mile delivery system design and application," in *2020 IEEE International Smart Cities Conference (ISC2)*. IEEE, 2020, pp. 1–7.
- [57] A. M. Raivi, S. A. Huda, M. M. Alam, and S. Moh, "Drone routing for drone-based delivery systems: A review of trajectory planning, charging, and security," *Sensors*, vol. 23, no. 3, p. 1463, 2023.
- [58] R. Bridgelall, T. Askarzadeh, D. Tolliver, M.-P. Consortium *et al.*, "Remote sensing of multimodal transportation assets using drones," Mountain-Plains Consortium, Tech. Rep., 2024.